Aspects of the Electroweak Theory

Helen Julia Porter

Thesis submitted to the University of Glasgow for the Degree of Doctor of Philosophy.

November 1990

Department of Physics and Astronomy, University of Glasgow.

Acknowledgements

I would like to thank both Professor I.S.Hughes and Professor R.P.Ferrier for the provision of facilities within the Department of Physics and Astronomy.

I am very grateful for the help and encouragement which has been consistently provided by my supervisor, Dr.C.D.Froggatt. I would also like to thank Dr.D.G.Sutherland for many critical but good-natured discussions which helped me to take a more objective view of my work. I am indebted to Professor J. Ambjørn of the Niels Bohr Institute in Copenhagen for his patience and willingness to assist me with even the most trivial points. I would also like to thank Dr.I.Barbour for his help with the work of Chapter 5; and all members of the theory group for their assistance generally. I would particularly like to thank both Russell Jenkins and David Alexander for useful suggestions. I owe thanks to the Science and Engineering Research Council for financial support.

Finally I would like to thank my parents for their support and encouragement over the last four years.

Declaration

The work of Chapters One and Two is original apart from the guidance of my supervisor, Dr. C.D.Froggatt. The remaining work of this thesis forms part of a collaboration with Professor J.Ambjørn, Professor M.Shaposhnikov and T.Askgaard. The FORTRAN code used to obtain the results discussed in this thesis is based upon a version written by Dr. M.Laursen. It has, however, undergone extensive modification and development. I would like to state that the results of Chapter Six and the consequent analysis is my own work. Chapter Five was done in collaboration with Dr. I.Barbour.

'Let me tell you a little story. Two Irishmen, Pat and Mike, were walking along Broadway, and one said to the other, "Begorrah, the race is not always to the swift," and the other replied, "Faith and begob, education is a drawing out, not a putting in." '

I must say it seemed to me the rottenest story I had ever heard, and I was surprised that Jeeves should have considered it worth shoving into a speech. However, when I taxed him later with this, he said that Gussie had altered the plot a good deal, and I dare say that accounts for it.

"Right Ho, Jeeves", P.G.Wodehouse.

Contents

Abstract

This thesis is divided into two quite distinct parts, linked only by the central role of the electroweak theory in each. The first part is concerned with the experimentally observed $\Delta I = 1/2$ selection rule in weak Kaon decays, and we consider an extension to the Standard Model which might allow a satisfactory theoretical explanation of the rule. The second part forms the major part of the thesis and is related to the well-known baryon asymmetry of the Universe. We explore the possibility that the non-perturbative sector of the electroweak theory could play a central role in the production of such an asymmetry. We use lattice gauge techniques to simulate the electroweak interactions in the phase with restored $SU(2)$ symmetry and numerically calculate a rate for baryon number non-conservation processes which is then compared to the existing theoretical predictions.

Ma has recently proposed an extension to the Standard Model which contains new penguin diagrams and which should therefore contribute to $\Delta I = 1/2$ processes. The new model must be constrained to preserve the observed small $K_L - K_S$ mass difference. We correct and reanalyse the model and search the parameter space numerically to find suitable values for the new particle masses. We find that that the model is unable to provide the necessary enhancement to fully understand the rule.

The electroweak theory may play a major role in the generation of the baryon asymmetry of the Universe. It provides for fermion number non-conservation by allowing sphaleron type transitions across the potential barrier separating different topological sectors. These transitions are thought to become rapid at high temperature, but perturbative calculations are not possible because of infrared singularities. We have used lattice gauge theory to study the evolution of an $SU(2)$ gauge-Higgs system in the high temperature, unbroken symmetry phase. A Minkowski metric was used so that we were able to measure the rate of sphaleron transitions in real time, by following the development of the Chern-

Simons number, N_{cs}, which is closely related to the topological charge. We include a description of the problems relating to the measurement of topological quantities on the lattice and compare the results of using different techniques to measure them.

Using 8^3, 12^3 and 16^3 spatial lattices we found that the transitions were unsuppressed and $\Gamma = \kappa(\alpha_W T)^4$ where $\kappa \simeq 0.1 - 1.0$. This has important implications for the possibility of the electroweak theory washing out a baryon excess at the time of the phase transition; particularly for Grand Unified Theories which conserve baryon minus lepton number. There was good scaling behaviour with both the lattice size and gauge coupling. In addition we measured the thermal fluctuations $< N_{cs}^2 >$ within a given topological sector. We found reasonable agreement with the perturbative estimate. Larger lattice sizes are needed to measure the sphaleron transition rate in the low temperature, broken symmetry phase. Problems relating to energy conservation have so far prevented the addition of a driving term $\mu_B N_{cs}$ which modifies the effective action in the presence of a non-zero fermionic density; μ_B is the fermionic chemical potential. With this term added into the simulation it might be possible to see evidence for sphaleron transitions playing a direct role in baryon number generation.

Chapter 1

Introduction to the New Model

1.1 The Standard Model and the $\Delta I = \frac{1}{2}$ Rule

The Standard Model describes the fundamental interactions of elementary particles up to energies of about 100 GeV and distances of about 10^{-16}cm [1]. Its success as the minimal model needed to predict the behaviour of matter with its inherent symmetries, has been considerable. The most famous of its triumphs must be the prediction of the W and Z bosons whose existence was confirmed experimentally in 1983.

The Standard Model combines the strong, weak and electromagnetic interactions and can be mathematically described as an $SU(3) \times SU(2) \times U(1)$ gauge theory. Elementary particles are grouped into families or generations, each of which consists of a pair of quarks and leptons. There are thought to be three generations in all; the first comprising the u and d quarks and the electron and its neutrino, e and ν_e. The c, s, t and b quarks and the μ, τ, ν_μ and ν_τ leptons complete the spectrum.

The $SU(3)$ sector describes the strong force through Quantum Chromodynamics (Q.C.D.). This determines how hadrons interact; the quarks which make up the hadron have a colour quantum number and interact through the exchange of virtual coloured gluons. The experimentally observed rule that quarks are never found in isolation, but must always exist within hadrons, which is known as "confinement", is consistent with the premise that physical particles are colourless. The actual mechanism is much more complicated and

has not actually been proved theoretically. $SU(3)$ is a non-Abelian gauge theory and this allows interactions between the gluons themselves. So as two quarks are pulled apart the self interactions between the gluons increase and the force between the quarks becomes more attractive. This property that the interaction actually increases with the separation and hence decreases with increased virtual energy is referred to as asymptotic freedom. Asymptotic freedom itself is not sufficient to explain quark confinement; although we see the correct behaviour of the interaction at short distances using perturbation theory, it is not clear yet that the same behaviour is necessarily true at larger separations. Lattice gauge theories are doing much to explore the problem in the regime where perturbation theory breaks down.

The $SU(2) \times U(1)$ sector is the electroweak model of Weinberg and Salam. Electroweak interactions were first seen in nuclear β decay. They are characterised by parity violation and only allow the interaction of left-handed fermions. Charge conjugation invariance is also violated by the weak interactions; the amplitude for a weak decay process is not necessarily identical to the amplitude for the same process but where anti-particles replace the particles. The Higgs mechanism provides a method of giving the gauge bosons mass which avoids introducing non-renormalizable terms into the Lagrangian; $SU(2) \times U(1)$ is spontaneously broken to $U(1)_{em}$ by the Higgs doublet. The $W^{\pm}$ and Z acquire mass through this symmetry breaking, while the photon remains massless. In addition, the fermions are able to acquire mass during the symmetry breaking via the Yukawa couplings. Although each of C and P invariance is broken by the interactions a two generation model conserves CP. In the three generation model there is a small amount CP non-conservation which is introduced by the fermion mass mixing matrix. This matrix is parameterized by three mixing angles and an additional complex phase which describes the extent of CP violation. The most widely used parameterization of this matrix is that of Kobayashi and Maskawa.

Quantum electrodynamics (Q.E.D.) describes the electromagnetic interactions of electrons through the exchange of virtual photons. It is described by

$U(1)_{em}$; which is an Abelian gauge group.

Although the Standard Model is highly successful and has a pleasing mathematical basis it is not a complete description of the physical world. Indeed the non-perturbative region of the model has not been extensively explored, although lattice gauge calculations do provide some way of testing. Despite being such an important and obvious force of nature, gravity has no part in this model; it still lacks a complete quantum description although superstring theories have done much to provide a partial quantum field description if only at much higher energies and dimensions. There are a large number of unknown parameters in the Standard Model whose values can only be determined through experiments, rather than having a theoretical motivation.

One very major problem associated with the Standard Model is the so-called $\Delta I = 1/2$ rule, which is observed experimentally in Kaon decay and non-leptonic hyperon decays [2]. In particular [3]

$$\frac{\Gamma(K_S^0 \to \pi^+\pi^-)}{\Gamma(K^+ \to \pi^+\pi^0)} \approx 450 \tag{1.1}$$

K_S^0 is just the short-lived weak neutral Kaon mass eigenstate. [1] Both K_S^0 and K^+ have isospin $I = 1/2$. The space wavefunction of the final two pion state is symmetric, so that the isospin wavefunction must also be symmetric; that is $I = 0$ or 2. However, since the $\pi^+\pi^0$ state has $I_3 = 1$, the $I = 0$ state is excluded and $I = 2$. So while $K^+ \to \pi^+\pi^0$ represents $\Delta I = 3/2$ or $\Delta I = 5/2$, $K_S^0 \to \pi^+\pi^-$ may be a mixture of $\Delta I = 1/2$, $\Delta I = 3/2$, or $\Delta I = 5/2$. This is consistent with a rule of preferring $\Delta I = 1/2$ decays, and it can further be deduced that the ratio of amplitudes for the $\Delta I = 1/2$ and $\Delta I = 3/2$ processes is

$$\frac{A(\Delta I = \frac{1}{2})}{A(\Delta I = \frac{3}{2})} \approx 22 \tag{1.2}$$

Despite such a phenomenon first having been seen over thirty years ago the $\Delta I = 1/2$ rule still lacks a decisive explanation.

Progress in understanding this effect was made when it was realised that

[1] The mass eigenstates for the Kaon system are different with respect to the strong and weak forces because the latter do not conserve flavour.

these Kaon decays cannot be considered solely as weak processes; Q.C.D. corrections become important in two ways which increase our understanding of the experimental ratio eq(1.1). The first is that the amplitude $K \rightarrow \pi^+\pi^0$ is suppressed when hard gluon effects are calculated. This can be understood qualitatively by realising that there are two identical $\overline{u}$ quarks in the final $\pi^+\pi^0$ state; and so the Pauli exclusion principle is influencing the decay.

The second is the introduction of the so-called penguin diagram [4] [5] shown in figure 1.1:

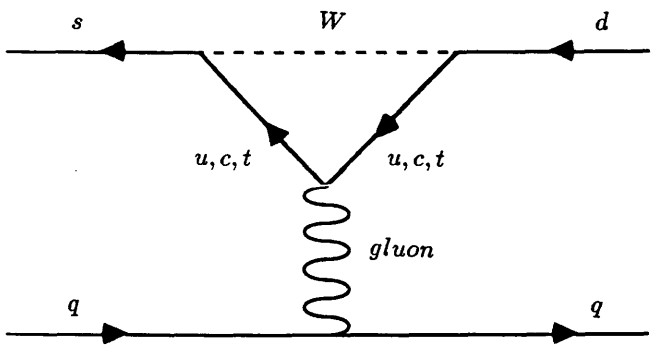

Figure 1.1

The Standard Model penguin diagram.

whose effective Hamiltonian is given by:

$$H_{penguin} = \frac{G_F}{\sqrt{2}} \sin\theta_c \cos\theta_c c(\mu) \times (\overline{s}\gamma_\mu(1-\gamma_5)\lambda^a d)(\overline{u}\gamma^\mu\lambda^a u + \overline{d}\gamma^\mu\lambda^a d + \overline{s}\gamma^\mu\lambda^a s) \tag{1.3}$$

Here θ_c is the Cabibbo angle, G_F the Fermi coupling constant, λ^a the colour matrices and μ the renormalisation scale. This diagram represents a pure $\Delta I = 1/2$ change because the gluon cannot carry any isospin number; but the d quark has $I = 1/2$ and the s quark has $I = 0$. Although the Wilson coefficient $c(\mu)$ is not large the matrix elements are significant. From eq(1.2) it is seen that the penguin diagram gives rise to a $(V-A) \times V$ structured operator, which will consequently contribute to both $(V-A) \times (V-A)$ and $(V-A) \times (V+A)$ type operators. In the limit of exact chiral symmetry a left handed operator can only annihilate left handed quarks; but mesons contain left and right handed

quarks as their quark structure is of course just $q\bar{q}$. This means that the matrix elements of operators like $(V-A)\times(V-A)$ must be proportional to the quark masses because they give the scale of the chiral symmetry breaking. So for mesons which are made from light quarks $(V-A)\times(V-A)$ operators are helicity suppressed. Operators of the form $(V-A)\times(V-A)$ are typical when purely weak matrix elements for kaon decay are evaluated. Such a suppression will not apply to an operator like $(V-A)\times(V+A)$ so the penguin is expected to produce a large effect, despite being a loop correction type diagram.

Quantifying the effects of Q.C.D. is very difficult. Despite improving lattice gauge techniques for estimating non-perturbative effects, calculations are generally restricted to the perturbative region $\mu \geq 1$ GeV. It is possible that these non-perturbative effects may play a major role in the understanding of the $\Delta I = 1/2$ rule. In fact the full amplitude should be independent of the renormalisation scale μ. However, the matrix elements, by definition must be calculated at the scales of the initial and final physical states; ie m_K and m_π. This is much lower than the 1 GeV scale needed before reasonable estimates of the Wilson coefficients can be made.

In addition there is no reliable method to evaluate the hadronic matrix elements even at the low energy scales m_K and m_π. One approach to this problem is to use the bag model in which the mesons are treated as resonances of two quark states and the matrix elements calculated as eigenstate equations. Vacuum insertion techniques are also frequently used; a $|0><0|$ state is inserted between the two quark bilinear operators. It is clear that in following this procedure the contribution of all other intermediate states will be ignored and that the amplitudes will not necessarily be consistent with chiral perturbation theory. However the simplicity of this method and the lack of any other that can be proven to be more reliable has made it very popular.

Thus, considerable controversy surrounds the predicted $\Delta I = 1/2$ amplitude from the Standard Model; however, it is generally thought to provide about 20% of the experimental amplitude. With such serious doubts, speculation flourishes about new interactions and particles that might be the true explanation of the

rule.

1.2 A Review of the Ma Model

Over the past few years extensions to the Standard Model have been considered in an effort to provide a plausible explanation for the $\Delta I = 1/2$ rule [6] [7]; given the uncertainties related to calculations within the Standard Model. The underlying idea is that new heavy particles could act as propagators for new penguin diagrams and so increase the $\Delta I = 1/2$ amplitude. Ma [7] has considered such a mechanism; using superstring theory to give a physical motivation for the existence and behaviour of the new fields. String theories are formulated at energies above the Planck scale, and usually in more than four dimensions; to get a connection with much lower energies requires some compactification scheme down to four dimensions. Such schemes indicate that E_6 is one likely candidate for the unifying gauge group below the Planck scale, eventually breaking down to $SU(3) \times SU(2) \times U(1)$; but with additional particles appearing [8]. Fermions belong to the **27** representation of E_6, which decomposes under $SO(10)$ into $\mathbf{16} + \mathbf{10} + \mathbf{1}$. The full set of quarks and leptons associated with a particular generation is contained within the **16**, but in addition the **16** contains two new scalar bosons; one a singlet, ϕ_1, and one part of a doublet ϕ_2. The **10** contains a new vector like quark h whose left and right handed components transform in the same way under $SU(2)$, unlike the quarks of the Standard Model. The new scalar bosons couple the Standard Model quarks to these new h quarks and allow the possibility of new $\Delta I = 1/2$ interactions. The only requirement on the mechanism that Ma proposes is that the $K_L - K_S$ mass difference is kept within the experimentally known limits. This mass difference, Δm_K, is given by $-2Re < K^0|\mathcal{H}_{eff}|\overline{K}^0 >$. The new interactions allow new box diagrams to contribute to Δm_K; again the Φ boson replaces the W and the h quarks replace the usual u, c, and t propagators. Ma does not attempt to constrain the free parameters of the theory systematically, rather he tries to show that such a model is likely to have a large window of allowed parameter values. Instead of using

the most general Lagrangian possible he neglects the pseudoscalar interactions of the new particles and looks at the couplings to the first and second generation quarks only. This reduces the number of free parameters in the theory and makes the model tractable. The Lagrangian used takes the form:

$$\mathcal{L}_{int} = (g_1 \overline{d} h_1 + g_2 \overline{s} h_2)\phi + h.c. \tag{1.4}$$

where ϕ is a linear combination of ϕ_1 and ϕ_2, g_1 and g_2 are the new coupling constants of the theory and *h.c.* stands for the hermitian conjugate. Generation symmetry is assumed in the Lagrangian in that the d quark couples to h_1 and the s quark couples to h_2; h_1 and h_2 belonging to the first and second generations. However, h_1 and h_2 are gauge rather than mass eigenstates so that mixing is allowed; through some angle defined to be θ. It is this mixing which allows the mass eigenstates H_1 and H_2, with mass m_1 and m_2 respectively to act as new fermion propagators in a new penguin diagram shown in figure 1.2 below.

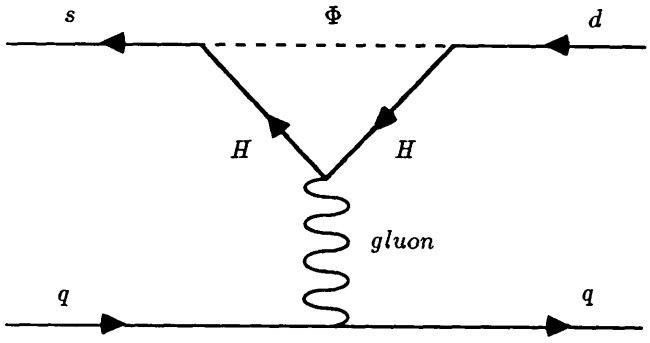

Figure 1.2

The new penguin diagram in Ma's model.

An analogy can be made with the Standard Model, with its Yukawa coupling of the Higgs boson to the quarks. As spontaneous symmetry breaking takes place the Higgs particle acquires its vacuum expectation value and the Yukawa term becomes a quark-quark type coupling term. Then the Yukawa coupling constant must be proportional to the quark mass. Here, however, there is no such reason to expect that the coupling constants g_1 and g_2 should be small. In any case, it must be assumed that the new quarks and the new

scalar bosons are heavy, $\geq$ 40 GeV., otherwise their existence would have been detected experimentally.

Ma calculates the amplitude for fig. 1.2 and the associated $K_L - K_S$ mass difference. He then shows that the coefficients of the amplitude for the new penguin diagram may be large, while the mass difference remains very small for some example parameter choices; in particular the new particle masses are less than 150 GeV. Unfortunately, when these chosen parameter values are substituted into the equation giving the mass difference an error is made which substantially changes the results of the work. (See Appendix A for details)

A very much more serious flaw in Ma's investigations is that the original Lagrangian eq(1.3) does not contain any parity violating part, and so the contribution to $K \rightarrow 2\pi$ must be zero from this consideration alone. So while the amplitude for the new penguin may be very large the hadronic matrix elements are actually zero.

In Chapter two we study a generalisation of the Lagrangian of eq(1.2) in detail; the motivation is still the E_6 gauge group but the pseudoscalar interaction terms are now included rather than neglected [9]. In the spirit of Ma's paper we do not include all possible couplings, but just consider a Lagrangian which has the generic structure required to generate a new penguin diagram contributing to the $\Delta I = 1/2$ amplitude. To restrict the number of free parameters in the theory we confine the model to two generations, assuming like Ma that the couplings of for example an H_3 quark to the s and d quarks are very small, which is natural since generation symmetry is already assumed in the very structure of the original Lagrangian.

Choudhury and Joshi [10] have studied the induced neutral strangeness changing sdZ_0 weak vertex of the original non-parity violating Lagrangian which affects the rate of $K^0 \rightarrow \mu^+\mu^-$ decay. They concluded that Ma's model would be too constrained by experimental limits on this vertex to explain the $\Delta I = 1/2$ rule. The vertex could certainly be recalculated using a generalised Langrangian, but the work of Chapter 2 is restricted to the constraints on the free parameters of the model imposed by Δm_K; and this alone seems sufficient

to rule such a model out.

Chapter 2

The New Model

2.1 Introduction

This chapter considers how a generalized version of Ma's Lagrangian may enhance $\Delta I = 1/2$ processes through the introduction of the new penguin diagrams that are discussed in Chapter 1. We begin by setting out the new interaction Lagrangian which differs from the one investigated by Ma in that pseudoscalar interactions are no longer neglected. In Section 2.2 the amplitude for the process $K^0 \to \pi^+\pi^-$ is evaluated, and the size of the $K_L - K_S$ mass difference, Δm_K, predicted by the new model is determined. Both the amplitude and the mass difference are expressed as functions of the new model's parameters, and Section 2.3 considers how to explore the parameter space to determine regions where the new penguin amplitude is large enough explain the $\Delta I = 1/2$ rule, while at the same time Δm_K remains inside experimental limits. Results and conclusions are presented in Section 2.4.

2.1.1 The New Lagrangian

Assuming only the same kind of generation symmetry as Ma, the full form of the Lagrangian describing the possible couplings of the new vector-like h quarks to the s and d quarks of the Standard Model is:

$$\begin{aligned}\mathcal{L} =& \frac{g_A}{2}\overline{h}_1(1+\gamma_5)d{\phi_1}^\dagger + \frac{g_B}{2}\overline{h}_2(1+\gamma_5)s{\phi_1}^\dagger \\ &+\frac{g_C}{2}\overline{h}_1(1-\gamma_5)d{\phi_2}^\dagger + \frac{g_D}{2}\overline{h}_2(1-\gamma_5)s{\phi_2}^\dagger + h.c.\end{aligned} \tag{2.1}$$

To simplify the analysis it is assumed that only the new couplings g_B and g_C are non-zero, i.e. $g_A = g_D = 0$. Thus

$$\mathcal{L} = \frac{g_B}{2}\overline{h}_2(1+\gamma_5)s{\phi_1}^\dagger + \frac{g_C}{2}\overline{h}_1(1-\gamma_5)d{\phi_2}^\dagger + h.c. \tag{2.2}$$

It should be recognised that couplings of the opposite chirality would certainly need to be included when estimating the induced strangeness-changing weak neutral current processes such as $K_L \to \mu^+\mu^-$.

In addition to mixing between the h quarks, mixing must also be allowed between the new scalar bosons, ϕ_1 and ϕ_2, to obtain a non-zero $d \to s$ type interaction; from eq.(2.2) it is seen that the s quark may only couple to ϕ_2 while the d quark may only couple to ϕ_1. The mixing angle is denoted by α. It is also assumed that the second of the mass eigenvalues is much greater than the first; so that only one scalar boson Φ, with mass M, is included in the calculations of this chapter. Amplitudes are calculated in the approximation that all external momenta are small compared to the new particle masses. The Feynman rules for the Lagrangian are given in Appendix B.

2.2 The New Penguin Amplitude and the Contribution to the $K_L - K_S$ Mass Difference

Having introduced chirality into the Lagrangian the penguin diagram is finite and the self energy diagrams vanish. The amplitude for the penguin vertex is given by

$$\Gamma^{a\mu}_{penguin} = iw_j k^\mu \overline{s}(1-\gamma_5)\lambda^a d \times I_{(i)} - w_j k_\nu \overline{s}(1-\gamma_5)\sigma^{\nu\mu}\lambda^a d \times I_{(ii)} \tag{2.3}$$

where w_j is defined to be

$$w_j \equiv (-1)^j m_j \frac{1}{4}\frac{1}{16\pi^2} g_S g_B g_C \sin\theta\cos\theta\sin\alpha\cos\alpha \tag{2.4}$$

and the integrals are

$$I_{(i)} = \int_0^1 dx \int_0^{1-x} dz \frac{(2x+z-1)}{(m_j^2 + (M^2 - m_j^2)z)} \tag{2.5}$$

$$I_{(ii)} = \int_0^1 dx \int_0^{1-x} dz \frac{(z-1)}{(m_j^2 + (M^2 - m_j^2)z)} \tag{2.6}$$

The first of these integrals is zero, leaving only a tensor type interaction for the penguin amplitude. This differs from the original non-parity violating theory discussed in Chapter 1, where the first term survived as a vector type term. The total amplitude for the new penguin diagram of fig. 1.2 is given by

$$\Gamma = \frac{1}{2} B k_\nu \bar{s} \sigma^{\mu\nu} (1 - \gamma_5) \lambda^a d \times \frac{g_S}{2m_G^2} \bar{q} \lambda^a \gamma_\mu q \tag{2.7}$$

where k is the gluon momentum, and a gluon "mass" is defined as $m_G^2 \equiv k^2$. B is defined by

$$B = \frac{1}{2} g_S g_B g_C \sin\theta \cos\theta \sin\alpha \cos\alpha (f_1' - f_2') \tag{2.8}$$

and

$$f_j' = \frac{m_j}{16\pi^2} \left(\frac{3M^2 - m_j^2}{2(M^2 - m_j^2)^2} + \frac{M^4}{(M^2 - m_j^2)^3} \ln \frac{m_j^2}{M^2} \right) \tag{2.9}$$

We want to calculate the invariant amplitude for $K^0 \to \pi^+\pi^-$, assuming that the effective Lagrangian from eq.(2.7) is solely responsible for the decay. It would be equally possible to calculate the invariant amplitude of the process $K^0 \to \pi^0\pi^0$.

$$A(K^0 \to \pi^+\pi^-) = \frac{g_S B}{4m_G^2} < \pi^+\pi^- | \partial_\mu (\bar{s}\sigma^{\mu\nu}(1 - \gamma_5)\lambda^a d)(\bar{q}\gamma_\nu \lambda^a q) | K^0 > \tag{2.10}$$

The relevant matrix element has been calculated by Deshpande [11] using the vacuum insertion approximation. We use his result modified by a factor m_K^2/m_σ^2 which is necessary to give the correct chiral transformation behaviour [12]. m_σ is the mass of a 0^+ scalar boson; taken to be 0.7 GeV.

$$A(K^0 \to \pi^+\pi^-) = -\frac{g_S B}{4m_G^2} \frac{8}{3} \frac{f_\pi m_K^2 m_\pi^2}{(m_d + m_u)} \left(\frac{m_K^2}{m_\sigma^2} \right) \left(\frac{f_k}{f_\pi} + 1 + \frac{f_K}{f_\pi} \frac{m_K^2}{m_\sigma^2} \right) \tag{2.11}$$

where f_K and f_π are the Kaon and Pion decay constants. The quark masses

m_u and m_d are taken to be current masses, in agreement with Deshpande.

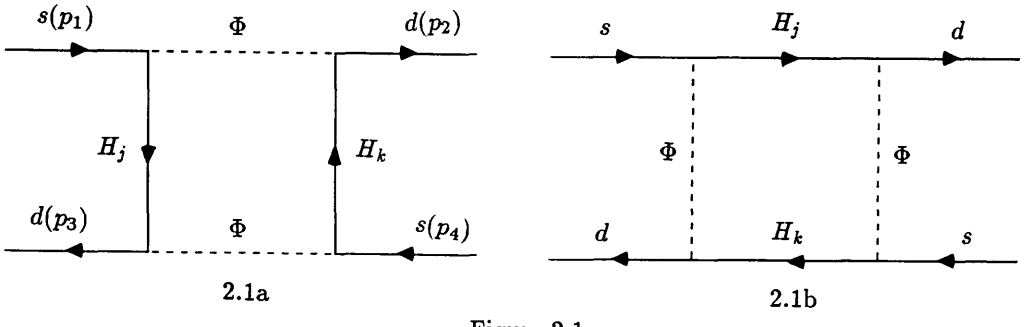

Figure 2.1

2.1a and 2.1b show the new box diagrams for the $K_L - K_S$ mass difference.

The next stage is the calculation of the induced $K_L - K_S$ mass difference, Δm_K, that the new interactions would generate, through the box diagrams of fig. 2.1a and fig. 2.1b. The amplitude for fig. 2.1a is given by

$$I_a = -i\,4\nu\,\overline{d}(p_3)(1+\gamma_5)s(p_1)\,\overline{d}(p_2)(1+\gamma_5)s(p_4)\,(F'_{11}+F'_{22}-2F'_{12}) \tag{2.12}$$

where

$$\nu \equiv \frac{1}{16}(g_B g_C \sin\theta\cos\theta\sin\alpha\cos\alpha)^2 \tag{2.13}$$

and

$$F'_{jk} = i\frac{m_j m_k}{(2\pi^4)}\int d^4k \frac{1}{(k^2-M^2)^2(k^2-m_j^2)(k^2-m_K^2)} \tag{2.14}$$

This integral can be evaluated to give

$$F'_{jk} = \frac{m_j m_k}{16\pi^2}\left\{\frac{1}{(M^2-m_j^2)(M^2-m_k^2)}+\frac{1}{(m_k^2-m_j^2)} \times\left[\frac{m_k^2}{(M^2-m_k^2)}\ln\frac{m_k^2}{M^2}-\frac{m_j^2}{(M^2-m_j^2)}\ln\frac{m_j^2}{M^2}\right]\right\} \tag{2.15}$$

$$F'_{jj} = \frac{{m_j}^2}{16\pi^2}\left\{\frac{2}{(M^2-m_j^2)^2}+\frac{(M^2+m_j^2)}{(M^2-m_j^2)^3}\ln\frac{m_j^2}{M^2}\right\} \tag{2.16}$$

The contribution from figure 2.1b has a relative minus sign. In addition there is a colour supression factor of 1/3; this is because the Φ boson carries no colour quantum number and so, unlike the case shown in 2.1a, the initial s and $\overline{d}$

quarks are unable to change colour during the interaction.

$$I_b = +i\frac{4}{3}\nu\,\bar{d}(p_2)(1+\gamma_5)s(p_1)\,\bar{d}(p_3)(1+\gamma_5)s(p_4)\,(F'_{11}+F'_{22}-2F'_{12}) \qquad (2.17)$$

From I_a and I_b we wish to construct $\mathcal{L}_{eff}$ and evaluate $< K^0|\mathcal{L}_{eff}|\overline{K}^0 >$. The vacuum insertion technique is to be used, so I_b must be Fierz rearranged before its contribution to $\mathcal{L}_{eff}$ can be ascertained. Moreover, since K is a pseudoscalar particle, only axial vector and pseudoscalar terms can contribute to a non-zero amplitude. Anticipating this we note that

$$\bar{d}(p_2)(1+\gamma_5)s(p_1)\,\bar{d}(p_3)(1+\gamma_5)s(p_4) = \frac{1}{2}\bar{d}(p_3)(1+\gamma_5)s(p_1)\,\bar{d}(p_2)(1+\gamma_5)s(p_4) \qquad (2.18)$$

and obtain

$$I_a + I_b = -i\frac{10}{3}\nu\,\bar{d}(1+\gamma_5)s\,\bar{d}(1+\gamma_5)s\,(F'_{11}+F'_{22}-2F'_{12}) \qquad (2.19)$$

$$\Delta m_K = -\frac{20}{3}\nu\,(F'_{11}+F'_{22}-2F'_{12})\,Re\left\{< K^0|\bar{d}\gamma_5 s|0 >< 0|\bar{d}\gamma_5 s|\overline{K}^0 >\right\} \qquad (2.20)$$

Following [4] we use

$$< 0|\bar{d}\gamma_5 s|\overline{K}^0 >= \frac{if_K}{(2m_K)^{\frac{1}{2}}}\frac{m_\pi^2}{(m_u+m_d)} \qquad (2.21)$$

This is larger than the corresponding element used by Ma, but it is more consistent with the Dirac equation when this element is compared to the axial vector matrix element. m_u and m_d are current quark masses. Thus the $K_L - K_S$ mass difference predicted by the new Lagrangian is given by:

$$\Delta m_K = \frac{10}{3}\nu\frac{f_K^2 m_\pi^4}{m_K(m_u+m_d)^2}(F'_{11}+F'_{22}-2F'_{12}) \qquad (2.22)$$

This expression will be used in the next section where we deal with the constraints on the allowed values of the parameters of the new model.

2.3 Constraints on the Model

The first condition to be satisfied is

$$|A(K^0 \to \pi^+\pi^-)|_{Ma} > w \times |A(K^0 \to \pi^+\pi^-)|_{expt} \tag{2.23}$$

w is some arbitrary parameter that can be changed according to whether we want the model to provide a full or partial explanation of the $\Delta I = 1/2$ puzzle.

Secondly the mass difference, Δm_K, predicted by the new Lagrangian must be less than the known experimental value:

$$|\Delta m_K|_{Ma} < |\Delta m_K|_{expt} \tag{2.24}$$

then these two inequalities are combined to give

$$\rho \times \frac{|(F'_{11} + F'_{22} - 2F'_{12})|}{(f'_1 - f'_2)^2} < \frac{1}{w^2}\left(\frac{\Delta m_K}{m_K}\right)_{expt} \frac{1}{|A(K^0 \to \pi^+\pi^-)|^2_{expt}} \tag{2.25}$$

where ρ has been defined as

$$\rho \equiv \frac{15}{8}\frac{f_K^2}{f_\pi^2}\frac{1}{g_S^4}\frac{m_G^4}{m_\sigma^6}\left[\left(\frac{m_K^2}{m_\sigma^2}\right)^2\left(\frac{f_K}{f_\pi} + 1 + \frac{f_K}{f_\pi}\frac{m_K^2}{m_\sigma^2}\right)^2\right]^{-1} \tag{2.26}$$

The advantage of combining the constraints in this way is that the dependence on g_B, g_C, α and θ vanishes to leave dependence only on the mass ratios of the new quarks to the scalar boson Φ:

$$x \equiv \frac{m_1}{M}, \quad y \equiv \frac{m_2}{M} \tag{2.27}$$

Unfortunately the disadvantage of squaring the penguin amplitude in this way is that the inequality, eq.(2.25), becomes extremely sensitive to small changes in the parameters such as m_σ which are not at all well known.

Using the experimental values:

$$|A(K^0 \to \pi^+\pi^-)|_{expt} = 2.744 \times 10^{-7} GeV. \tag{2.28}$$

and

$$\left(\frac{\Delta m_K}{m_K}\right)_{expt} = 0.707 \times 10^{-14} \tag{2.29}$$

The Q.C.D. coupling constant g_S is chosen to have a value corresponding to $\alpha_S = g_S^2/4\pi = 1/2$. The effective gluon mass is assumed to be 0.5 GeV. Then

$$|(F'_{11} + F'_{22} - 2F'_{12})| - \frac{0.67}{w^2} \times (f'_1 - f'_2)^2 < 0 \tag{2.30}$$

The left hand side of this expression is a complicated function of the mass ratios x and y, and for this reason a numerical search is used to find the regions which satisfy the inequality.

For every such region in which (2.30) holds we can reapply (2.23) to find the minimum values of the mass of the new boson Φ, M, and of the product $(g_B g_C)$ which are allowed. Defining $f = f' \times 16\pi^2 M$:

$$f(x) = x\left(\frac{3-x^2}{2(1-x^2)^2} + \frac{1}{(1-x^2)^3} ln x^2\right) \tag{2.31}$$

Then defining $f(x) \equiv f_1$ and $f(y) \equiv f_2$ eq.(2.23) becomes:

$$(g_B g_C \sin\theta \cos\theta \sin\alpha \cos\alpha) > \frac{w}{|f_1 - f_2|} \times M \times 6.2\ 10^{-5} \tag{2.32}$$

It is then assumed that both of the new vector-like quarks must have masses greater than 40 GeV; otherwise they would already have been detected. Then a minimum value of M can be determined for every x and y coordinate pair lying inside the allowed region; and hence an overall minimum value of M can be found for the whole area. Alternatively, the minimum value of $M/(|f_1 - f_2|)$ can be found for each x, y pair, and if all possible coordinate pairs inside the allowed region are scanned we obtain a minimum for $(g_B g_C \sin\theta \cos\theta \sin\alpha \cos\alpha)$. In practice, of course, we can never test all possible coordinate pairs and consequently we divide the region under scrutiny into a finite sized mesh.

2.4 Numerical Results and Conclusions

Locating all possible regions which satisfy the constraint (2.30) is crucial. Preliminary searches at $w = 1.0$ failed to find any regions of interest, so more detailed searches were performed at a smaller value of w, $w = 0.1$. The motivation for this was simply that the negative regions should be larger the smaller

the value of w; and so once areas are found a $w = 0.1$ it is possible to "home-in" on such areas for more realistic values of w. In fact, if w is much smaller than 0.1 much of the positive quadrant of the x, y plane turns negative.

A full search from 0.001 to 100.0 was made at $w = 0.1$. Three negative regions were found, one at small x and small y, and the second and third at small x and large y, and large x and small y respectively. When trying to move to larger values of w it became clear that the inequality (2.30) is extremely sensitive to variations in w. This is illustrated in figures 2.2 and 2.3 where the allowed region shrinks drastically as w is increased by a factor of just 2. Approximations were made to try to estimate the bounds on the negative regions for $w = 1.0$, a value of w at which the new penguin amplitude would match that of the experimental data. From the results at small w we know to look where x and y are both small, and where one of the pair is small but the other very large. At small x and small y the formula (2.30) simplifies; then setting $y = x(1 + \epsilon)^{1/2}$ gives an easily soluble quadratic. The solution approximately describes where the line $y = x$ crosses into the negative region. This gave $x, y \approx \exp(-120)$. Similarly the formula (2.30) simplifies for small x (y) and large y (x). The curve $y = 1/x$ provides some means to pin-point the negative region; substituting $y = 1/x$ dictates where this region intersects with the curve. The graph of fig. 2.4 indicates clearly the usefulness of this. For $w = 1.0$ this point is estimated to be at $x = \exp(-236)$. Finally, the results of the searches for minimum M and $g_B g_C$ for $w = 0.1$ and $w = 0.2$ are given in Table 1.1. It is assumed that $\sin\theta \cos\theta \sin\alpha \cos\alpha$ obtains its maximum value $1/4$. In every case the region specified was divided into a mesh of about 1000×1000; and each mesh point investigated.

w	Area Searched	$M_{min}(GeV)$.	$(g_B g_C)_{min}$	$M(GeV)$. at$(g_B g_C)_{min}$
0.1	x: 0.00025 $\rightarrow$ 0.25 y: 0.00025 $\rightarrow$ 0.25	777.0	0.238	1760.0
0.1	x: 0.0004 $\rightarrow$ 0.4 y: 10.0 $\rightarrow$ 15.0	180.0	0.0117	180.0
0.2	x: 0.000005 $\rightarrow$ 0.005 y: 0.000005 $\rightarrow$ 0.005	28000.0	158.0	63500.0
0.2	x: 0.000007 $\rightarrow$ 0.007 y: 100.0 $\rightarrow$ 7100.0	7170.0	7.19	7170.0

Table 1.1

For large $y(x)$ and small $x(y)$ we find that the overall minimum value of M coincides with the minimum possible value for the couplings. Further, as the area searched is increased to include larger $y(x)$ values so both the minimum mass of Φ and minimum values of the couplings decrease. However, although M and the coupling values are becoming more plausible, the difference in the new quark masses is many orders of magnitude. The table clearly shows that as w approaches any workable value the range of possible mass ratios x and y diminishes quite rapidly; already at $w = 0.2$ not only are choices of available x and y extremely artificial, but the minimum allowed couplings suggest that perturbation theory is not valid in these regions.

We have shown that using reasonable approximations to calculate the effects of the new penguin diagram by standard perturbative techniques the new model cannot match the experimental $\Delta I = 1/2$ amplitude. Even to produce about 20% of the experimentally observed amplitude requires the new particles to have masses at the TeV. scale, and such large values of the couplings of the new Lagrangian that the use of perturbation theory is highly suspect.

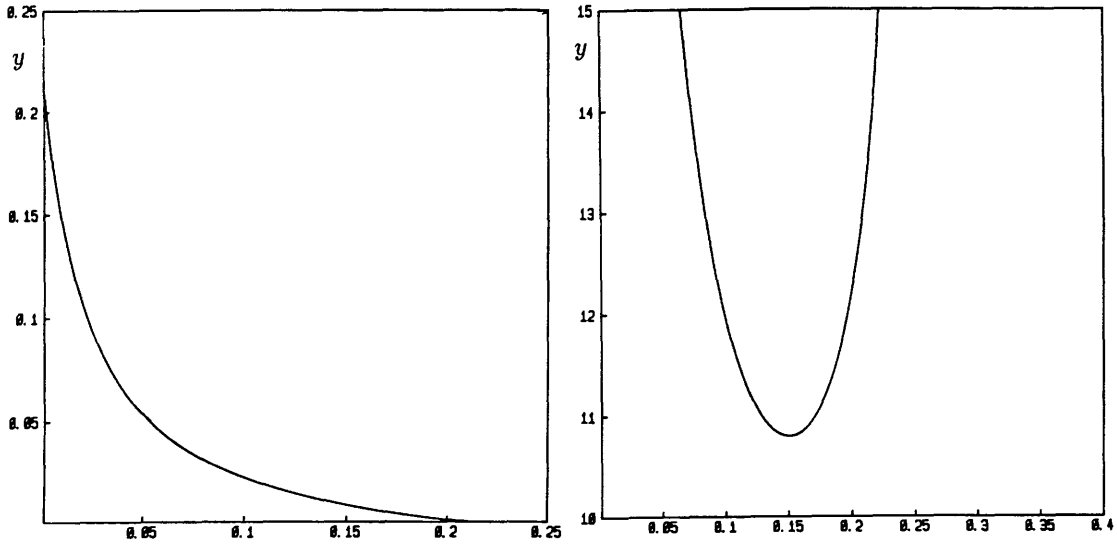

2.2a 2.2b

Figure 2.2

Curves which show the boundary of the allowed regions for $w = 0.1$ in the x, y plane. In 2.2a the allowed region lies below the curve and in 2.2b the allowed region lies within the curve.

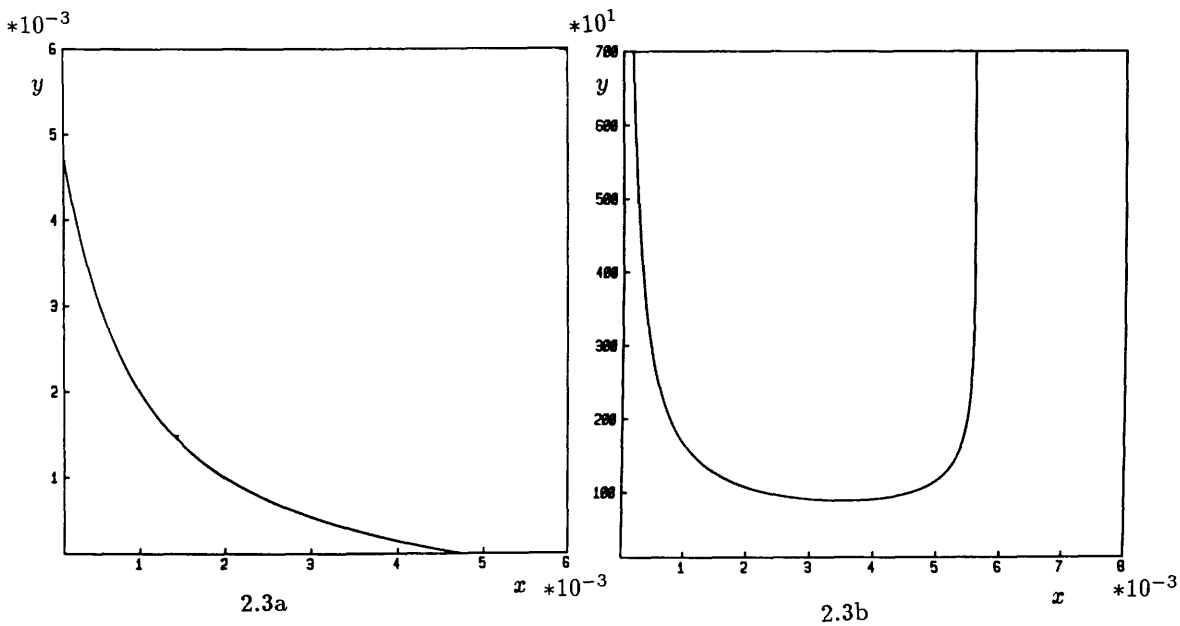

2.3a 2.3b

Figure 2.3

Curves which show the boundary of the allowed regions for $w = 0.2$ in the x, y plane. In 2.3a the allowed region lies below the curve and in 2.3b the allowed region lies within the curve.

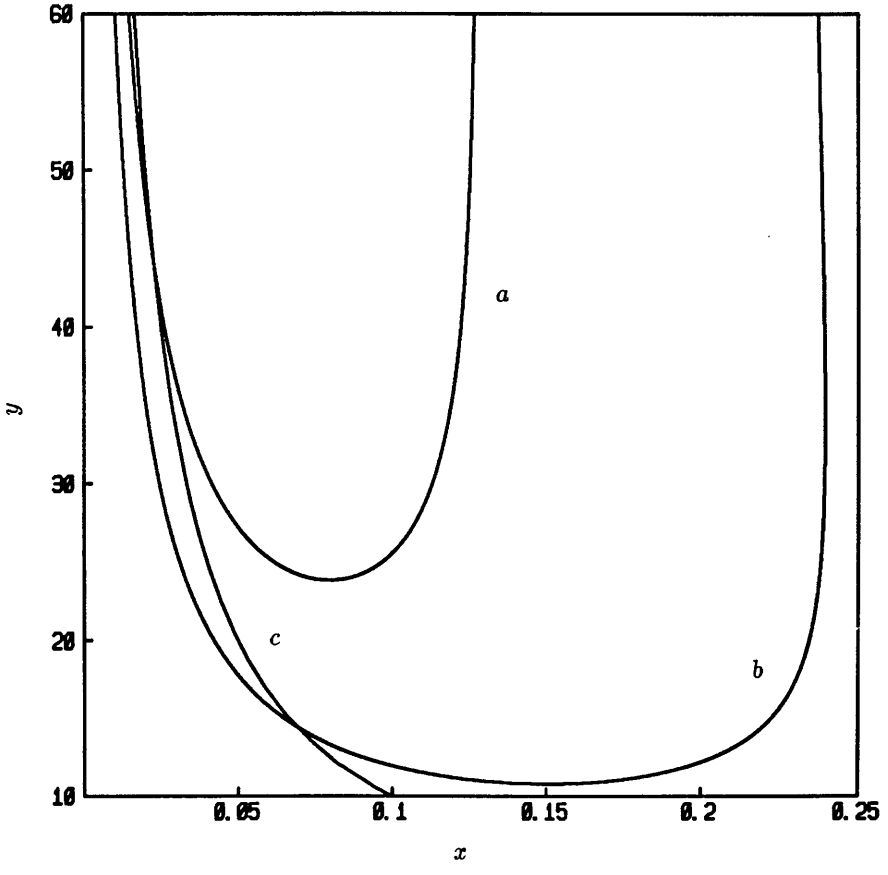

Figure 2.4

Curve a surrounds the allowed region for $w = 0.12$ at large y, curve b the allowed region for $w = 0.1$. The function $y = 1/x$ is shown by c.

Chapter 3

The Electroweak Theory and Baryon Number Non-Conservation

3.1 Introduction

The remainder of this thesis relates to baryon number non-conservation within the electroweak theory. Interest in this aspect of the Standard Model has grown recently, with the realization that it may have an important role in the production of the baryon asymmetry of the Universe (B.A.U.). The theoretical background for the existence of such baryon number violating processes and their connection with topological quantities is the subject of this chapter. The need for a numerical method of testing theoretical predictions of the rate of such transitions is motivated, and we also outline a model recently proposed by Shaposhnikov in which the addition of fermions to the system may actually allow B.A.U. to be created at the time of the $SU(2)$ phase transition.

We begin by briefly reviewing the evidence for the existence of B.A.U., and the conditions which any model seeking to provide a mechanism for its production must fulfil.

3.2 Baryogenesis and Cosmology

Existing experimental evidence indicates that the Universe contains significantly more matter than anti-matter [13]. Cosmic rays, which provide information about our own galaxy, have a measured ratio of antiprotons to protons of about 3.10^{-4}. The actual ratio of antiprotons to protons within the galaxy is thought to be much smaller, the antiprotons which are detected are produced in secondary reactions such as $p + p \rightarrow 3p + \overline{p}$. Taking our galaxy to consist of matter, it seems reasonable to suggest that matter and anti-matter are separated on the galactic scale. However, galaxies predominantly exist in clusters rather than individually and it can be shown that a cluster containing some galaxies composed of matter and some composed of anti-matter would emit large quantities of γ rays as annihilation occurred. The estimated size of such signals is larger than the measured background γ ray flux; so for the Universe to contain equal quantities of matter and anti-matter forces separation to take place at mass scales between 10^{12} and $10^{14} M_{\odot}$ i.e. the mass of a typical cluster. Such a separation must occur at $T > 40$MeV. otherwise, in particular, nucleons and anti-nucleons will continue to annihilate down to nucleonic densities which are lower than those observed today. The cosmological horizon, that is the maximum distance between two points for them to remain causally connected, at $T > 40$ MeV. is too small for separation to occur at such large mass scales. It must be concluded that baryon-antibaryon symmetry is broken in the course of the evolution of the Universe.

The asymmetry can also be expressed as the ratio of the number of baryons to the number of photons.

$$\frac{n_b}{n_\gamma} \approx 10^{-9} \tag{3.1}$$

n_γ, the photon number density is given by the cosmic microwave background. The smallness of this ratio suggests that if there was initially a matter-antimatter asymmetry then only a tiny fraction of the initial baryons escaped annihilation, and survived until present times and temperatures.

The three criteria that must be satisfied if baryogenesis is to occur were

identified by Sakharov in 1967 [14]. The first of these is the existence of a baryon number violating process. The second is that both C and CP must be violated; a state with a baryon number B is odd under both C and CP, so only a state having $B = 0$ can be C and CP invariant. C and CP violation break the symmetry between particles and anti-particles, so that the production rate of baryons may exceed that for anti-baryons. Finally thermal non-equilibrium is needed to prevent the annihilation rate of baryons matching their production rate.

3.3 Instantons and Topology

One very important characteristic of non-Abelian gauge theories is their complex vacuum structure. This can be seen most easily by considering a simple gauge theory in Euclidean space, with a Lagrange density $\mathcal{L} = -1/4 F_{\mu\nu} F_{\mu\nu}$, where $F_{\mu\nu} = F^a_{\mu\nu} T^a$ and T^a are the representation matrices of the gauge group. For the Euclidean action $S = \int d^4x \mathcal{L}$ to remain finite requires that

$$F_{\mu\nu} \to 0 \tag{3.2}$$

$$|x| \to \infty \tag{3.3}$$

Normally we would take this to mean

$$A_\mu \to 0 \tag{3.4}$$

$$|x| \to \infty \tag{3.5}$$

However we may be more general than this. Under a gauge transformation U

$$A_\mu \to U^{-1} A_\mu U + U^{-1} \partial_\mu U \tag{3.6}$$

so that the gauge transformed condition on A_μ becomes

$$A_\mu \to U^{-1} \partial_\mu U \tag{3.7}$$

which of course still ensures $F_{\mu\nu}$ approaches zero at spatial infinity. A gauge field in the form $U^{-1}\partial U$ is known as "pure gauge". The boundary of four dimensional Euclidean space is given by the space S^3, a hypersphere. A gauge transformation $U(x)$ at this boundary is therefore a mapping from S^3 to the space of the particular gauge group determining the theory. Mappings between spaces can be characterised into homotopy classes, each with an associated winding number, or topological charge Q [15]. (This is also called the Pontryagin index.) We shall refer to a gauge transformation which has a zero winding number as *trivial* or *small*, and one with non-zero winding number as *non-trivial* or *large*. $U(1)$ is the simplest theory to consider, in this case the gauge transformations U are mappings from $S^3 \rightarrow S^1$. Every such mapping can be continuously deformed into the trivial mapping, that is from S^3 into a single point; and it becomes meaningless to discuss a winding number for $U(1)$. So only non-Abelian gauge theories have an associated winding number. For example $SU(2)$ has S^3 as the space of its gauge group. Mappings from $S^3 \rightarrow S^3$ certainly have a winding number. This all implies that every finite energy Euclidean configuration has some index Q associated with it, and that it is impossible to make a continuous deformation of the configuration into another with a different winding number Q without violating the finiteness of the action.

It can be shown that [16]

$$Q = \frac{g^2}{16\pi^2} \int d^4x Tr(F_{\mu\nu}\tilde{F}_{\mu\nu}) \tag{3.8}$$

where

$$\tilde{F}_{\mu\nu} = \frac{1}{2}\epsilon_{\mu\nu\rho\lambda}F_{\rho\lambda} \tag{3.9}$$

the dual of $F_{\mu\nu}$. Since Q is a conserved quantity, it seems natural that it should have an associated current. This is the Chern-Simons current:

$$K_\mu = \epsilon_{\mu\nu\rho\lambda}Tr(F_{\nu\lambda}A_\rho + \frac{2ig}{3}A_\nu A_\lambda A_\rho) \tag{3.10}$$

Then

$$Q = \int dt \frac{\partial}{\partial t} N_{cs} \tag{3.11}$$

where

$$N_{cs} = \frac{g^2}{16\pi^2} \int d^3x K_0 \tag{3.12}$$

$$N_{cs} = \frac{g^2}{16\pi^2} \int d^3x \epsilon_{ijk} Tr(F_{ij}A_k + \frac{2ig}{3} A_i A_j A_k) \tag{3.13}$$

N_{cs} is the Chern-Simons number. It can be shown that N_{cs} is gauge invariant under trivial gauge transformations only [17]; if a non-trivial gauge transformation is made then:

$$N_{cs} \rightarrow N_{cs} + n_q \tag{3.14}$$

where n_q is the winding number of the gauge transformation. We may also define a Chern-Simons density:

$$n_{cs} = \frac{g^2}{16\pi^2} \epsilon_{ijk} Tr(F_{ij}A_k + \frac{2ig}{3} A_i A_j A_k) \tag{3.15}$$

Using the positivity condition

$$\int Tr(F_{\mu\nu} \pm \tilde{F}_{\mu\nu})^2 d^4x > 0 \tag{3.16}$$

it follows that

$$\int Tr(F_{\mu\nu}F_{\mu\nu}) d^4x > \left| \int Tr(F_{\mu\nu}\tilde{F}_{\mu\nu}) d^4x \right| = \frac{16\pi^2 Q}{g^2} \tag{3.17}$$

where we have used eq.(3.8). Thus we obtain

$$S_E \geq \frac{8\pi^2 Q}{g^2} \tag{3.18}$$

Thus for any winding number the Euclidean action, S_E, has a definite minimum. In fact this occurs when

$$F_{\mu\nu} = \pm \tilde{F}_{\mu\nu} \tag{3.19}$$

Solutions of (3.19) are known as *instantons*. The instanton is analogous to tunnelling amplitudes in semi-classical quantum mechanics. The amplitude for barrier penetration can be shown to be

$$\int [dq] e^{-S_E} \tag{3.20}$$

where $\int[dq]$ sums over all the paths between the states on either side of the barrier. In the saddle point approximation such an integral is dominated by the minimum of S_E. This allows the instanton to be interpreted as tunnelling between two vacuum states. Since tunnelling is allowed between different vacua it seems reasonable to construct a complete vacuum state as a superposition of the individual vacua. This is the "θ" vacuum.

$$|\theta>=\sum_n e^{-in\theta}|n> \tag{3.21}$$

Here $|n>$ are the individual vacua, each separated by finite energy barriers. This has an obvious analogy with the Bloch vacuum of Solid State Physics, which is constructed from a periodic potential where tunnelling between vacua alters the classical energy level degeneracy.

3.4 Sphalerons

In this section we shall introduce the concept of sphalerons and describe how they may enable the electroweak theory to provide a large rate for the baryon number violating process at high temperatures. We begin by discussing the relationship between instanton type events and baryon number non-conservation.

In Q.E.D. the coupling between the electromagnetic current, j_μ, and the gauge field, A_μ, leads to charge conservation even in the full quantum theory, despite the appearance of the Adler-Bell-Jackiw anomaly [18]. To prevent spoiling the gauge invariance of the Lagrangian the anomaly takes effect on the chiral current, j^5_μ, which is no longer exactly conserved in the limit of massless fermions. In the same way there is an anomaly in the electroweak theory, but now the gauge field couples only to left-handed quarks and lepton doublets. Thus neither the vector nor the axial vector current are exactly conserved; and in particular:

$$\partial^\mu J^B_\mu = N_f \frac{g^2}{16\pi^2} Tr(F_{\mu\nu}\tilde{F}^{\mu\nu}) \tag{3.22}$$

where N_f is the number of families. We have neglected the $U(1)$ part. In

addition,

$$\partial^\mu K_\mu = Tr(F_{\mu\nu}\tilde{F}^{\mu\nu}) \tag{3.23}$$

and so

$$\partial^\mu (J^B_\mu - N_f \frac{g^2}{16\pi^2} K_\mu) = 0 \tag{3.24}$$

$$\tilde{J}^B_\mu = J^B_\mu - N_f \frac{g^2}{16\pi^2} K_\mu \tag{3.25}$$

where $\tilde{J}^B_\mu$ is a conserved quantity. A change in fermion number is related to an event changing the topological number of the system. In other words not only will an instanton move the system into a topologically different vacuum, there is a corresponding change in the baryon number.

$$B(t_2) - B(t_1) = N_f(N_{cs}(t_2) - N_{cs}(t_1)) \tag{3.26}$$

There is a similar anomaly in the leptonic current, which leads to the anomaly free combination of Baryon minus Lepton number, $B - L$. Thus the electroweak theory has two of the three necessary ingredients for baryogenesis; C and CP violation and baryon number changing processes. In 1976 't Hooft [19] showed that the rate of such instanton events was exponentially suppressed as $\exp(-4\pi/\alpha_W)$ which seemed far too small to have any relevance to the baryon asymmetry of the Universe (B.A.U). However 't Hooft's calculation was at zero temperature and in 1985 Kuzmin, Rubakov and Shaposhnikov (KRS) [20] suggested that finite temperatures could allow thermal fluctuations over the barriers between the different topological sectors. Such fluctuations are classical unlike the quantum nature of instanton events; and they argued that therefore the rate of such transitions should be given by a Boltzmann factor:

$$\frac{dN_f}{N_f dt} = TC \exp(-E_{sph}/T) \tag{3.27}$$

where C is some function of temperature. E_{sph} is the height of the potential barrier separating the different topological vacua, and is also the energy of the "sphaleron" which is the name given to the static unstable solution to the

classical equations of motion, sitting at the top of the potential barrier. The situation is illustrated by figure 3.1 below:

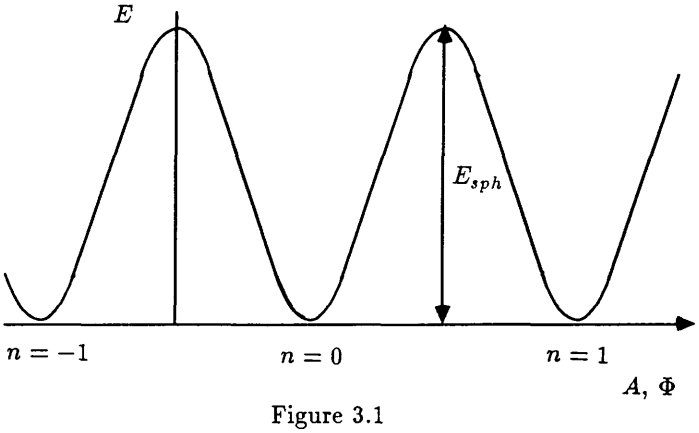

Figure 3.1

Schematic dependence of the static energy of the gauge-Higgs system upon the configuration $A(x)$, $\Phi(x)$. The minima represent vacuum states with different topological numbers, n.

It is helpful to consider the selection rules for a sphaleron process. For each generation 3 quarks and 1 lepton will be produced by the decay of a sphaleron, ensuring that $B - L$ is conserved.

This solution to the classical equations for a gauge-Higgs system was first found numerically by Dashen, Hasslacher and Neveu [21]. The solution has the form:

$$\begin{aligned} A_i &= i\left(\epsilon_{ijk}\frac{x_j\tau_k}{r^2}\right) f(\xi) \\ \Phi &= \frac{v(T)}{\sqrt{2}}\left(i\frac{\tau_a x_a}{r}\right)\begin{pmatrix}0\\1\end{pmatrix} h(\xi) \end{aligned} \tag{3.28}$$

where $\xi = g_W(T)v(T)r$ with $r^2 = x^2$ and $g_W(T)$ and $v(T)$ being the temperature dependent expressions for the gauge coupling constant and the vacuum expectation value of the Higgs field respectively. $h(\xi)$ and $f(\xi)$ are determined by substituting in the above solution into the Hamiltonian, and demanding that it be minimized. Then

$$E_{sph} = \left(\frac{2M_W(T)}{\alpha_W(T)}\right) B\left(\frac{\lambda(T)}{\alpha_W(T)}\right) \tag{3.29}$$

$M_W(T)$ and $\lambda(T)$ are the temperature dependent W mass and the Higgs self

coupling coefficient. $B(\lambda/\alpha_W)$ varies between 1.5 and 2.7 as λ varies between 0 and ∞, so that E_{sph} lies between 8 and 14 Tev. In addition, Klinkhamer and Manton [22] showed that the radius of the sphaleron is $\sim 1/2M_W$ and that it has a topological number of 1/2. In the one-loop approximation the temperature dependence of M_W for $T < T_c$ is as follows:

$$M_W(T) = M_W(0)\left(1 - \frac{T^2}{T_c^2}\right)^{1/2} \tag{3.30}$$

so that $M_W(T)$ goes to zero as T approaches the critical temperature T_c, and the transition rate given by eq.(3.27) consequently becomes very large. However, above T_c the idea of the sphaleron sitting on the minimum energy path for a topological transition is no longer correct, and semiclassical methods become invalid. The critical temperature, T_c, is thought to be about 300 GeV.

The most immediate consequence of the work by KRS was the prediction that the B.A.U. produced by any Grand Unified Theory (G.U.T.) which preserved Baryon minus Lepton number would be washed out during the electroweak phase transition if the transition rate above the phase transition is unsuppressed. G.U.T.'s had been able to provide a reasonable mechanism for baryon asymmetry production as well as unifying $SU(3)$, $SU(2)$ and $U(1)$. The anomalous electroweak processes themselves preserve B-L. The solution to the rate equation shows that if $dN_f/N_f dt = \beta T$ then at the time of the phase transition [20]

$$B(T_c) = \frac{1}{2}(B_{in} - L_{in}) + \frac{1}{2}(B_{in} + L_{in})e^{-A} \tag{3.31}$$

with

$$A \sim \beta \times 10^{15} \tag{3.32}$$

so if the initial baryon and lepton numbers are equal the baryon number at the time of the $SU(2)$ phase transition would vanish.

Since the initial work of KRS, significant effort has been made to provide more rigorous calculations of the semiclassical transition rate below T_c, in particular to determine C, and there has been discussion about whether or not the rate is suppressed above T_c.

Arnold and McLerran [23] calculated the prefactors multiplying the Boltzmann factor for $T < T_c$. They worked with $\lambda \sim g^2$ and calculated the path integral for the rate of baryon number violation using a Gaussian expansion about a static sphaleron background. In addition, there are six zero modes corresponding to transformation symmetries of the sphaleron which have to be calculated separately from the Gaussian integrals. They found that the rate of sphaleron transitions per unit time and per unit volume is

$$\Gamma = c(\alpha_W T)^4 \left(\frac{E_{sph}}{T}\right)^7 \exp\left(-\frac{E_{sph}}{T}\right) \tag{3.33}$$

for $2M_W(T)/\alpha_W(T) \gg T \gg 2M_W(T)$. c is a constant independent of temperature. Their results have been confirmed elsewhere [24]. Using this formula they showed that sphaleron transitions are sufficient to dissipate any $(B + L)$ excess which may have been created at some point in the early Universe. They worked only in the region where the equation (3.33) is valid, and used a chemical potential to describe the baryon excess.

Above T_c, where semiclassical calculations break down, scaling arguments show that

$$\Gamma = \kappa(\alpha_W T)^4 \tag{3.34}$$

with κ an unknown coefficient. Most authors assume that κ is of the order 1; that the suppression is algebraic rather than exponential. However, Cornwall [25] argues that not only does the potential barrier height continue to rise linearly with T above T_c, but that it always exceeds T by a substantial factor. This is because the W boson acquires a magnetic mass $\sim g^2 T$; making the exponent of the Boltzmann factor very large. In fact, Cornwall argues that this number is between 13 and 40; and that it is independent of both T and g. In other words κ is very small because it is determined by this Boltzmann factor.

The need to resolve these arguments is clear; if these sphaleron processes are unsuppressed, not only will they destroy theories in which G.U.T. models create B.A.U, but they may provide some part of a mechanism which generates the baryon asymmetry within the Standard Model.

3.5 Shaposhnikov's Model

This model [26] [27] describes a scenario in which the B.A.U. is produced entirely within the Standard Model, specificially through the electroweak interaction. Instead of G.U.T.'s generating B.A.U. at $T > 10^{12} - 10^{15}$ GeV, the relevant temperatures for baryogenesis in this scheme are only $\sim 10^2$ GeV.

The starting point is the observation that in the presence of a non-zero fermionic density a high temperature gauge theory has its effective action modified by a term $-\mu_B N_{cs}$; μ_B being the chemical potential [28]. Depending on the shape of the effective potential it can become energetically favourable to "trade" baryons for a change in N_{cs} number. It is not possible to calculate the shape of this potential above the phase transition because of infrared divergences which appear when perturbation theory is used. Possible effective potentials for the Chern-Simons density, n_{cs}, and the effect of a non-zero chemical potential are

illustrated below:

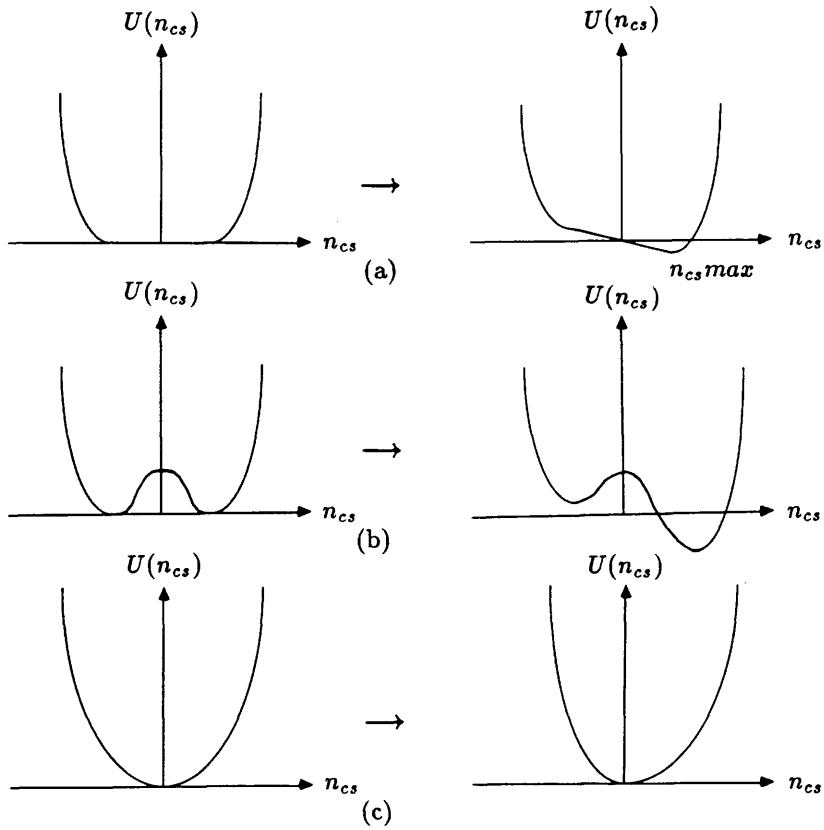

Figure 3.2

Possible potentials $U(n_{cs})$ for the Chern-Simons density. The effect of a non-zero chemical potential μ_B is shown.

Figure 3.2a shows the situation where the potential starts with a non-trivial degeneracy, 3.2b the case where there is finite degeneracy corresponding to domains of space with different signs of Chern-Simons density, and 3.2c illustrates the case where the potential has trivial degeneracy. Under appropriate conditions the potentials 3.2a and 3.2b allow the system to attain a net non-zero Chern-Simons number, and we see intuitively that this will take place more readily for 3.2a than 3.2b where we need either some kind of tunnelling process or a mechanism to eat up the metastable state by the stable state.

Shaposhnikov emphasises that this movement in N_{cs} is "orthogonal" to that

associated with sphaleron transitions, this is schematically illustrated below:

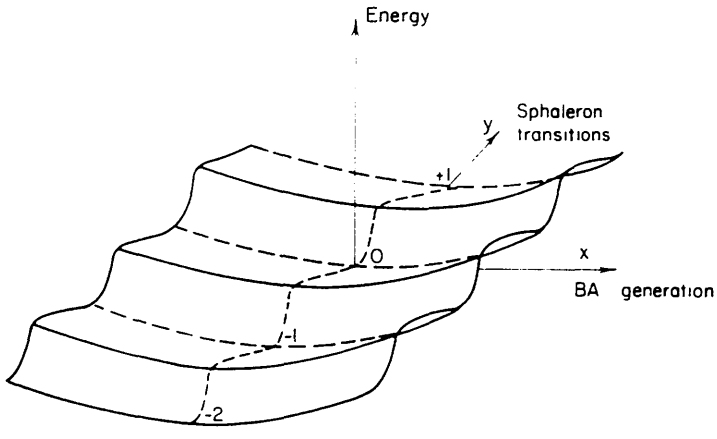

Figure 3.3

Schematic dependence of the energy on the configuration of the gauge and Higgs fields. Periodicity in the direction y corresponds to the large gauge transformations. (From M.Shaposhnikov, Nucl. Phys. B299 (1988) 797.)

The idea is that there is no energy barrier to cross in the x axis and so the system moves through classes of gauge inequivalent configurations [29].

As the electroweak phase transition takes place any non-trivially shaped $U(n_{cs})$ becomes unstable as the gauge bosons acquire mass, and the N_{cs} is re-released as fermions. The total number of baryons produced will be $N_f Tr\rho_0 Q$, where ρ_0 is the equilibrium density matrix describing the state just above the phase transition and Q is the difference of Chern-Simons numbers between the symmetric phase and the broken symmetry phase:

$$Q = \frac{g^2}{16\pi^2}\int_{t_c}^{\infty} d^4x Tr(F_{\mu\nu}\tilde{F}_{\mu\nu}) = N_{cs}(T_c) - N_{cs}(0) \tag{3.35}$$

N_{cs} at the time of the phase transition depends both on the shape of the potential and on δ_{ms}, the microscopic asymmetry of the Baryon number non-conserving processes which measures the extent of CP violation.

$$\delta_{ms} = \frac{\Gamma(in \to out) - \Gamma(\overline{in} \to \overline{out})}{\Gamma(in \to out) + \Gamma(\overline{in} \to \overline{out})} \tag{3.36}$$

Γ are the decay widths, and in and out represent the initial and final states.

The procedure for calculating δ_{ms} is not well understood and remains an area of contention [30]. However, it has been suggested that it might arise from a 14-loop Feynman diagram. The high order of the diagram is because the amplitude of CP violation in the B non-conserving processes is proportional to the imaginary part of the quark-Higgs Yukawa coupling. The sign of δ_{ms} is not even known; but it arises from the phase δ of the Kobayashi-Maskawa matrix. Therefore, the model actually connects the sign of B.A.U., that is whether there are more baryons than anti-baryons or vice versa, with the sign of CP violation in K^0 physics. Current estimates, based on naïve loop counting put δ_{ms} between 10^{-16} and 10^{-20}, which rules out the possibility of potentials like those shown in figures 3.2b and 3.2c enabling baryogenesis in the Standard Model. (It has been estimated [27] that δ_{ms} for these potentials would have to be larger than 10^{-4} and 10^{-6} respectively). The existence of extra Higgs could increase δ_{ms} and make such potentials workable; with an additional Higgs doublet CP violation arises at the two loop level [26].

If the potential has non-trivial degeneracy as in 3.2a the condition for $n_{cs}max$ to be attained becomes [26]

$$4\left(\frac{M_0}{T_C}4\pi{\alpha_W}^2\delta_{ms}\right)^{\frac{1}{2}} \gg 1 \tag{3.37}$$

Here $M_0 = M_{pl}/1.66N_{eff}^{1/2}$ where M_{pl} is the Planck mass and N_{eff} the effective number of massless degrees of freedom, usually about 10^2 in the Standard Model. It seems possible that this condition is satisfied given the uncertainty in δ_{ms}. The number of baryons actually produced will be proportional to $n_{cs}max$, another quantity whose value is uncertain. Dimensional arguments give

$$n_{cs}max \simeq (\alpha_W T)^3 \tag{3.38}$$

The asymmetry must survive from the time of the phase transition until the present time. If the B non-conserving processes are in thermal equilibrium during the phase transition then all of the asymmetry will be washed away. This means that the phase transition should be first order, and such a constraint

forces an upper bound on the Higgs particle [31]

$$M_H < 45GeV \tag{3.39}$$

which in turn forces the rather unfortunate upper bound on the top quark mass:

$$M_t < 80GeV \tag{3.40}$$

This bound on the top quark mass arises from demanding that the minimum of the one loop effective potential $V(\Phi)$ at $\Phi^2 = v^2$ be an absolute rather than just a local minimum [32]. Recent experiments indicate that $M_H > 41.6$ GeV [33] and $M_t > 77$ GeV [34], and it appears that Shaposhnikov's model with one Higgs doublet is almost ruled out. However the situation with two Higgs doublets changes the bounds on the Higgs and top quark masses and so there is still the possibilty of baryogenesis at the electroweak scale [35]. Turok [36] is also studying a model with an extended Higgs sector.

If the Higgs is too light then the system supercools [37]. Large entropy generation is associated with a supercooled phase transition and this itself restricts the model. The baryon to entropy ratio $n_B/S \sim 10^{-10}$, so if the Universe supercools a correspondingly larger number of baryons must be produced at the phase transition to preserve the experimentally observed ratio. The lower limit becomes

$$M_H > M_{Coleman-Weinberg} \sim 10GeV \tag{3.41}$$

3.6 Numerical Simulations

The model described above relies heavily on several key assumptions. It is important that their validity, or otherwise, be tested; both for the model itself and more generally so that the role of the electroweak theory in relation to baryogenesis can be better understood. The problems raised are by their very nature non-perturbative; perturbation theory at finite temperature is well known to amass infrared divergences [38], fortunately lattice gauge theories provide a useful method of simulating quantum field theories non-perturbatively [39].

One of the first numerical investigations was made by Ambjørn, Laursen and Shaposhnikov [40]. They exploited the fact that at high temperatures a four dimensional field theory becomes effectively three dimensional and studied a three dimensional $SU(2)$ gauge-Higgs system. Configurations at $T > T_c$ were generated by a Monte Carlo routine, then these configurations were taken through the phase transition into the cold, broken phase and the change in the topological charge, $Q = N_{cs}(T_c) - N_{cs}(T_f)$, was measured, T_f is the final temperature of the system. The purpose of this was to address two important questions:

- Does the potential $U(n_{cs})$ have non-trivial degeneracy?
- If so, can baryons be produced from configurations of non-trivial N_{cs} during the phase transition?

If the potential really has non-trivial degeneracy then the distribution of Q should reflect this by being non-Gaussian, that is a broader and flatter distribution might be expected. In fact, the results were not clear cut, they suggested that indeed the potential could be non-trivially degenerate, but this was by no means certain. The measurement of non-trivial Q, eg ~ 2 for larger lattices suggests that the change in baryon number can be significant.

The remaining work in this thesis is an attempt to build upon and extend this simulation. The main difference is that real time, as opposed to fictitious Monte Carlo time, is incorporated and the system allowed to evolve under the classical equations of motion. There is no high temperature approximation; but the lattice remains three dimensional and represents the spatial fields at a given moment in time. This allows for real time studies of sphaleron transitions and the addition of the driving term $-\mu_B N_{cs}$ to the system. We shall continue to study a gauge-Higgs system; there is no need to add fermions directly onto the lattice because their contribution to the scenario is modelled by the $\mu_B N_{cs}$ term itself. The $U(1)$ part of the electroweak theory has no influence on the baryon number non-conservation and is negelected to leave the $SU(2)$ part only as in [40].

The details of the lattice program, including the treatment of the momenta

variables and associated Gauss constraint are described in Chapter 4. Chapter 5 discusses different ways of measuring Q and the related problems and difficulties. Chapter 6 describes the runs made using $\mu_B = 0$, i.e. with no driving term. This work was done in order to determine the rate of sphaleron transitions. Analysis of the resultant data is given in detail. The problems associated with non-zero μ_B are discussed in Chapter 7 and some preliminary results are described. Overall conclusions and possible areas of future research follow Chapter 7.

Chapter 4

Numerical Description

4.1 Introduction

In this chapter we discuss in detail the formulation of our particular lattice system. A short review of lattice gauge theory and Monte Carlo methods is given in the remainder of this section. Section 4.2 deals with the motivation for using classical statistics, and contains a discussion about recent work closely related to that undertaken in this thesis. In section 4.3 we proceed with a full description of our rather unconventional approach, which is necessary in order to obtain real time evolution. Section 4.4 describes how a suitable starting configuration is obtained and appropriate checks which are made to ensure that the program is performing as expected. Section 4.5 considers the implementation of the real time classical evolution equations. It must be stressed that more usually the evolution of the lattice system occurs within fictitious "computer" time, because the final state is all that is generally required; we are of course not so much interested in the final state of the system as in how it gets there!

4.1.1 Lattice Gauge Theories

Perturbative calculations of quantum field theories are plagued by singularities, which are normally removed by regularization and then renormalization. If we want to study a field theory beyond the range of perturbation theory then we again need a technique of regularization and ultimately renormalization. In 1974 Wilson [41] introduced the powerful numerical approach of lattice gauge

theory whereby space and time are discretized. Particles and gauge fields are defined only at the sites and along the links of the lattice. If the lattice spacing is a then all wavelengths shorter than $2a$ are meaningless and ultraviolet divergences are automatically removed. The continuum limit is obtained by taking $a \rightarrow 0$ and using renormalization group theory to ensure that observable quantities approach their physical values. The lattice system has a finite number of degrees of freedom, as we shall see this provides a useful check on the numerical simulations. A further advantage is that a field theory on a lattice has a close analogy with statistical mechanics; for example the strong coupling expansion is equivalent to the high temperature expansion of statistical mechanics. The gauge field is represented by the link variable

$$U_{x,\hat{i}} = \exp(-iagT^a A_i^a(x)) \tag{4.1}$$

where T^a are the representation matrices of the gauge group. A "plaquette" is the product of four link variables about a square on the lattice. Since

$$U_{x,\hat{i}} \rightarrow V_x U_{x,\hat{i}} V^\dagger_{x+\hat{i}} \tag{4.2}$$

under a gauge transformation then the trace of the plaquette will clearly be gauge invariant. The pure gauge part of the (Euclidean) action can be built up from these plaquettes allowing local gauge invariance to be preserved on the lattice. The Wilson action is

$$S = \sum_{\square} \beta(1 - \frac{1}{n} ReTrU_{\square}) \tag{4.3}$$

where $U_{\square}$ denotes a plaquette and $\sum_{\square}$ the sum of all plaquettes on the lattice. The factor n is the dimension of the group matrices; for example if we have an $SU(2)$ gauge theory then $n = 2$. β is simply a normalization factor whose value is obtained from the continuum limit. This limit is obtained by substituting eq.(4.1) into eq.(4.3) and taking the leading order terms in a. This gives

$$U_{\square} = \exp(-ia^2 g F^a_{\mu\nu} T^a) + \mathcal{O}(a^3) \tag{4.4}$$

where

$$F_{\mu\nu} = \partial_\mu A_\nu - \partial_\nu A_\mu - ig[A_\mu, A_\nu] \tag{4.5}$$

This leads to

$$S = \frac{\beta g^2}{2n} \int \frac{1}{2} Tr(F_{\mu\nu} F_{\mu\nu}) d^4x + \mathcal{O}(a^6) \tag{4.6}$$

Thus if we identify $\beta = 2n/g^2$ we obtain the usual continuum gauge action.

Often of course, we need other types of fields than just the gauge fields on the lattice. This chapter discusses the formalism of a gauge-Higgs system; so we must understand fully how a scalar field is treated on the lattice [42]. Scalar fields sit at the lattice sites rather than along the links, so terms like Φ_x^2 are straightforward, Φ_x denotes the scalar field associated with the site x. A derivative term such as $\sum_x (\partial_i \Phi_x)^2$ is as we would expect from a naïve approach to discretization of space.

$$\begin{aligned} \sum_x (\partial_i \Phi_x)^2 &= \sum_x \frac{(\Phi_{x+\hat{i}} - \Phi_x)^\dagger (\Phi_{x+\hat{i}} - \Phi_x)}{a^2} \\ &= \frac{1}{a^2} \sum_x \left(2\Phi_x^2 - \Phi_x^\dagger \Phi_{x+\hat{i}} - \Phi_{x+\hat{i}}^\dagger \Phi_x \right) \end{aligned} \tag{4.7}$$

To make the derivative term covariant requires the insertion of a gauge field along the link connecting adjacent Φ fields:

$$\sum_x (D_i \Phi_x)^2 = \frac{1}{a^2} \sum_x \left(2\Phi_x^2 - \Phi_x^\dagger U_{x,x+\hat{i}} \Phi_{x+\hat{i}} - \Phi_{x+\hat{i}}^\dagger U_{x+\hat{i},x} \Phi_x \right) \tag{4.8}$$

This gives the correct continuum limit as $a \to 0$. The time components are treated using the same approach.

Having identified a suitable method of discretizing the terms in a gauge-Higgs action, the next subsection will outline Monte Carlo methods which are widely used to numerically obtain configurations at thermal equilibrium.

4.1.2 Monte Carlo Methods

Suppose we need to calculate the expectation value of some operator O within a system. C represents a configuration of the variables in the system. Then

$$< O >= \frac{1}{Z} \int (dC) O(C) e^{-S(C)} \tag{4.9}$$

Z is the partition function:

$$Z = \int (dC) e^{-S(C)} \tag{4.10}$$

The summation over all possible configurations is generally impractical, even on a lattice system the number of terms in the integral becomes enormous very quickly with lattice size. Monte Carlo methods were devised well before the advent of lattice gauge theories to overcome these problems and evaluate the integral numerically for statistical mechanical systems. They generate configurations C such that the probability of producing a particular configuration is

$$P(C) = \frac{1}{Z} e^{-S(C)} \tag{4.11}$$

Then

$$< O >= \frac{1}{N} \sum_{n=1}^{N} O_n(C) + \mathcal{O}(\frac{1}{\sqrt{N}}) \tag{4.12}$$

where N is the total number of configurations and $O_n(C)$ is the value of the operator, O, on the n^{th} configuration generated by the Monte Carlo algorithm. Suppose we let $W(C', C)$ be the transition probability for one step of the updating algorithm to change a configuration C to C'. Then

$$P(C) = \sum_{C'} W(C', C) P(C') \tag{4.13}$$

If the algorithm attains the objective that $P(C) = 1/Z \exp(-S(C))$ then at equilibrium we have

$$e^{-S(C)} = \sum_{C'} W(C', C) e^{-S(C')} \tag{4.14}$$

which is a condition on W at every stage of the updating. It can be shown that this condition is sufficient to ensure that any algorithm which satisfies it and which explores the phase space fully will eventually generate configurations with the desired weighting (4.11). In practise, the majority of Monte Carlo algorithms are based on the detailed balance condition:

$$W(C', C) e^{-S(C)} = W(C, C') e^{-S(C')} \tag{4.15}$$

There is, for example the heat bath algorithm in which each variable in turn is replaced with a value selected randomly with a weighting given by the Boltzmann factor of the current action. That is $W(C, C') \propto \exp(-S(C))$, and so is independent of C', thus satisfying (4.15) automatically.

We use the so-called Metropolis algorithm in our code because of its simplicity of application. A test variable V' is selected to replace the existing variable V. The probability of choosing V' to replace V must be identical to the probability of choosing V to replace V'. If the change in the action, $\triangle S$, is negative, i.e. if the new action is less than the existing action, then V' is accepted. If $\triangle S$ is positive a random number between 0 and 1 is picked, if this number is less than $\exp(-\triangle S)$ then the change is still accepted.

In practice, we have some parameter or scale which determines how close the new test variable is to the current value, i.e. how fast the phase space is explored. It is convenient to adjust this parameter to attain an acceptance rate of about 50% for the new variables. On the lattice we must "hit" each site or link sequentially, we cannot calculate $\triangle S$ if two things are being changed simultaneously. It becomes advantageous in terms of computer time to hit each variable a number of times before moving onto the next site or link. The optimum number of hits is best determined experimentally. As the number of hits increases the Metropolis algorithm approaches the heat bath.

4.2 Motivation for a Classical Description of the System

In this section we present the arguments which motivate the use of classical statistics on our lattice system. Since the overall objective of the simulations is to model sphaleron processes it must first be shown that a sphaleron can be described classically. This section finishes with a discussion of how such a classical approach allows an identification of the temperature of the system, T, with the inverse of the lattice spacing a^{-1}.

We consider the elementary excitations which combine coherently to form

the sphaleron in the broken symmetry phase. These have mass $\sim M_W$ and momentum of order $\sim 1/r_{sph}$, where r_{sph} is the size of the sphaleron which in this phase is about M_W^{-1}. That the typical momentum is the inverse of the size of the sphaleron arises from considering Fourier components of an extended object. Since the energy of the sphaleron $E_{sph} \sim M_W/\alpha_W$ we see that about $1/\alpha_W$ excitations are needed to form the sphaleron. Defining E_{ex} to be the energy of such an individual excitation

$$E_{ex} = \sqrt{\left(\frac{1}{r_{sph}^2} + M_W^2\right)} \simeq \sqrt{2} M_W \tag{4.16}$$

In the region for which the semiclassical rate formula eq.(3.33) is valid $T \gg M_W$, thus in this region $E_{ex} \ll T$. This means that classical statistics are enough to describe the formation of the sphaleron. Above the phase transition the sphaleron-like configurations are expected to have energy $\propto T$ and spatial extension of order $(\alpha_W T)^{-1}$; hence the characteristic momentum of the fluctuations forming the sphaleron, $\alpha_W T$, is again much less than T, and we see that classical statistics still suffice. A more intuitive picture is of the sphaleron as a large object in space-time which may be smeared out or blurred by quantum effects; but because the spatial size of such quantum effects in the hot plasma is of order T^{-1} compared to the sphaleron size $\sim (\alpha_W T)^{-1}$, we should be able to neglect the quantum "blurring" without drastically altering the behaviour of the sphaleron.

The spatial discretization of a lattice provides a natural cut-off to regularize the Rayleigh-Jeans divergence of a classical system. In the continuum, quantum effects remove the divergence and it can be shown that the maximum wavelength, λ_{max}, of the spectrum of a blackbody depends on its temperature, T through:

$$\lambda_{max} \propto \frac{1}{T} \tag{4.17}$$

This suggests that on the lattice a can be identified with $1/T$. From the discussion above we see then that quantum effects have a spatial size of about one lattice spacing; so to give a sensible description of sphaleron processes on

the lattice, we must ensure that the sphaleron is large compared to the lattice spacing. In what follows we will need to use $aT \sim 1$. In fact, we may try and justify this by taking a free bosonic system and calculating the energy in the continuum limit and comparing it with the energy predicted by the classical equipartition theorem. We have

$$\frac{V}{(2\pi)^3}\int d^3k|k|\frac{1}{\exp(E/T)-1} = \frac{V}{a^3}T \tag{4.18}$$

then

$$\frac{V}{(2\pi)^3}4\pi\int d|k|\frac{|k|^3}{\exp(|k|/T)-1} = \frac{V}{a^3}T \tag{4.19}$$

Performing the integral yields:

$$\frac{1}{2\pi^2}T^4\Gamma(4)\zeta(4) = \frac{T}{a^3} \tag{4.20}$$

where ζ is Riemann's ζ function. Thus

$$(aT)^3 = \frac{30}{\pi^2}, \qquad aT = 1.4 \tag{4.21}$$

We must be aware that if, for example, we chose a fermionic system with different statistics then the ratio would change, but we see that we are well within a factor of 2 accuracy.

This suggests the possibility of observing topological transitions directly be performing microcanonical simulations of classical statistics of gauge theories on a computer. The first lattice studies of topological transitions in real time and using classical statistics were carried out in two dimensions. In [43] the process of kink-antikink pair creation in $\lambda\phi^4$ theory was studied, and in [44] sphaleron transitions in the broken symmetry phase of a $U(1)$ Abelian Higgs model were investigated by Grigoriev, Rubakov and Shaposhnikov (GRS). The numerical results of GRS are in very close agreement with the analytic predictions of the sphaleron transition rate for this model [45]. The work of the remainder of this thesis is based on an almost identical lattice formalism as for [44]; except that we will use $3+1$ dimensions, and use a non-Abelian theory.

4.3 The Lattice System

Given knowledge of the equations of motion, a classical system can be completely described by its coordinates and momenta at any particular time. In the same way we discretize space but keep time continuous so that the 3-dimensional spatial lattice describes both the fields and their momenta; to which the equations of motion can be applied. In this section we define many of the notations to be used and derive the discretized form of the equations of motion. The system is shown to be constrained by the particular gauge choice $A_0 = 0$, the temporal gauge, and finally the Hamiltonian, H, of the system is constructed. Since the classical probability of a configuration is given by the Gibbs canonical distribution $\exp(-H/T)$, H is needed for the Metropolis algorithm which is used to generate suitable starting configurations. We will denote the spatial size of the lattice by N.

In what follows we define the Higgs field associated with each site on the lattice as:

$$\Phi = \begin{pmatrix} \phi_1 + i\phi_2 \\ \phi_3 + i\phi_4 \end{pmatrix} = \begin{pmatrix} \Phi_1 \\ \Phi_2 \end{pmatrix} \tag{4.22}$$

This compares with the alternative description used in [40]:

$$\Phi = \begin{pmatrix} \Phi_1^* & \Phi_2^* \\ -\Phi_2 & \Phi_1 \end{pmatrix} = R.V \quad R \in R_+ \quad V \in SU(2) \tag{4.23}$$

Explicitly they have the following connection

$$\begin{aligned} \phi_1 &= \ \ RV_4 \\ \phi_2 &= -RV_3 \\ \phi_3 &= \ \ RV_2 \\ \phi_4 &= -RV_1 \end{aligned} \tag{4.24}$$

The components of V have been defined by

$$V \equiv V_4 + i\tau_a V_a \tag{4.25}$$

so that $V_1^2 + V_2^2 + V_3^2 + V_4^2 = 1$. We use this form of decomposition of the $SU(2)$ matrices throughout. In the continuum the Lagrangian of the $SU(2)$-Higgs

theory is

$$\mathcal{L} = -\frac{1}{4}F_{a\mu\nu}F^{a\mu\nu} + |D_\mu\Phi|^2 - M^2|\Phi|^2 - \lambda|\Phi|^4 \tag{4.26}$$

The equations of motion can be obtained from $\mathcal{L}$ by the variational principle. To find the discrete form of such equations the lattice version of the action is first constructed. Then the equations of motion are derived directly from this lattice action. The advantage of such an approach is that we automatically keep all the internal symmetries of the theory, in particular gauge invariance, in the time evolution; provided of course that the discretized action respects them. Instead of the standard Euclidean version we use the Minkowski version, with metric (+ - - -); we want real time simulations. The size of the time-like link is $a\triangle t$, the size of the space-like link is a. Then using $S = \int d^4x\mathcal{L}(x)$ and replacing the integral with a sum over all sites x and d^4x by a^4, we find the lattice version of the action is:

$$\begin{aligned} S_L =& \beta_G \left\{ \frac{1}{\triangle t^2} \sum_{\Box^0} \left(1 - \frac{1}{2} Tr U_{\Box^0}\right) - \sum_{\Box} \left(1 - \frac{1}{2} Tr U_{\Box}\right) \right\} \\ &+ \frac{\beta_H}{2} \left\{ \frac{1}{\triangle t^2} \sum_x \left(2\Phi_x^\dagger \Phi_x - \Phi_x^\dagger U_{x,\hat{0}} \Phi_{x+\hat{0}} - \Phi_{x+\hat{0}}^\dagger U_{x,\hat{0}}^\dagger \Phi_x\right) \right. \\ &\qquad \left. - \sum_x \left(6\Phi_x^\dagger \Phi_x - \sum_{\hat{i}} \left(\Phi_x^\dagger U_{x,\hat{i}} \Phi_{x+\hat{i}} + \Phi_{x+\hat{i}}^\dagger U_{x,\hat{i}}^\dagger \Phi_x\right)\right) \right\} \\ &- \beta_R \sum_x (\Phi_x^2 - v^2)^2 \end{aligned} \tag{4.27}$$

where v is the lattice vacuum expectation value of the Higgs field, $\Box^0$ denotes the time-like plaquettes and $\Box$ denotes the space-like plaquettes. $\hat{i}$ and $\hat{0}$ denote spatial and time-like directions respectively. Throughout we use periodic boundary conditions on the lattice. β_G is the lattice gauge coupling constant, β_H and β_R are the lattice Higgs and radial Higgs coupling constants respectively. In future we will drop the subscript on S_L and use S to mean the lattice action. The couplings β_G, β_H and β_R have the following connection with the

continuum variables M, λ and g:

$$\begin{aligned} M^2 &= \frac{2(1-2\beta_R-3\beta_H)}{\beta_H a^2} \\ \lambda &= \frac{4\beta_R}{\beta_H^2} \\ g^2 &= \frac{4}{\beta_G} \end{aligned} \tag{4.28}$$

and the W and Higgs masses are given by

$$M_W^2 = \frac{\beta_H(2\beta_R+3\beta_H-1)}{2\beta_G\beta_R a^2}, \qquad M_H^2 = \frac{4(2\beta_R+3\beta_H-1)}{\beta_H a^2} \tag{4.29}$$

The lattice vacuum expectation value of the Higgs field is given by

$$v^2 = 1 + \frac{(3\beta_H-1)}{2\beta_R} \tag{4.30}$$

It should be noted that the lattice Higgs field has been rescaled to be $a\sqrt{(2/\beta_H)}$ of the continuum Higgs field. The connections are only at tree-level; and are chosen in this particular form so that the final 3-dimensional Hamiltonian that we shall actually put onto the lattice can be rewritten in terms of the "hopping" parameter, in the standard way [46].

The gauge choice $A_0 = 0$ corresponding to $U_{x,\hat{0}} = 1$ on the lattice removes the time-like links as variables, and (4.27) describes a set of gauge-Higgs systems at different time-slices. It is appropriate to introduce the momenta fields E and P here:

$$\begin{aligned} U_{x+\hat{o},\hat{i}} &\equiv \triangle t E(x,\hat{i}) U_{x,\hat{i}} \\ P_x &\equiv (\Phi_{x+\hat{o}} - \Phi_x)/\triangle t \end{aligned} \tag{4.31}$$

The product $\triangle t E(x,\hat{i})$ is an element of $SU(2)$ which will be described in terms of components

$$E = E_4 + i\tau^a E^a \tag{4.32}$$

while the P fields are complex doublets:

$$P_x = \begin{pmatrix} p_1 + ip_2 \\ p_3 + ip_4 \end{pmatrix} \tag{4.33}$$

If the E and U fields of eq.(4.31) are expanded in terms of a and Δt it can be seen that the continuum electric field F_{0i}, which we will denote $\mathcal{E}_i$, is identified with $E_i^a \tau_i^a$ [1].

It should be noted that the gauge fixing $A_0 = 0$ excludes time dependent gauge transformations on the lattice; this can be seen by studying eq.(4.31) under a gauge transformation V:

$$U_{x+\hat{0},\hat{i}} \rightarrow V_{x+\hat{0}} U_{x+\hat{0},\hat{i}} V^{\dagger}_{x+\hat{0}+\hat{i}} \tag{4.34}$$

so then if both sides of the equation are to transform identically

$$\Delta t E(x,\hat{i}) U_{x+\hat{i}} \rightarrow V_{x+\hat{0}} E(x,\hat{i}) U_{x+\hat{i}} V^{\dagger}_{x+\hat{0}+\hat{i}} \tag{4.35}$$

but we require

$$U_{x,\hat{i}} \rightarrow V_x U_{x,\hat{i}} V^{\dagger}_{x+\hat{i}} \tag{4.36}$$

which not only sets $V_{x+\hat{0}} = V_x$, but forces E to transform according to

$$E(x,\hat{i}) \rightarrow V_x E(x,\hat{i}) V_x^{\dagger} \tag{4.37}$$

so that the gauge field momenta transform differently from the gauge fields.

Variation of the gauge fixed action with respect to $U_{x,\hat{k}}$ (by taking the Lie derivative to ensure remaining on the $SU(2)$ manifold) and setting $\nabla S = 0$ gives the E field equations of motion:

$$E^a(x,\hat{k}) = E^a(x-\hat{0},\hat{k}) - \Delta t \left\{ \sum_{\hat{i}\neq\hat{k}} \Big(U_{x,\hat{k}} U_{x+\hat{k},\hat{i}} U^{\dagger}_{x+\hat{i},\hat{k}} U^{\dagger}_{x,\hat{i}} + U_{x,\hat{k}} U^{\dagger}_{x-\hat{i}+\hat{k},\hat{i}} U^{\dagger}_{x-\hat{i},\hat{k}} U_{x-\hat{i},\hat{i}} \Big)^a \right.$$
$$\left. + \frac{\beta_H}{\beta_G} Im\, (\Phi_x^{\dagger} \tau^a U_{x,\hat{k}} \Phi_{x+\hat{k}}) \right\} \tag{4.38}$$

The P field equations are obtained by varying S with respect to $\phi_j(x)$:

$$P_x = P_{x-\hat{0}} + \Delta t \left\{ \sum_{\hat{i}} (U_{x,\hat{i}} \Phi_{x+\hat{i}} + U^{\dagger}_{x-\hat{i},\hat{i}} \Phi_{x-\hat{i}}) - \left(6 + 4\frac{\beta_R}{\beta_H} (\Phi_x^2 - v^2) \right) \Phi_x \right\} \tag{4.39}$$

[1] This identification will be discussed in detail in chapter 7

All variables on the RHS of equations (4.38) and (4.39) except E and P are evaluated at time t.

In addition, we have a constraint on the gauge fixed system. If we vary (4.27) with respect to $U_{x,\hat{0}}$, and demand that $\nabla S = 0$ in the usual way, then we have another equation to be satisfied. Fixing the gauge turns this equation into a constraint:

$$\left.\frac{\partial S}{\partial U_{x,\hat{0}}}\right|_{U_{x,\hat{0}}=1} = 0 \tag{4.40}$$

This is the Gauss constraint which can be easily studied in the continuum; if we apply the Euler-Lagrange equations to (4.26) and fix the gauge $A_0 = 0$ then we find the constraint:

$$D_i \mathcal{E}_i = 0 \tag{4.41}$$

Furthermore, it can be shown that this constraint commutes with the Hamiltonian, so that it must be time independent. Thus, if we set up an initial lattice configuration with some value for the quantity $D_i\mathcal{E}_i$, not necessarily exactly zero, then the value of $D_i\mathcal{E}_i$ should remain invariant. It is clear that the longitudinal component of the $\mathcal{E}$ field determines whether this law is satisfied, since the longitudinal and transverse components of the electric field are defined by $\nabla \mathcal{E}^T = 0$ and $\nabla \times \mathcal{E}^L = 0$ respectively.

Applying (4.40) gives

$$G_x \equiv \frac{-i}{\triangle t}\left\{\frac{\beta_G}{2}\sum_i (U^\dagger_{x-\hat{i},\hat{i}} E^\dagger(x-\hat{i},\hat{i}) U_{x-\hat{i},\hat{i}} - E^\dagger(x,\hat{i}))^a + \frac{\beta_H}{2} Im(\Phi^\dagger_x \tau^a P_x)\right\} = 0 \tag{4.42}$$

G_x is the constraint at each site, x, of the lattice.

Details of the derivation of the E and P field equations of motion, and the form of the Gauss constraint are found in Appendix C.

4.4 Preparing a Hot Configuration

This section describes how the 4-dimensional action, S, of eq.(4.27) is reformulated as a set of 3-dimensional spatial lattices at different times. The approach is very similar to the Hamiltonian formalism of lattice gauge theory which was

first advocated by Kogut and Susskind [47], except that here we must take into account the Minkowski rather than Euclidean metric. The implementation of the Gauss constraint is considered, and the performance of the Metropolis algorithm in generating starting configurations for the time evolution is evaluated.

We need to generate a hot configuration which can be used as the starting point for the real time simulation. Therefore we need to represent the Hamiltonian of the system on the lattice. To do this we take the $\triangle t \to 0$ limit of (4.27) and sum the kinetic and potential energies to give the total energy (rather than the difference, which gives back the action).

$$\begin{aligned} H =& \frac{\beta_G}{2} \sum_{x,\hat{i}} E^a(x,\hat{i}) E^a(x,\hat{i}) + \frac{\beta_H}{2} \sum_x P_x^\dagger P_x \\ &+ \beta_G \sum_{\square} \left(1 - \frac{1}{2} Tr U_{\square}\right) + 3\beta_H \sum_x \Phi_x^\dagger \Phi_x - \beta_H \sum_{x,\hat{i}} Re(\Phi_x^\dagger U_{x,\hat{i}} \Phi_{x+\hat{i}}) \\ &+ \beta_R \sum_x (\Phi_x^\dagger \Phi_x - v^2)^2 \end{aligned} \tag{4.43}$$

The kinetic energy is the sum of the first two terms while the remaining terms give the potential energy. Although we put H in this form directly onto the lattice and refer to it as the "Hamiltonian", we are actually going to identify it with E/T, where E is the energy of the system. The motivation for such an identification is seen by considering equations (4.27) and (4.43); both the lattice action, S and H are proportional to a^4, but whereas the action belongs to a 4-dimensional lattice the Hamiltonian sits on a 3-dimensional lattice so there is an extra factor a:

$$\begin{aligned} S &\to \int d^4x \mathcal{L} \\ H &\to a \int d^3x \mathcal{H} \end{aligned} \tag{4.44}$$

We use $aT \simeq 1$. This means that H of eq.(4.43) must be identified with E/T in the continuum. Further, since the gauge part of H dominates we deduce that $\beta_G \sim 1/T$.

4.4.1 The Gauss Constraint

Configurations generated by using this Hamiltonian alone will not satisfy the Gauss constraint. In order to ensure the constraint we use:

$$H_{eff} = H + \xi G^2 \tag{4.45}$$

where

$$G = \sum_x \triangle t^2 G_x^2 \tag{4.46}$$

and ξ is some parameter which governs the accuracy by which the constraint is satisfied. The Metropolis algorithm will generate configurations with a distribution

$$e^{(-H_{eff})} = e^{(-H)} e^{(-\xi G^2)} \tag{4.47}$$

the effect as $\xi \to \infty$ is to multiply the usual distribution $\exp(-H)$ by $\delta(G)$; the delta function of the constraint. In practise, the extra term slows down the Metropolis updating quite considerably; for every new field the square of the constraint has to be recalculated. We chose a value of ξ which allowed a compromise between the final size of the constraint and the computer time taken to thermalize the system. This was $\xi = 2.5$ which meant that the size of the constraint term G^2 was about 6% of the remaining total energy H.

Once a configuration has been obtained in this way from the Metropolis we can reduce the value of G to as close to zero as we like by applying the following "cooling" equations:

$$\frac{\partial U_{x,\hat{i}}}{\partial t} = -\frac{\partial(\xi G^2)}{\partial U_{x,\hat{i}}}; \quad \frac{\partial \phi_i}{\partial t} = -\frac{\partial(\xi G^2)}{\partial \phi_i} \tag{4.48}$$

These are simply the Langevin equations with no noise term and force the system to minimize ξG^2. We do not expect this cooling to affect the physical components of the configuration, it is simply killing the longitudinal components of the electric field. Indeed experimentally we see very little change to the total energy. The only quantities which change in any non-negligible way are the value of the constraint and the average value of $E_i^a E_i^a$. The latter decreases by about 1% which affects the total energy by a decrease of typically 0.3%.

The ratio of the final value of the constraint to its initial value was about 10^{-7}, orders of magnitude more significant than any effects on the remaining energy of the system. If we were to use a lower value of ξ then we would see a greater change in the total energy and $E_i^a E_i^a$.

4.4.2 Choice of Coupling Constants

The value of the Higgs coupling, β_H, determines whether we are in the broken or the unbroken phase. The tree level formula eq.(4.30) shows how v^2 changes from a positively to a negatively valued parameter as β_H decreases through numbers close to $1/3$. This behaviour is clearly illustrated by figure 4.1a where we see a sharp phase transition as β_H is varied, but β_R and β_G are kept fixed at 0.005 and 8.0 respectively. We expect the phase transition to take place at $\beta_H = 0.33$, this is the value of β_H at which v^2 passes through zero, given that $\beta_R = 0.005$. It is interesting to note that the phase transition takes place at a larger value of β_H than we expect; that is the change of phase is occurring at a lower "temperature" than anticipated. Alternatively, we could deduce that the lattice system is hotter than predicted. We use β_R to fix the ratio of the W to the Higgs mass. β_G behaves as the inverse of temperature; this is shown by figure 4.1b; as β_G is increased the value of $< \Phi^2 >$ slowly increases and the

system moves further towards the broken symmetry regime.

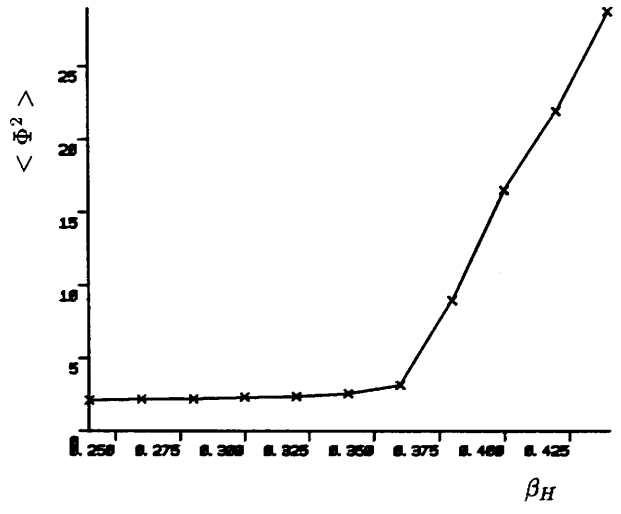

Figure 4.1a

Measurement of $< \Phi^2 >$ after metropolis on an 8^3 lattice. $\beta_G = 8.0, \beta_R = 0.005$ while β_H is varied.

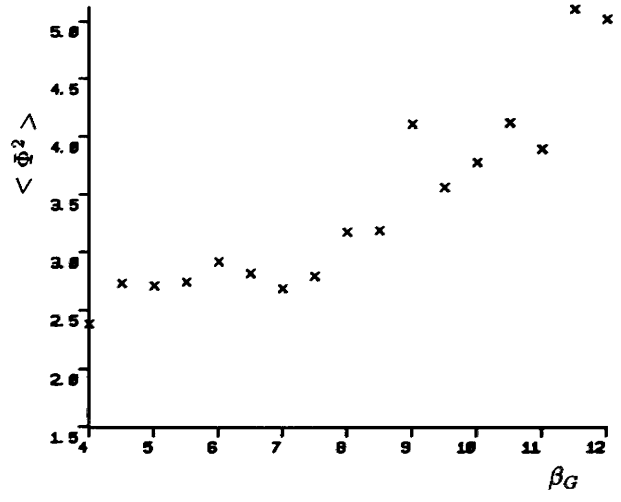

Figure 4.1b

Measurement of $< \Phi^2 >$ after metropolis on an 8^3 lattice. $\beta_H = 0.36, \beta_R = 0.005$ while β_G is varied.

4.4.3 Performance of the Metropolis Algorithm

We discuss here specifically the eleven independent starting configurations of the data sets which are analysed later for time development with $\mu_B = 0$; they provide a wide range of lattice sizes and couplings. We used 5000 sweeps of the Metropolis algorithm to ensure that thermal equilibrium was reached. The number of hits at each site and link was chosen to be 5. The majority of computer time for each simulation was used up in the time evolution so that the cost of setting up a good starting configuration is not particularly expensive in relative terms.

The lattice system has twenty degrees of freedom associated with each site. There are four each for the Higgs field and its conjugate momenta P, because these are expressed as complex doublets made from four independent components. Each site has three associated links, so if we consider the gauge fields there will be three $SU(2)$ matrices associated with a particular site. Only three of the four components of an $SU(2)$ matrix can be independent because $\sum_i U_i^2 = 1$. A further degree of freedom is removed from each field by the Gauss constraint, leaving six degrees of freedom for the gauge fields affiliated to each site. There will of course be an identical number of degrees of freedom for the conjugate field E, so we have $4 * 2 + 6 * 2 = 20$ degrees of freedom altogether. We can use the classical equipartition of energy to compare the value of the lattice Hamiltonian with its anticipated value.

$$\frac{E}{T} = \frac{1}{2} n_f \tag{4.49}$$

where n_f is the number of degrees of freedom. In every case the total energy is greater than expected by about 1 - 2.5 %, so that the lattice is slightly hotter than expected. For example, if we have an 8^3 lattice we would ideally hope to see the lattice Hamiltonian take a value close to $10N^3 = 5120$; in reality this quantity is typically 5190. The Gauss constraint term corresponds to three degrees of freedom and we find that there is good agreement between the value of this term (before the gauss cooling) and $1.5N^3$. We also study the division of energy between kinetic and potential sectors and find that the energy is

close to being divided equally between the two. It seems then, that despite the difficulties with the identification of the temperature on the lattice we are seeing a remarkable confirmation of the assumptions that have been made. We have a good test that the Metropolis is working well.

4.5 Time Evolution at $\mu_B = 0$

The situation at $\mu_B \neq 0$ is described in Chapter 7, here we are concerned with the time development at $\mu_B = 0$ and in particular the numerical schemes used for the work of Chapter 6.

The majority of simulations were performed using a straightforward implementation of the the first order equations of motion for the fields given by eqs.(4.31), (4.38) and (4.39).

A timestep of $\triangle t = 0.05$ was found to be the most suitable. Although there was a reasonably good conservation of energy, we always found a small but significant rapid increase in the energy at the start of the time evolution. The difference of the average energy from the starting energy expressed as a percentage of the starting energy varied from between 0.2 - 0.5 %. This motivated the study of a second order scheme, we chose the leapfrog method because it is well known to conserve phase space [48]. The implementation of the leapfrog method is discussed in Appendix D. Trial runs showed an improvement in the performance of the time evolution; as the step size $\triangle t$ increased the leapfrog method maintained accuracy notably better than the first order scheme for the same step size. We chose to study N_{cs} as a function of time in these tests since it is the quantity to be measured for the determination of the sphaleron transition rate. In addition there was no detectable initial rise in energy for $\triangle t = 0.05$. Unfortunately only two of the thirteen runs to be described in Chapter 6 were made using the leapfrog scheme, but they do provide a useful check on the numerical reliability of the first order schemes.

We also studied the behaviour of the Gauss constraint. It was very encouraging to discover that in all but one (still unexplained) of the first order

simulations there was an exact conservation of the constraint (as far as we were able to detect, given that the constraint can only be written out to so many decimal places. We used 6 decimal places in all, a typical staring value for the Gauss constraint was 0.000039). This seems quite remarkable over the 150000 timesteps and would seem to confirm that the first order scheme is behaving well. For the leapfrog method there was an initial unexplained increase in the constraint but thereafter it remained constant. This increase was of the order of a factor of 100, which is large, but because our starting constraint is so small the final value of the constraint is still reasonably close to zero.

4.6 Computer Running Times

The main results presented in the remainder of this thesis were obtained from running the lattice program on the CRAY X-MP at Rutherford. A typical run on a 12^3 lattice took about 2100 seconds for 5000 sweeps of the Metropolis algorithm. The total time for a complete run, with time development over 150000 timesteps and 5000 sweeps of the Metropolis, was approximately 19000 seconds. This corresponds to the program being run for $\mu_B = 0$ with no cooling into the broken phase. A reduction in lattice size to 8^3 or an increase to 16^3 necessitated a factor of about 3 change in the required computer time. In fact, at the 16^3 sizes vectorization becomes more efficient and an increase of slightly less than a factor 3 is needed.

Chapter 5

Topological Measurements

5.1 Introduction

In Chapter 3 the connection between the rate of baryon number non-conservation and topology was explained. Consequently it is clear that the determination of both the sphaleron transition rate, and the shape of the Chern-Simons potential from lattice simulations will entail the measurement of topological quantities.

In their paper Ambjørn, Laursen and Shaposhnikov [40] describe the technique they used to measure the change in the topological charge, Q, between the symmetric and broken phases. The moment of the phase transition was mimicked by an instantaneous change in the Higgs coupling constant, β_H, to one in the cold phase, typically 0.4 or 0.42. The system was then made to adjust to this change by applying "cooling" equations; in this case the Langevin equations without the noise term. Meanwhile, the sum of $Tr(F_{\mu\nu}\tilde{F}^{\mu\nu})$ on the lattice is measured at every time step; if the lattice size is large enough and the timestep small enough this summation should be a reasonable approximation to the integral over 4-space. The results showed how the measured values of Q depended not only on the lattice size but also on the choice of the final value of β_H.

In this chapter we discuss these problems in detail, and describe the effect that different "cooling" procedures have. Much of the motivation for this work was the discovery that the same lattice configurations could produce very different distributions of Q depending upon whether the representation of the Higgs

field was as in (4.22) or (4.23).

5.2 Naïve Symmetric Measurement of Q

Whatever the specific details of the cooling equations that are used, they all move the system from time t_i^c to time $t_{i+1}^c \equiv t_i^c + \triangle t^c$. If we can find the difference $\triangle Q_i$ between the topological charge of the system at time t_i^c and the system at time t_{i+1}^c, then we can obtain the total change in the topological charge of the system between any two times simply by summing $\triangle Q_i$. Of course, $\triangle t^c$ must be small enough for this approximation to be sensible. The method used to extract $\triangle Q_i$ which is described here is based on the work of Di Vecchia et al [49]. The implementation of this method into computer code was originally done by Laursen, and we have taken over the routines from his program virtually unaltered.

The idea is to embed the 3-dimensional lattice into a 4-dimensional space-time lattice by replacing the time-like links. These are simply assigned to be the unit matrix for consistency with the gauge choice $A_0 = 0$. The separation of the space-like planes within the lattice is $\triangle t^c$. Thus from the space-like configurations at times t_{i-1}^c, t_i^c and t_{i+1}^c we can obtain $F_{\mu\nu}\tilde{F}_{\mu\nu}(x, t_i^c)$.

$$F_{\mu\nu}\tilde{F}_{\mu\nu}\Big|_{lattice} = \frac{1}{16}\sum_{\alpha,\beta=1}^{4} \epsilon_{\mu\nu\lambda\zeta}\left\{\frac{1}{2}TrU_{\mu\nu}^{\alpha}U_{\lambda\zeta}^{\beta} - \frac{1}{4}TrU_{\mu\nu}^{\alpha}TrU_{\lambda\zeta}^{\beta}\right\}(x) \qquad (5.1)$$

where $U_{\mu\nu}^{\alpha}$ are the four plaquettes in the $\mu\nu$ plane originating at site x, as shown in figure 5.1.

$$U_{\mu\nu} = U_{\mu}(x)U_{\nu}(x + e_{\mu})U_{\mu}^{\dagger}(x + e_{\nu})U_{\nu}^{\dagger}(x) \qquad (5.2)$$

e_{μ} is the vector in the μ^{th} direction with length equal to the lattice separation. Figure 5.1 illustrates how $F\tilde{F}(x)$ is calculated. The second term in eq.(5.1) normalizes the expression so that if, for example, all the links are set to the unit matrix the topological charge will be zero. Finally we obtain a lattice prescription for the difference in topological charge between two times t_1 and

t_2:

$$Q(t_2) - Q(t_1) = \frac{1}{16\pi^2} \sum_{t_n=t_1}^{t_2} \sum_{x \in lattice} TrF\tilde{F}|_{lattice}(x, t_n) \tag{5.3}$$

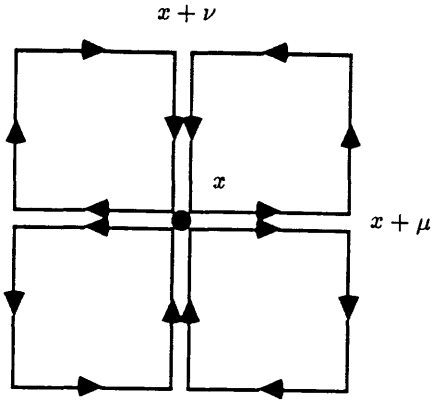

Figure 5.1

The four plaquettes in the $\mu\nu$ plane which are used for calculating $F\tilde{F}$ at the point x.

The next section describes four possible approaches to cooling the system.

5.3 Different Cooling Methods

5.3.1 Langevin Method Using the $SU(2)$ Representation of Φ

This is the method that was used by Ambjørn, Laursen and Shaposhnikov in their initial investigations. They used the lattice Langevin equations, but with the noise term omitted, to cool the system. The cooling is very similar to the method of reducing the size of the Gauss constraint which has been discussed in Chapter 4. Only the gauge and Higgs fields, U and Φ are cooled, so that it is really the potential energy of the system which is minimized. In addition they take account of the measure associated with the system. If we consider the path integral

$$I = \int [d\Phi] e^{-S^c} \tag{5.4}$$

then in the $R.V$ representation of Φ (given by eq.(4.23).

$$\begin{aligned} I &= \int R^3 [dR][dV] e^{-S^c} \\ &= \int [dR][dV] e^{-(S^c - 3\log R)} \end{aligned} \tag{5.5}$$

The R^3 term arises explicitly from the Jacobian of the coordinate transformation. Thus they work with an *effective* action $S^c_{eff} = S^c - 3\log R$. S^c is given by

$$\begin{aligned} S^c =& \beta_G \sum_{\square} \left(1 - \frac{1}{2} Tr U_{\square}\right) + 3\beta_H \sum_x \Phi^\dagger_x \Phi_x - \beta_H \sum_{x,\hat{i}} Re(\Phi^\dagger_x U_{x,\hat{i}} \Phi_{x+\hat{i}}) \\ &+ \beta_R \sum_x (\Phi^\dagger_x \Phi_x - v^2)^2 \end{aligned} \tag{5.6}$$

Under the Langevin equation for the R field:

$$\frac{\partial S^c_{eff}}{\partial R} = -\frac{\partial R}{\partial t^c} \tag{5.7}$$

where t^c is the "cooling" time. It is apparent that

$$\frac{\partial R}{\partial t^c} = -\left(\frac{\partial S^c}{\partial R} - \frac{3}{R}\right) \tag{5.8}$$

It is not immediately clear whether or not the treatment of such an effective action is justified. As we shall see the $3/R$ term plays a very important role in the measurement of Q, and the final state of the system which is reached after cooling has finished.

5.3.2 Langevin Cooling Using the Rectangular Coordinate Representation of Φ

In this representation of the Higgs field there is no ambiguity about treating the effective action. The measure term simply cannot contribute. Again only the potential energy of the system is minimised. It was the striking difference in the results of the Q measurements compared to the original Langevin, inclusive of the $3/R$ term which led to the investigations of this chapter.

5.3.3 Analytic Cooling

We devised the following method of cooling the system in order to have an alternative approach to the Langevin equations. In the following we use the rectangular coordinate representation of the Higgs field.

The system can be cooled by using the exact solutions to $\partial S/\partial \phi_i = 0$ and $\partial S/\partial U_{x,i} = 0$ at every site and along every link respectively. After a few iterations the system will have minimized its energy; it cannot of course reach the mimimum in just one sweep through the lattice because of couplings between adjacent sites, for example forcing $\partial S/\partial \phi_i = 0$ at one site will affect the action at neighbouring sites.

Solving $\partial S/\partial \phi_i = 0$ leads to

$$\phi_i(x) = \frac{\beta_H \alpha_i}{y} \tag{5.9}$$

where the α_i are defined through

$$\begin{pmatrix} \alpha_1 + i\alpha_2 \\ \alpha_3 + i\alpha_4 \end{pmatrix} = \sum_{j=\pm 1}^{\pm 3} U_{x,\hat{j}} \Phi_{x+\hat{j}} \tag{5.10}$$

and

$$y = 6\beta_H + 4\beta_R(\Phi_x^2 - v^2) \tag{5.11}$$

Substituting (5.9) into (5.11) results in the following cubic equation for y.

$$y^3 + (4\beta_R v^2 - 6\beta_H)y^2 - 4\beta_R \beta_H^2 \sum_{i=1}^{4} \alpha_i^2 = 0 \tag{5.12}$$

Using Cardano's formula it can be shown that there is only one real root of this equation, which is given by

$$y = \sqrt[3]{\left\{ -\left(\frac{a^3}{27} + \frac{b}{2}\right) + \sqrt{\left(\frac{b^2}{4} + \frac{a^3 b}{27}\right)} \right\}} + \sqrt[3]{\left\{ -\left(\frac{a^3}{27} + \frac{b}{2}\right) - \sqrt{\left(\frac{b^2}{4} + \frac{a^3 b}{27}\right)} \right\}} - \frac{a}{3} \tag{5.13}$$

with $a = (4\beta_R v^2 - 6\beta_H)$ and $b = -4\beta_R \beta_H^2 \sum_{i=1}^{4} \alpha_i^2$ The root always gives a positive value for Φ^2. In addition the sign of $\partial^2 S/\partial \phi_i^2(x)$ ensures that the action is always minimized.

Lagrange multipliers are used to solve $\partial S/\partial U_i = 0$ because the four components of the gauge field must satisfy:

$$U_1^2 + U_2^2 + U_3^2 + U_4^2 = 1 \tag{5.14}$$

We work with

$$S' = S + \lambda g \tag{5.15}$$

where λ is the Lagrange multiplier, and g is the constraint:

$$g = U_1^2 + U_2^2 + U_3^2 + U_4^2 - 1 \tag{5.16}$$

In this case the sign of λ determines whether we minimize or maximize the action. The solutions take the form

$$(U_{x,\hat{j}})_i = -\frac{x_i}{2\lambda} \tag{5.17}$$

where λ is positive and

$$x_i = -\beta_G(\sum \sqcap_i)^\dagger + \beta_H \beta_i \tag{5.18}$$

$\sum \sqcap_i$ denotes the sum of the "staples" associated with a particular gauge link in the i^{th} direction and the β_i are defined by

$$\sum_{i=1}^{4} \beta_i (U_{x,\hat{j}})_i = -Re(\Phi_x^\dagger U_{x,\hat{j}} \Phi_{x+\hat{j}}) \tag{5.19}$$

The identification of β_i from this equation is clear once the right hand side is written out in terms of matrix components. Numerically the cooling is very fast. For this reason we introduce an artificial step size to slow down the cooling, eg:

$$\phi(t + \Delta) = \phi(t) + \Delta(\phi_s(t) - \phi(t)) \tag{5.20}$$

ϕ_s is the exact solution; a choice of $\Delta = 1$ corresponds to removing this slowing process.

5.3.4 Real Time Equations of Motion

Here, the real time equations of motion are used in place of cooling routines. We used the rectangular coordinate representation of the Higgs field. As in all the other methods described in this section β_H was abruptly increased to simulate entry into the broken symmetry phase. Since no actual minimization of energy takes place this method is not so straightforward to apply as the other cooling procedures; it is not clear when "cooling" is over. The advantage of this approach is that it should be more physical because it includes the dependence on the E and P fields.

5.4 Comparison of Different Cooling Methods

In this section we compare the results of using the four different sets of cooling equations that have been described above. We shall see that Q depends on the chosen cooling procedure, although physically Q is expected to depend only on the initial configuration.

The first step is to check that we are minimizing the energy of the system as expected. We see that S^c will be minimized when the first and fourth terms of eq.(5.6) vanish, and if the second and third terms cancel each other out. Thus we expect the Higgs field at each site to take on the vacuum value, $\Phi_x^2 = v^2$, and $TrU_\Box = 2$ for every plaquette on the lattice. This certainly happens where we use the Langevin cooling method with a rectangular coordinate representation of the Higgs field, and additionally where analytic cooling is used. In the case of cooling the effective action S^c_{eff}, using Langevin cooling and the $SU(2)$ representation of the Higgs field, we not surprisingly find that the *effective* action is minimized, but that the minima of S^c_{eff} and that of S^c are quite distinct. For example if we use S^c alone then we expect the term

$$\beta_R \sum_x (\Phi_x^2 - v^2)^2 \tag{5.21}$$

to become zero so that Φ_x^2 approaches v^2 during cooling. If we use S^c_{eff} we find

instead that

$$\beta_R \sum_x (\Phi_x^2 - v^2)^2 - 3 \sum log R_x \tag{5.22}$$

approaches its minimum. Solving for $\partial S^c_{eff}/\partial R = 0$ gives

$$4\beta_R (R_x^2 - v^2)^2 R_x = \frac{3}{R_x} \tag{5.23}$$

and we indeed find that the final value of R^2 satisfies this condition. The two terms in β_H then take on values appropriate to such a magnitude of R^2. Figure 5.2a shows the value of $\beta_R \sum_x (\Phi_x^2 - v^2)^2$ as cooling takes place using the Langevin method on S^c_{eff} and S^c with the Higgs field in the $SU(2)$ and rectangular coordinate representaions respectively. Figure 5.2b is similar, but the value of $\sum_x \Phi_x^2$ is studied. If we remove the $3/R$ term from the Langevin cooling but still keep the $R.V$ representation we find that each of the two terms in β_H approach zero individually, and that the vacuum term $\beta_R \sum_x (\Phi_x^2 - v^2)^2$ remains large. In fact it seems that the $3/R$ term was originally introduced by Ambjørn et al. to prevent the R coordinate going negative, and this is probably what we are seeing happen here. Using the real time development equations it is much harder to see what is really happening, we cannot expect to see the action being minimized because we expect energy to be conserved while the "cooling" is taking place.

Figure 5.3 compares the Q measurements obtained from the various methods. First, a configuration was generated by the Metropolis algorithm and then evolved through real time in the hot phase. After each time step the hot configuration was cooled to the broken phase and Q measured. The values of Q are then plotted against real time. It is interesting to observe that analytic cooling and the Langevin cooling using rectangular coordinates for the Higgs field gave similar results. With an $SU(2)$ representation of the Higgs field the charge Q varies much more rapidly. In fact, this particular time evolution corresponds to the variation of N_{cs} in figure 6.1; all the graphs were obtained from the same initial configuration and under identical conditions during the time evolution. The physical picture we have is based on the structure of the periodic potential shown in figure 3.1, the system starts off at some energy comparable to the

height of the potential barriers, and as cooling begins the system starts to roll into the nearest valley. If the system is near the potential barrier before cooling, then a small perturbation from its position in phase space may be enough to force it into a different valley when cooling begins. We expect the measured values of Q to be peaked around integers because of this picture, although we cannot expect Q to be necessarily integer because we are not integrating over all of time so the four integral d^4x is not complete. In fact the Q values we measure are separated by about 0.75 rather than 1. This is believed to be a result of lattice artifacts. This physical picture and distribution of the charge Q was outlined in [40] by Ambjørn et al. who studied measurements of the charge by cooling configurations generated by Metropolis. They used only the Langevin cooling with the $SU(2)$ representation of the Φ field. The results illustrated in figure 5.3 were obtained using an 8^3 lattice and a large final value of β_H ($\beta_H = 0.48$). Originally we used $\beta_H = 0.4$ or 0.42 for the cooling part, as was done in [40]; but we seemed completely unable to detect non-trivial Q using the Langevin method with rectangular coordinates. Increasing β_H seemed to allow non-trivial Q to be recorded, and on larger lattices we could obtain non-trivial Q even with $\beta_H = 0.4$ or 0.42. Again Ambjørn et al. discussed the dependence of their results on the choice of β_H. We have built on this and studied how each of the different methods depends on the choice of β_H, with no satisfactory conclusions about whether one method is superior to another. Figure 5.4 shows an example of different Q measurements which were *all* obtained from an identical starting configuration in the hot phase.

We have to conclude that the measurement of Q remains a problematic area. The hope that Q should depend only on the initial configuration is not realised. Of course measurements of topological charge have been investigated on the lattice before, and it is widely regarded as an area of difficulty. As stated previously this problem has significance for the measurement of the change in Chern-Simons number with time in the determination of the sphaleron transition rate at $\mu_B = 0$. However the explicit difficulties associated with the choice of cooling procedure are more pertinent to the search for an asymmetry in the

Q distribution, since Q is the difference in the Chern-Simons number between the unbroken and broken symmetry phases.

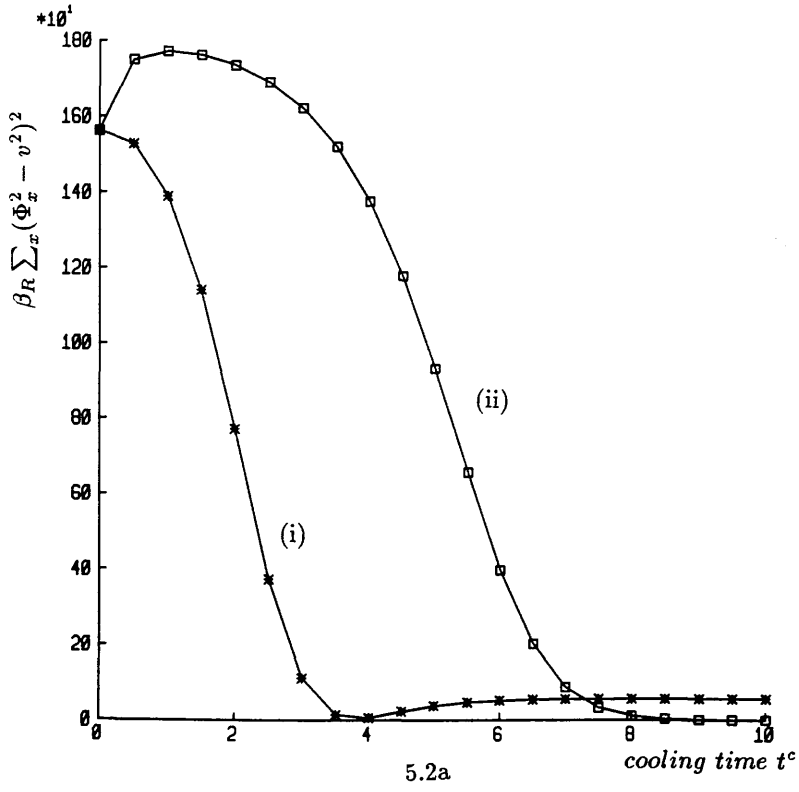

5.2a

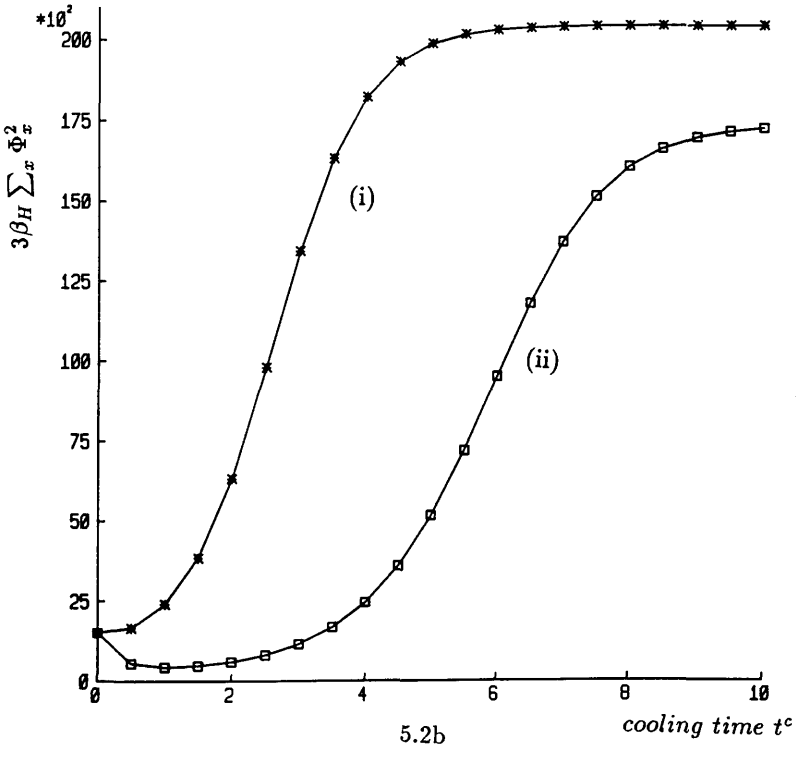

5.2b

Figure 5.2

Variation of (a) $\beta_R \sum_x (\Phi_x^2 - v^2)^2$, and (b) $3\beta_H \sum_x \Phi_x^2$ during cooling. The lattice size is 8^3 and at the start of cooling β_H is changed from 0.32 to 0.42. $\beta_G = 8.0$ and $\beta_R = 0.005$. (i) shows Langevin cooling with the Higgs field in the $SU(2)$ representation so the the effective action $S^c - 3logR$ is cooled, (ii) shows Langevin cooling for the Higgs field in rectangular coordinates.

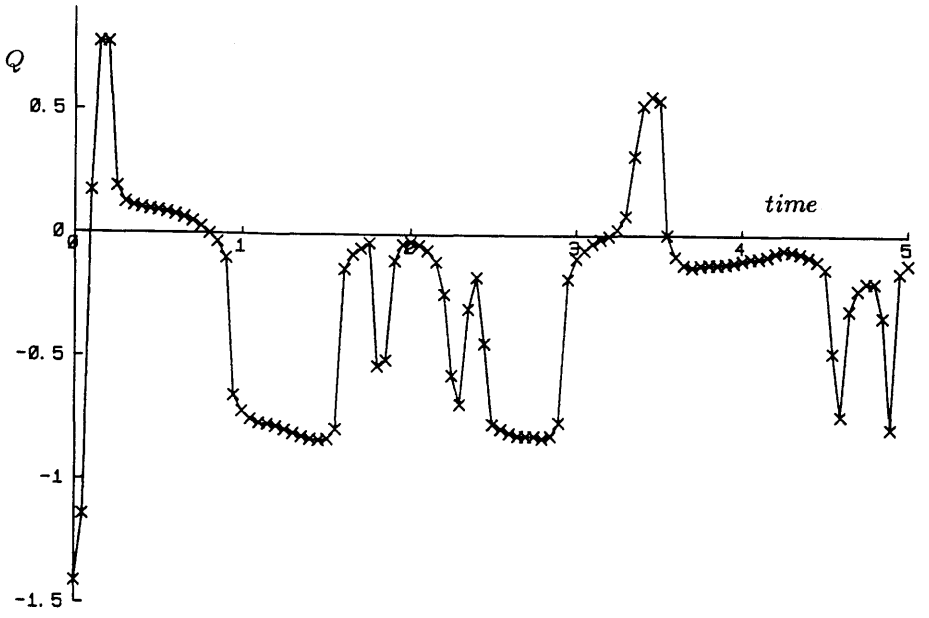
Q
0.5
0
-0.5
-1
-1.5
time
0
1
2
3
4
5

5.3a

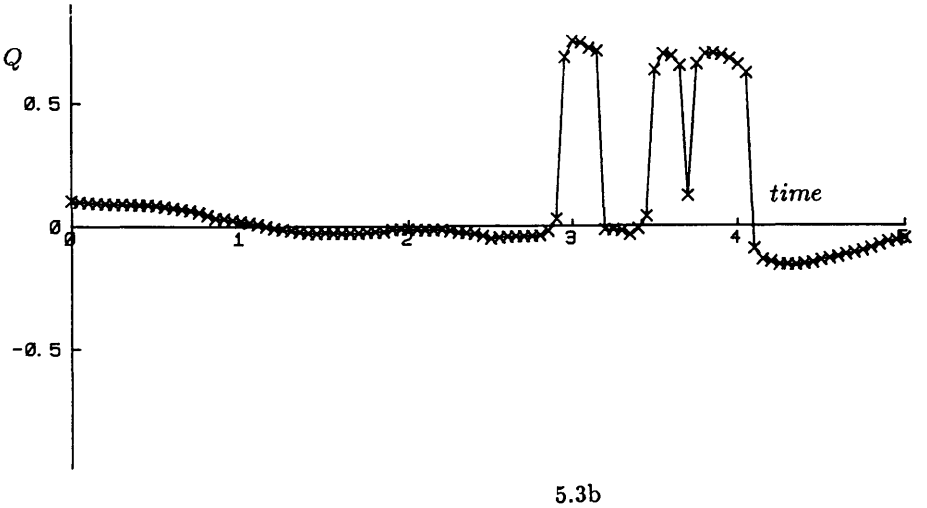
Q
0.5
0
-0.5
time
0
1
2
3
4
5

5.3b

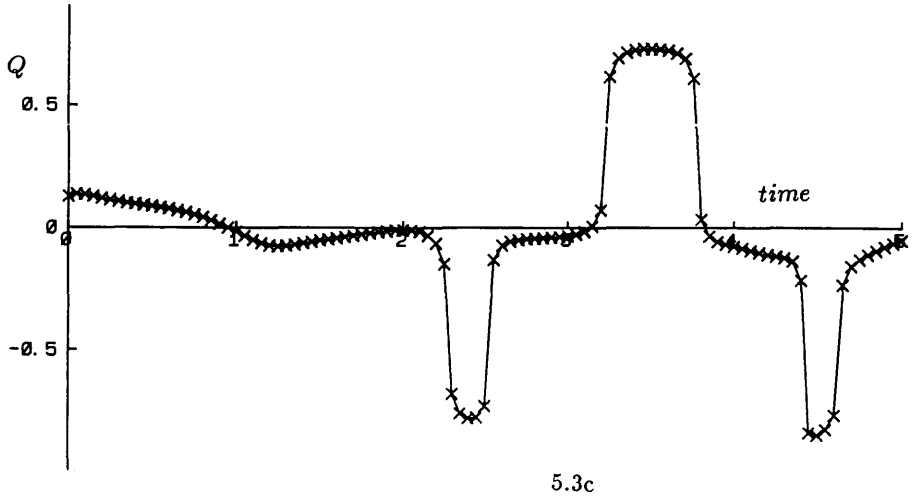
Q
0.5
0
-0.5
time
0
1
2
3
4
5

5.3c

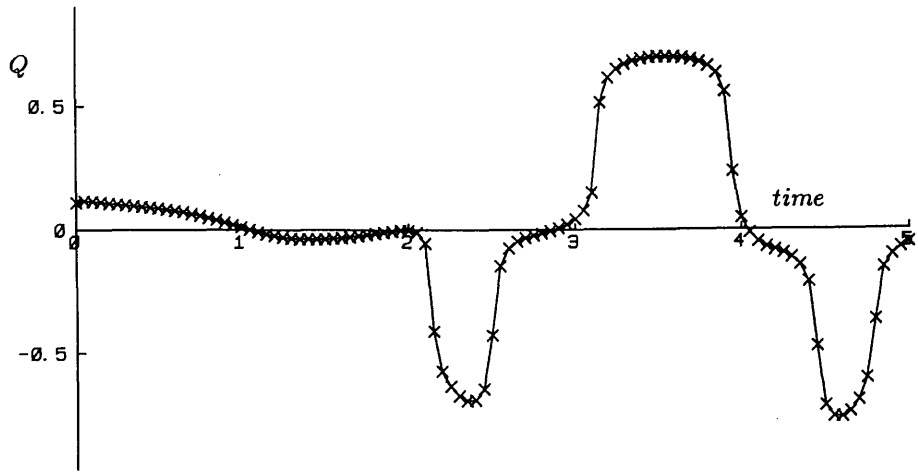

5.3d

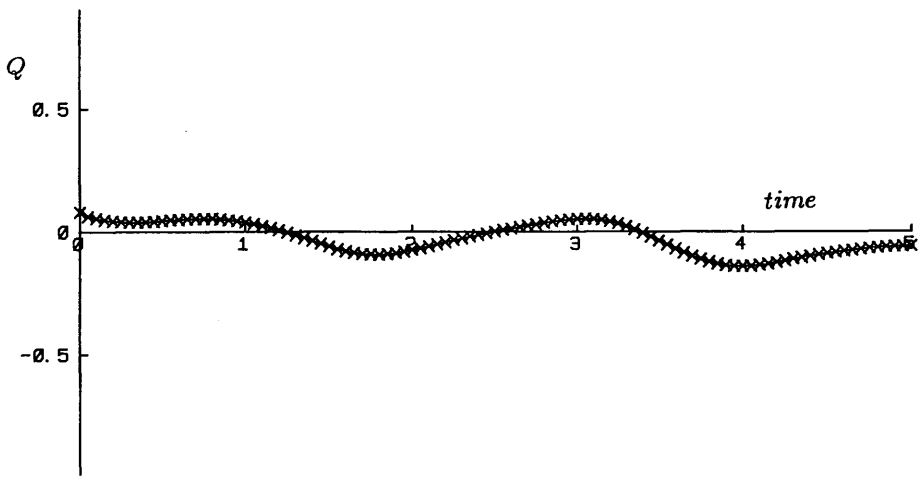

5.3e

Figure 5.3

Variation of Q with time. Different cooling procedures are used for each graph; but the initial configurations are identical. 5.3a shows the results of using the $SU(2)$ Higgs representation with Langevin cooling and the $3/R$ included. 5.3b is obtained as for 5.3a but the $3/R$ term is removed. 5.3c corresponds to using the new representation of the Higgs field with Langevin cooling, 5.3d and 5.3e the same representation with analytic cooling and the real time equations respectively. The initial coupling constants were $\beta_G = 9.0$, $\beta_H = 0.34$ and $\beta_R = 0.0016$. β_H was increased to 0.48 as cooling began. The lattice was 8^3. 200 cooling steps of $\Delta = 0.05$ were used except for d where the step was 0.25, and e where the step was 0.01 and 500 steps were used.

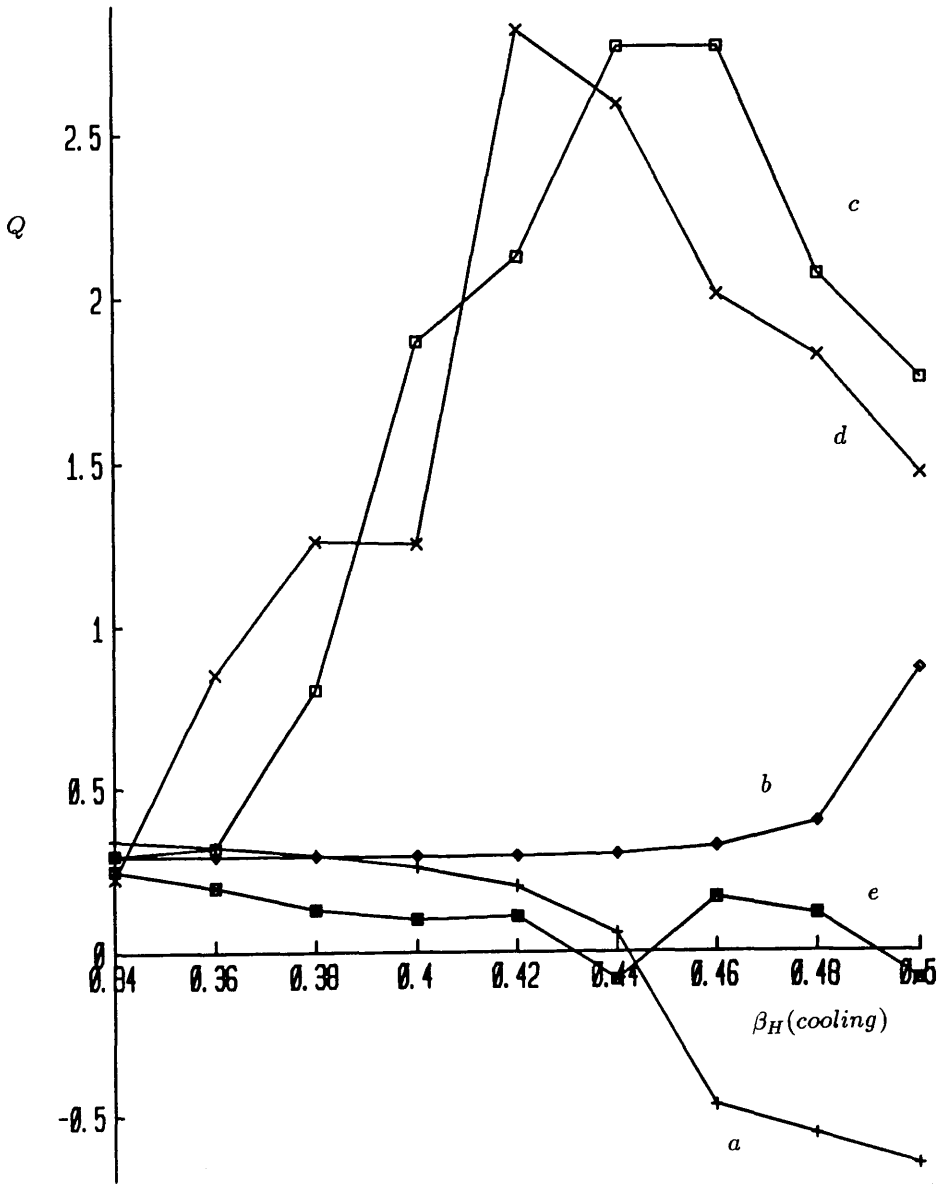

Figure 5.4

Variation of the measured charge Q with the final value of β_H. *Every* measurement corresponds to an identical initial configuration. Curve (a) shows the results of using the $SU(2)$ Higgs representation with Langevin cooling and the $3/R$ included. (b) is obtained as for (a), but the $3/R$ term is removed. (c) corresponds to using the new representation of the Higgs field with Langevin cooling, (d) and (e) the same representation with analytic cooling and the real time equations respectively. The initial coupling constants were $\beta_G = 8.0$, $\beta_H = 0.32$ and $\beta_R = 0.005$. The lattice was 16^3. 200 cooling steps of $\Delta = 0.05$ were used except for (d) where the step was 0.25, and (e) where the step was 0.01 and 500 steps were used.

Chapter 6

Sphaleron Transitions at $\mu_B = 0$

6.1 Introduction

The main objective of this chapter is the verification of the transition rate of fermion number non-conservation within the electroweak theory in the phase with restored symmetry [50] [51]. We shall begin with a discussion of the expected size of the thermal fluctuations of N_{cs}^2 which is particularly relevant to the choice of couplings and lattice sizes; if the thermal fluctuations are of the order of the sphaleron transitions themselves then measuring a transition rate for the sphalerons becomes extremely difficult. Next we consider the broken symmetry phase and discuss the limitations imposed by the available lattice sizes. Finally we consider the unbroken phase and discuss the interpretation of the data from the simulations which are made.

6.2 Thermal Fluctuations of $< N_{cs}^2 >$

Shaposhnikov has estimated the size of the thermal fluctuations of the Chern-Simons number within a topological sector using lowest order perturbation theory [50].

$$< N_{cs}^2 >= \left(\frac{g^2}{32\pi^2}\right)^2 \int\int d^3x d^3y \epsilon^{ijk}\epsilon^{lmn} < (F_{ij}^a A_k^a)(x)(F_{lm}^b A_n^b)(y) > \qquad (6.1)$$

Only lowest order gauge interactions are used so F_{ij} is as in Abelian gauge theory. Using

$$< A_i^a(x) A_j^b(y) >= \frac{1}{V} \int \frac{d^3k}{(2\pi)^3 2k^0} 2\delta^{ab}\delta_{ij} n_B(k) e^{-ik(x-y)} \tag{6.2}$$

where $n_B(k)$ is the Bose distribution function. The calculation is reasonably straightforward and is given in Appendix E, yielding:

$$< N_{cs}^2 >= \left(\frac{g^2}{32\pi^2}\right) \frac{48VT^3}{\pi^2} (\zeta(2) - \zeta(3)) \tag{6.3}$$

ζ is the Reimann ζ function. Translating this into lattice parameters gives

$$< N_{cs}^2 >= \alpha \frac{N^3}{\beta_G^2} \tag{6.4}$$

where

$$\alpha \simeq 1 \times 10^{-3} \tag{6.5}$$

where N^3 is the total number of sites on the lattice, and β_G the gauge coupling constant. We shall see that this is quite well satisfied in the confined phase.

6.3 The Higgs Phase

As discussed in Chapter 3, the transition rate in the broken symmetry phase has been calculated using semi-classical methods. Ideally we should begin by comparing the lattice transition rate with these predictions. Unfortunately, we shall show in this section that the maximum lattice sizes available to us are not large enough to allow this rate to be measured. The problem is essentially that there are just too many parameters to be fixed, while at the same time the temperature of the lattice system is hotter than the tree-level formulae would lead us to believe.

We begin by setting the Higgs mass to be equal to the W mass, which approximates the condition $\lambda \sim g^2$ that Arnold and McLerran [23] used in their analysis. Thus from eq.(4.28) $\beta_R = \beta_H^2/8\beta_G$. Further, the spatial size of the sphaleron is $\sim 1/M_W$; if we define $k \equiv 1/M_W a$ then k gives the size of the

sphaleron on the lattice. Thus for the lattice calculation to have meaning we need

$$2 \leq k \leq \frac{N}{4} \tag{6.6}$$

This ensures that the correlation length of the Higgs and W masses is at least two lattice spacings, and because we use periodic boundary conditions the sphaleron diameter must be at least one half of the size of the lattice. Next we consider eq.(3.33) which is the rate equation to be tested on the lattice. If we define $x \equiv 2M_W/T\alpha_W$ then this rate equation is valid in the region $x \gg 1$. Using $\alpha_W = \pi/\beta_G$ and $(aT)^3 = 30/\pi^2$ we find that the definition of x can be expressed as

$$x = \frac{2\pi}{(30/\pi^2)^{1/3}} \frac{\beta_G}{k} \tag{6.7}$$

Thus we also have

$$2 \leq \frac{2\pi}{(30/\pi^2)^{1/3}} \frac{\beta_G}{x} \leq \frac{N}{4} \tag{6.8}$$

x must be chosen such that the above equation can be satisfied, but more importantly so that the rate of sphaleron transitions is not too suppressed. If we choose x to be too large then we might never see a sphaleron event on the lattice. A value of x near 10 would seem reasonable.

We began with three free lattice parameters, β_G, β_H and β_R. We have translated the choice of β_G and β_H into choices of x and k. We see that the choices of β_R and x are almost automatic and the only remaining parameter k is itself restricted by eq.(6.6). Equation (4.29) describes the Higgs and W masses in terms of β_G, β_H and β_R; it translates into

$$\beta_G = \frac{\beta_H^2}{4(1 - \beta_H(3 - 1/4k^2))} \tag{6.9}$$

So that once k is chosen β_G is fixed through the choice of x in eq.(6.7), leaving a quadratic in β_H to be solved. Of course, we want β_H to be in the broken phase, i.e. $v^2 > 0$ and to keep β_G positive. The relationship between v^2 and β_H and k is as follows:

$$v^2 = 1 + \frac{(3\beta_H - 1)}{(1 - \beta_H(3 - 1/4k^2))} \tag{6.10}$$

once k has been chosen. Problems do not arise until we set up Metropolis configurations with coupling constants chosen according to the above rules. Then we see that the system is effectively in the unbroken symmetry phase (e.g. by measuring $< \Phi^2 >$); the temperature is too high and large thermal fluctuations are invalidating the tree level predictions. One possibility would be to move further into the broken phase by reducing k and thereby increasing the allowed values of β_H, but this is certainly not feasible on 8^3 lattices. It may be possible on larger lattices but we have not had the available computer time to explore this question thoroughly; as we have seen the relationships between different parameters is complicated so a lengthy systematic approach would be required. The alternative is to reduce the temperature by increasing β_G. This is more straightforward but we see from eq.(6.8) that an increase in lattice size is necessary. The verification of the rate in this phase requires a substantial amount of computing time and quite probably is not possible on the maximum available lattices we have at present (16^3).

6.4 The $SU(2)$ Symmetric Phase

Using $(aT)^3 = 30/\pi^2$ and $\alpha_W = g^2/4\pi = 1/\beta_G\pi$, the rate expression $\Gamma = \kappa(\alpha_W T)^4$ is converted into the number of transitions, $\mathcal{N}(t)$, expected on an N^3 lattice in time at.

$$\mathcal{N}(t) = 0.0452\kappa\frac{N^3}{\beta_G^4}t \tag{6.11}$$

Ideally we would like N^3/β_G^4 to be large. However, the the thermal fluctuations of N_{cs} are proportional to N^3/β_G^2, so we have a situation of competing interests. A range of N and β_G is chosen in an effort to balance the two. β_H is set at 0.34 which we know from earlier discussions ensures that we are just inside the unbroken symmetry phase, despite the tree-level predictions. We could of course choose a lower value of β_H and thus move further above the phase transition. If Cornwall's picture is correct then the periodic potential of figure 3.1 will continue to dominate however far above the phase transition we are. Alternatively, if the sphaleron transitions are unsuppressed, then at energies just

above T_c the potential should still influence the dynamics and make sphaleron processes much easier to identify and hence count. The radial Higgs coupling, β_R, is fixed by the requirement that $\lambda \sim g^2$.

We need to record N_{cs} as a function of time. Although N_{cs} is itself not gauge invariant eq(3.11) shows that the difference $N_{cs}(t_1) - N_{cs}(t_2)$ will be. Thus we measure $N_{cs}(t) - N_{cs}(t_0)$ where t_0 is the starting time for the time evolution. $N_{cs}(t) - N_{cs}(0)$ is determined by using the approach which has been described in Section 5.2; that is using the symmetric lattice version for the measurement of the the change in topological charge. There is no need for any cooling, the system remains in the unbroken symmetry phase throughout, so the cooling time is replaced by real time. Figure 6.1 shows a graph of $N_{cs}(t) - N_{cs}(t_0)$ against time, a measurement of N_{cs} has been made every timestep. With the aim of obtaining uncorrelated values of N_{cs} we only recorded it every 10 or every 100 timesteps. We were later to discover that runs with measurements every 10 timesteps were much more useful because of the improved statistics!

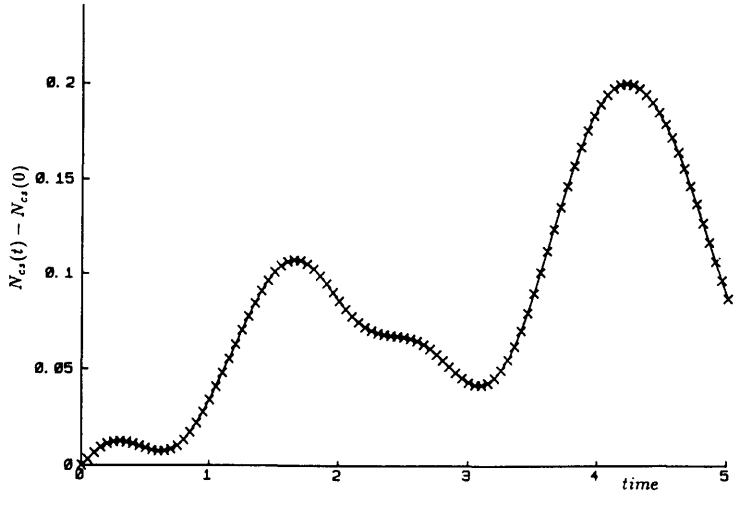

Figure 6.1

Typical plot of $N_{cs}(t) - N_{cs}(0)$ against time, a measurement of N_{cs} has been made after every timestep Δt. In this case $\Delta t = 0.05$, $\beta_G = 9.0$, $\beta_H = 0.34$ and $\beta_R = 0.0016$. The lattice size was 8^3.

We are looking for transitions larger than about 0.5 units of N_{cs}; the reason that we do not really expect to see integer transitions is that we are in a fi-

nite temperature regime and therefore we will not see vacuum configuration to vacuum configuration type processes. In addition, the discussions of Chapter 5 highlight the need for caution regarding the measurement of any topological quantity on the lattice. The resultant measurements of N_{cs} versus time are shown in figures 6.2 to 6.14. Where possible more than one initial starting configuration was used for a particular N and β_G, In most cases the thermal fluctuations appear to be large compared to the expected size of sphaleron type transitions. Figures 6.15, 6.16 and 6.17 show close ups of the data for what appear to be sharp, well defined jumps. In fact these jumps are smeared out by thermal fluctuations. It is clear that we need some kind of data analysis to support the envisaged picture of thermal fluctuations within plateaus, and rare but rapid transitions between sectors. We might hope to find some method which makes the counting of transitions more rigorous than a simple "by eye" approach.

We begin by noting that a plot of $R(i) \equiv N_{cs}(i) - N_{cs}(i+1)$, where $N_{cs}(i)$ is the i^{th} measurement of N_{cs} from the starting time, gives a very good fit to a Gaussian distribution. We expect this because the system is dominated by the thermal fluctuations. A typical distribution of R is shown in figure 6.18. We may then pose the question of what a random walk would look like if it were generated from a Gaussian distribution of variables with the same mean and standard deviation as the lattice data.

What we hope to see is a clear difference between the random walk data, consisting only of "thermal" fluctuations, and the lattice data which supposedly reflects a more complicated system, of which thermal fluctuations are only a part. Unfortunately, the random walk data looks very similar to the lattice data; there are "sharp" transitions, and worse still, close-ups of such transitions are in some cases as good as close ups of the lattice data where we might be tempted to claim a fairly clear sphaleron event. Figures 6.19 to 6.25 show representative random walks for each pair of N and β_G used. Close-ups are shown in figures 6.26 and 6.27.

We devised a method to identify particular points that could reasonably be

associated with a plateau. These points are then plotted and compared to a graph of the full data, the idea being that the number of "accepted" points of the lattice data should be larger than that of the random walk data, where there is no tendency to stick around a particular value of N_{cs}. Further, this analysis could help in the counting of transitions if we are able to identify plateaus satisfactorily.

A plateau will be characterised by thermal fluctuations about the mean value of N_{cs}, m, of the plateau. We expect the difference of the points from the mean, $x_i - m$, to be normally distributed about m. We also know that the standard deviation of this distribution, σ is related to the overall point to point standard deviation of the data set, which we will denote by S, i.e. the standard deviation of $R(i)$, such that $\sigma = S/\sqrt{2}$. If we then consider $2n+1$ consecutive points as a possible candidate for a plateau then we expect only a few to lie more than say 3 or $3.5 \times \sigma$ from the mean of the $2n+1$ points. In fact, given n we can calculate a limit on the number of such points ensuring that we would reject less than 2% of actual plateaus by chance. If this limit is satisfied then we accept the $(n+1)^{\text{th}}$ point as a point associated with a physical plateau. Every point in the full data set is considered in this way.

This technique shows up a clear difference between the lattice data and the random walk. Figure 6.28 illustrates how the number of points associated with plateaus varies according to the plateau length being imposed; there are clearly many more points being accepted from lattice data than from the random walk. Similar behaviour is seen in every data set. The difference is again highlighted in figure 6.29 where the accepted points are plotted out of a graph of N_{cs} versus time; the difference between the random walk and the lattice is quite dramatic.

The main difficulty with the credibility of our approach is that if the system really is in thermal equilibrium then the intervals Δt_i between successive sphaleron transitions should be distributed according to an exponential law:

$$p(\Delta t_i) = \exp(-\Gamma \Delta t_i) \tag{6.12}$$

That is the shorter plateau lengths are more likely than longer ones, our method

is best for finding longer plateaus. From figure 6.28 we might guess that a plateau length of about 50 measurements of N_{cs} is optimal, but this corresponds to a plateau length of 250 units of time, in the sets for which a measurement of N_{cs} is made every 5 units of lattice time. However, this is probably small enough to be useful, it is certainly small compared to the full time length of 7500 that has been used in all but one case. If we are to use this method to help count transitions then we should bear this problem of an artificially small cut off in plateau length in mind, and regard the method as an aid to the eye.

In Section 6.4.1 we give the results for the rate of sphaleron transitions from the lattice data. 6.4.2 contains a complementary discussion about the expected tendency of the values of N_{cs} to stick around integers. Finally, in Section 6.4.3 we measure $< N_{cs}^2 >$ within topological sectors to compare with the theoretical prediction of eq.(6.4).

6.4.1 Measurement of κ

We plotted out the accepted plateau points for a range of plateau lengths. Where there are 1500 measurements of N_{cs} in total we chose plateau lengths of 21, 41, 61, 81 and 101; where there are 15000 available points we used plateau lengths 41, 61, 81, 101, 121. These graphs were used as an aid to the eye, and in particular to estimate the error in counting up the number of transitions. In general we considered a gap betweeen two plateaus larger than about 0.5 as a sphaleron transition. It has to be admitted that the measurements are still highly subjective. Table 6.1 shows the estimated number of sphaleron

transitions for the different N and β_G that were used.

Measured Number of Sphaleron Transitions

$\beta_G \backslash N^3$	8^3	12^3	16^3
8.0	5 ± 2		
9.0	8 ± 4	23 ± 6	
10.0	2 ± 2	11 ± 2	29 ± 11
12.0			7 ± 3

Table 6.1 The measured number of transitions for the various β_G and lattice sizes.

We can use eq.(6.11) to extract the measured value of κ. The results are given in Table 6.2

Measured Value of κ

$\beta_G \backslash N^3$	8^3	12^3	16^3
8.0	$.1 \pm .05$		
9.0	$.3 \pm .2$	$.26 \pm .07$	
10.0	$.1 \pm .1$	$.19 \pm .03$	$.21 \pm .08$
12.0			$.10 \pm .04$

Table 6.2 The measured value of κ for the various β_G and lattice sizes.

From this table we may deduce

$$\kappa \geq 0.1 \tag{6.13}$$

This would seem to suggest that there is no exponential suppression of the rate. Thus if we have a sphaleron type object in the hot phase its mass cannot exceed the temperature by any substantial amount.

6.4.2 Binning N_{cs}

It seems reasonable to hope that a histogram of $N_{cs}(t)$ would show up the expected tendency of the system to stick around integer values of N_{cs}. Although we do find some convincing plots, it is difficult to draw an objective conclusion. Random walk data treated in an identical fashion does not look so very different from the lattice data. However, it is certainly true that the most plausible histograms from the lattice data are those for which we would expect the best results; i.e. those from the 8^3 lattice because the thermal fluctuations are smallest on this size lattice (c.f. eq.(6.4)). Figure 6.30 [1] is a good example and shows up a quite marked tendency for the N_{cs} values to peak around numbers close to integers. In fact the values of N_{cs} are peaked around multiples of nearer 0.8 than 1. This is related to the discussions of the previous chapter, where it is suggested that such an effect is due to lattice artifacts.

Unfortunately, using the selection method described above to pick out only those points associated with plateaus does not seem to be very successful. There is no decisive "cleaning" up of the peaks of the histogram. We could argue in defence of this that the number of points plotted will of course fall, and so the histogram will be less convincing anyway, just because there are fewer points plotted.

6.4.3 Measuring $< N_{cs}^2 >$

We are interested to see whether there is reasonable agreement between the lattice data and the perturbative formula eq.(6.4), and if the measurements scale well with the lattice size N and the coupling β_G. Unfortunately, it is not possible simply to measure the average value of $N_{cs}^2(t_i)$ because $N_{cs}(t_i)$ is really the difference in the Chern-Simons number between time 0 and time t_i; $N'_{cs}(t_i) = N_{cs}(t_i) - N_{cs}(0)$ where $N'_{cs}(t_i)$ is the true value of the Chern-Simons number.

The average value of $(N_{cs}(t_i) - N_{cs}(t_{i+n}))^2$ is determined for each lattice

[1] Figure 6.30 shows *all* the available data points, i.e. no selection process has been applied.

data set; $N_{cs}(t_{i+n})$ is the n^{th} measurement made from $N_{cs}(t_i)$. As n increases we anticipate that the correlation $< N_{cs}(t_i).N_{cs}(t_{i+n}) >$ will tend towards zero, so that $< (N_{cs}(t_i) - N_{cs}(t_{i+n}))^2 >$ will equal $2 < N_{cs}^2(t) >$. Figure 6.31 shows a typical graph of our results. In every case we see a distinct gradient to the "plateau" region of the curve; ideally we would have expected that the plateau should be completely flat, so we could easily read off the intercept as twice $< N_{cs}^2 >$. It is of course encouraging to see the marked contrast between the behaviour of the random walk data which varies as $\sqrt{n}$ and the lattice data. The error bars shown are very small because in the case illustrated there are 15000 actual measurements of $N_{cs}(t)$. It is apparent that there is a large systematic error in the approach we are using here, but it is still possible to estimate a value for $< N_{cs}^2 >$ from the graphs by looking at the intercept of the plateau slope with the y axis. The results are given in Table 6.3. and 6.4; 6.3 gives the measured value of α which is defined by eq.(6.4) to be $\beta_G^2/N^3 \times < N_{cs}^2 >$, Table 6.4 gives the actual measured $< N_{cs}^2 >$.

Measured $\alpha \times 10^{-4}$

$\beta_G \backslash N^3$	8^3	12^3	16^3
8.0	4.1 ± 1.0		
9.0	4.5 ± 1.0	4.8 ± 2.0	
10.0	4.2 ± 1.0	4.3 ± 1.5	3.4 ± 1.0
12.0			4.0 ± 1.0

Table 6.3 The measured value of α within a topological sector for the various β_G and lattice sizes. $\alpha \times 10^{-4}$ is expected to have a value close to 10 according to eq.(6.4).

Measured $< N_{cs}^2 >$

$\beta_G \backslash N^3$	8^3	12^3	16^3
8.0	0.0033 ± 0.0005		
9.0	0.003 ± 0.0005	0.01 ± 0.005	
10.0	0.0022 ± 0.0005	0.0074 ± 0.003	0.014 ± 0.002
12.0			0.011 ± 0.003

Table 6.4 The measured value of $< N_{cs}^2 >$ within a topological sector for the various β_G and lattice sizes.

It is reasonable to suggest that the slope of the plateau is due to "edge" effects between measurements of N_{cs} belonging to different topological sectors. As n increases, the likelihood of $N_{cs}(t_i)$ and $N_{cs}(t_{i+n})$ belonging to separate topological sectors increases. If this does happen then of course the difference of the values of N_{cs} squared will be larger than if both values belonged to the same sector.

The results given in Table 6.3 show good scaling with both the lattice size, N, and the gauge coupling β_G. Although α from the lattice data is smaller than predicted theoretically, the method of using the intercept of the slope of the "plateau" seems most likely to produce a lower bound on the size of thermal fluctuations.

6.5 Conclusions

Determination of the sphaleron transition rate in the broken symmetry phase seems to be impossible given the limitations both on available lattice sizes and computer time. Above the $SU(2)$ phase transition the large size of the thermal fluctuations was one of the main problems in the identification of sphaleron transitions, although it was encouraging to find that their size was in good agreement with perturbative estimates for all the lattice sizes and gauge couplings

that were used. A statistical approach to the lattice data seems to confirm the physical picture of rapid thermal fluctuations within each gauge sector superimposed on the slower underlying movement of N_{cs} between integer values via sphaleron transitions. However, since the system is at finite temperature the magnitude of sphaleron transitions will not necessarily be integer; we do not expect to see vacuum configuration to vacuum configuration type processes. Further, lattice artifacts affect the measurement of topological quantities and additionally, a direct identification of the physical temperature corresponding to the lattice system is difficult. The transition rate that was finally measured seems to confirm that above the $SU(2)$ phase transition the potential energy barriers separating the different gauge sectors are small compared to the temperature of the system. This is in disagreement with Cornwall [25] who has argued that the height of the barriers should continue to grow with increased temperature, and thus that the sphaleron transition rate should be very suppressed.

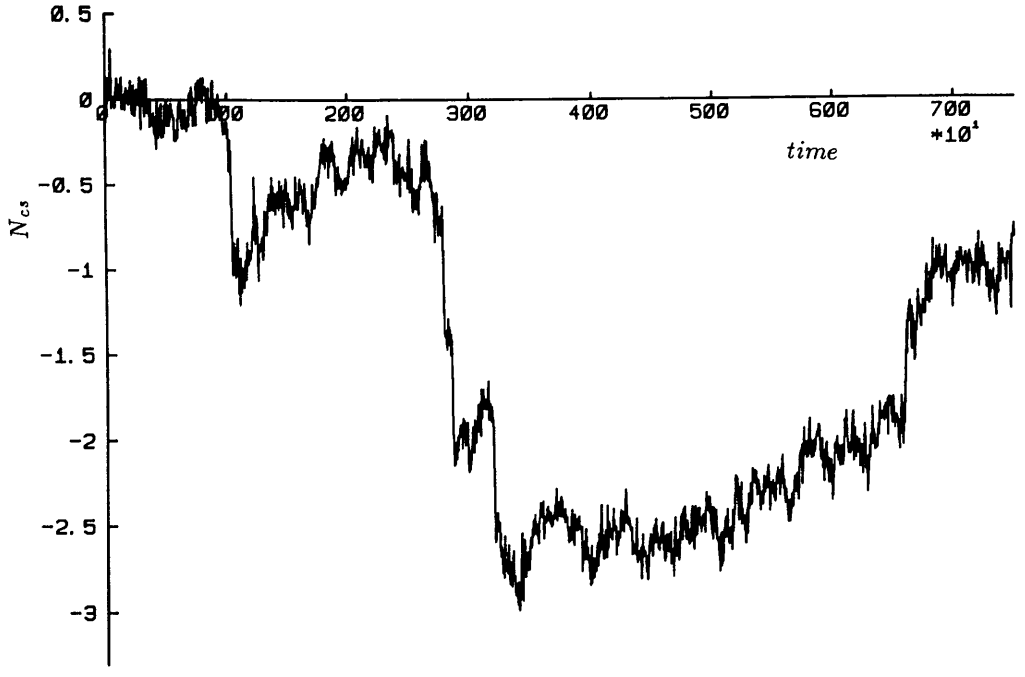

Figure 6.2

1^{st} order time evolution of N_{cs} for $\beta_G = 8.0$, $\beta_H = 0.34$ and $\beta_R = 0.00181$. The lattice size is 8^3 and $\Delta t = 0.05$.

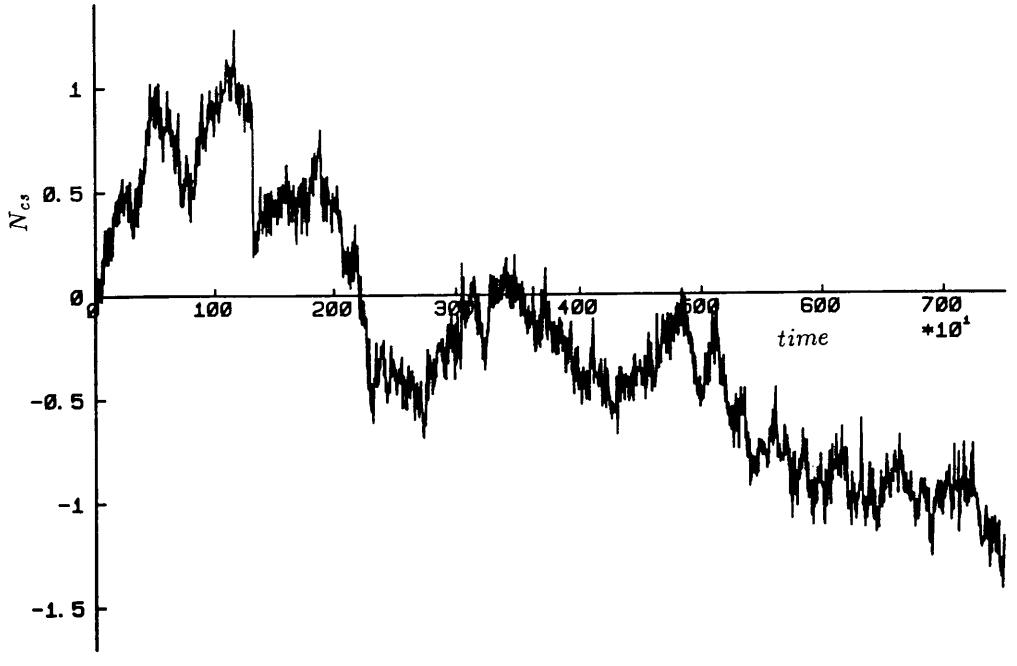

Figure 6.3

2^{nd} order time evolution of N_{cs} for $\beta_G = 8.0$, $\beta_H = 0.34$ and $\beta_R = 0.00181$. The lattice size is 8^3 and $\Delta t = 0.05$. The same starting configuration as in figure 6.2 is used.

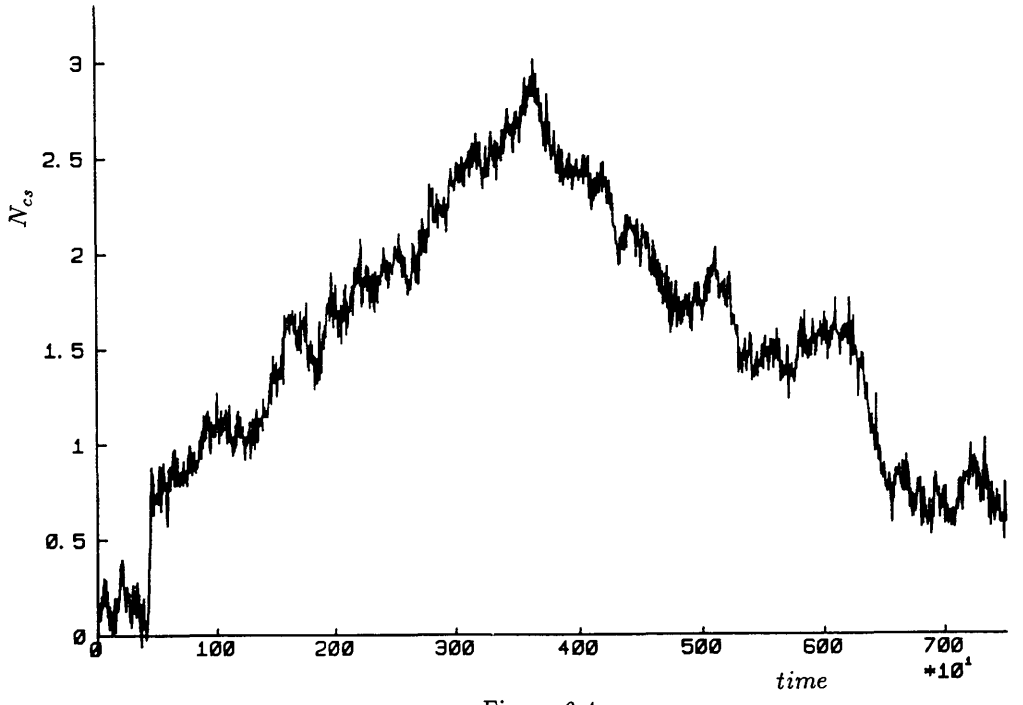

Figure 6.4

1^{st} order time evolution of N_{cs} for $\beta_G = 9.0$, $\beta_H = 0.34$ and $\beta_R = 0.0016$. The lattice size is 8^3 and $\Delta t = 0.05$.

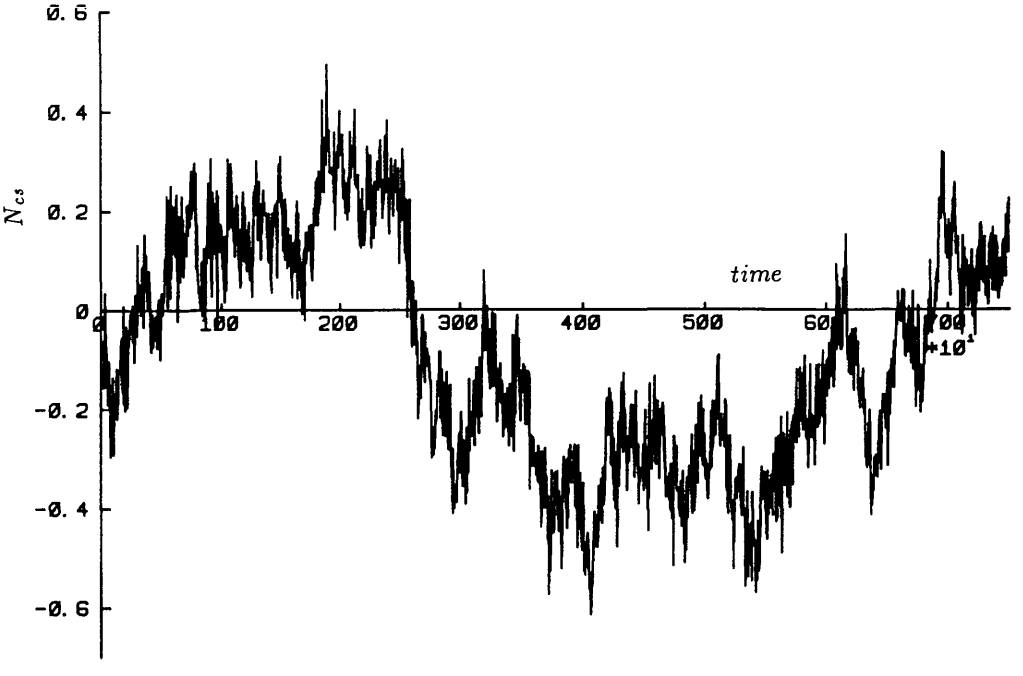

Figure 6.5

1^{st} order time evolution of N_{cs} for $\beta_G = 10.0$, $\beta_H = 0.34$ and $\beta_R = 0.0014$. The lattice size is 8^3 and $\Delta t = 0.05$.

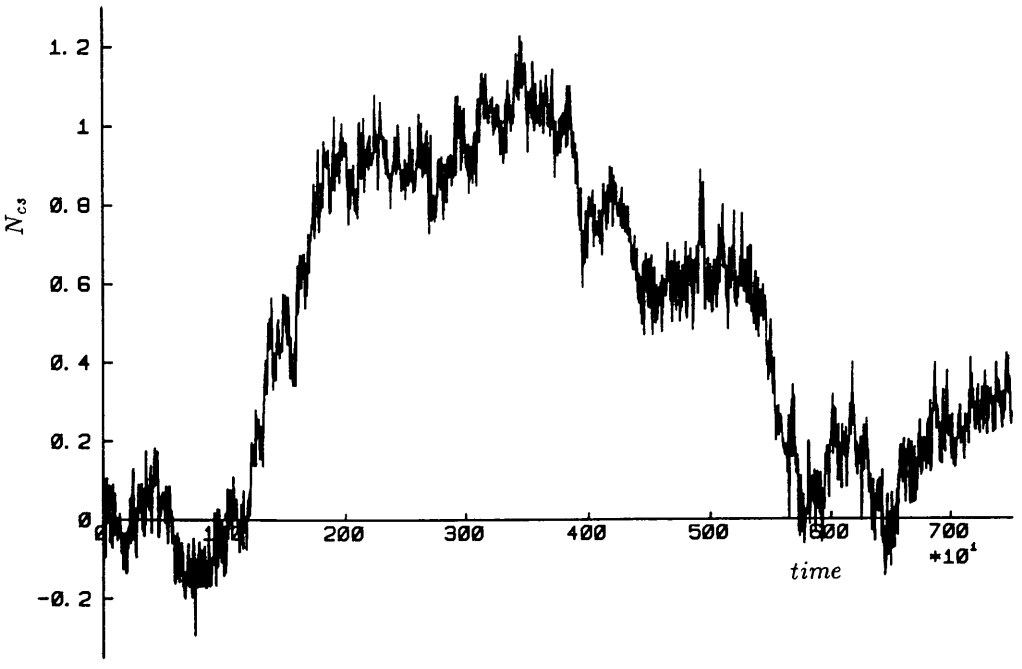

Figure 6.6

1^{st} order time evolution of N_{cs} for $\beta_G = 10.0$, $\beta_H = 0.34$ and $\beta_R = 0.0014$. The lattice size is 8^3 and $\Delta t = 0.05$.

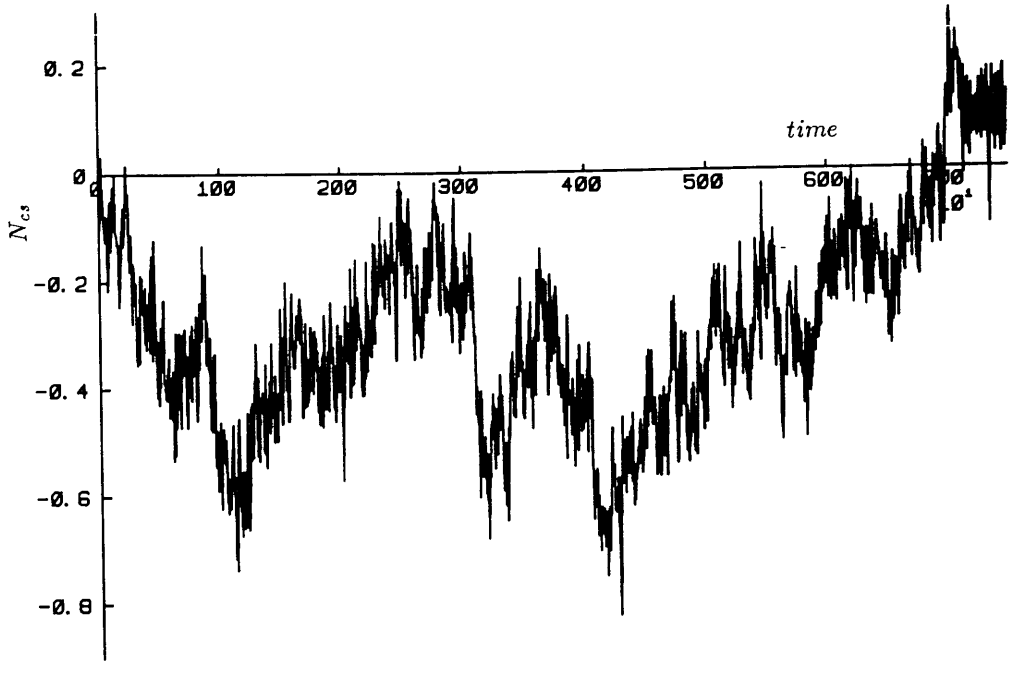

Figure 6.7

2^{nd} order time evolution of N_{cs} for $\beta_G = 10.0$, $\beta_H = 0.34$ and $\beta_R = 0.0014$. The lattice size is 8^3 and $\Delta t = 0.05$. The same starting configuration as in figure 6.6 is used.

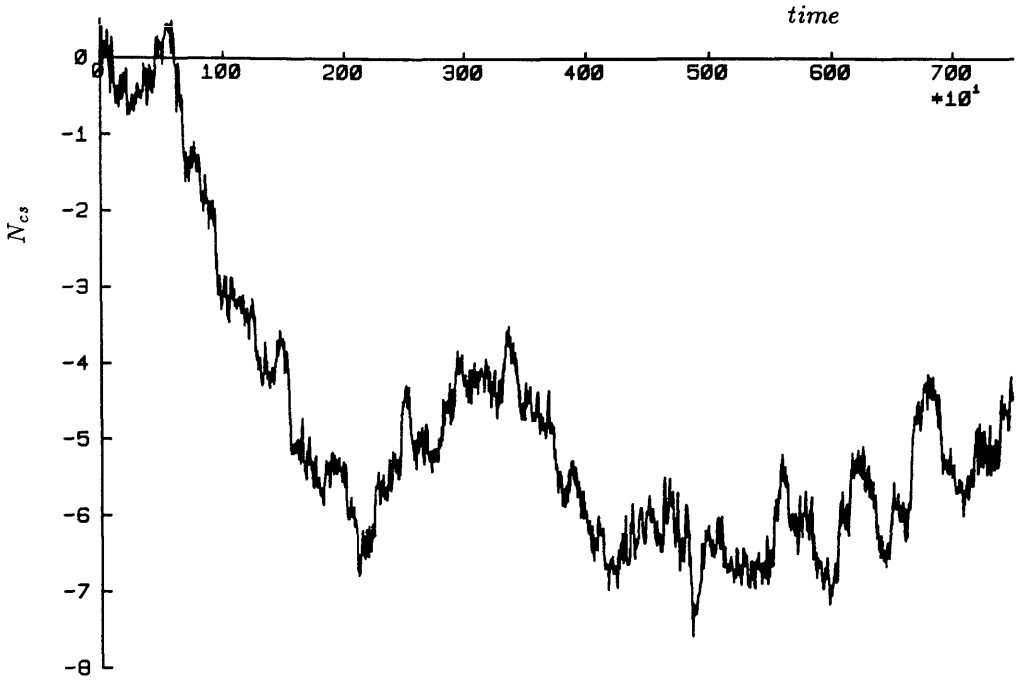

Figure 6.8

1^{st} order time evolution of N_{cs} for $\beta_G = 9.0$, $\beta_H = 0.34$ and $\beta_R = 0.0016$. The lattice size is 12^3 and $\Delta t = 0.05$.

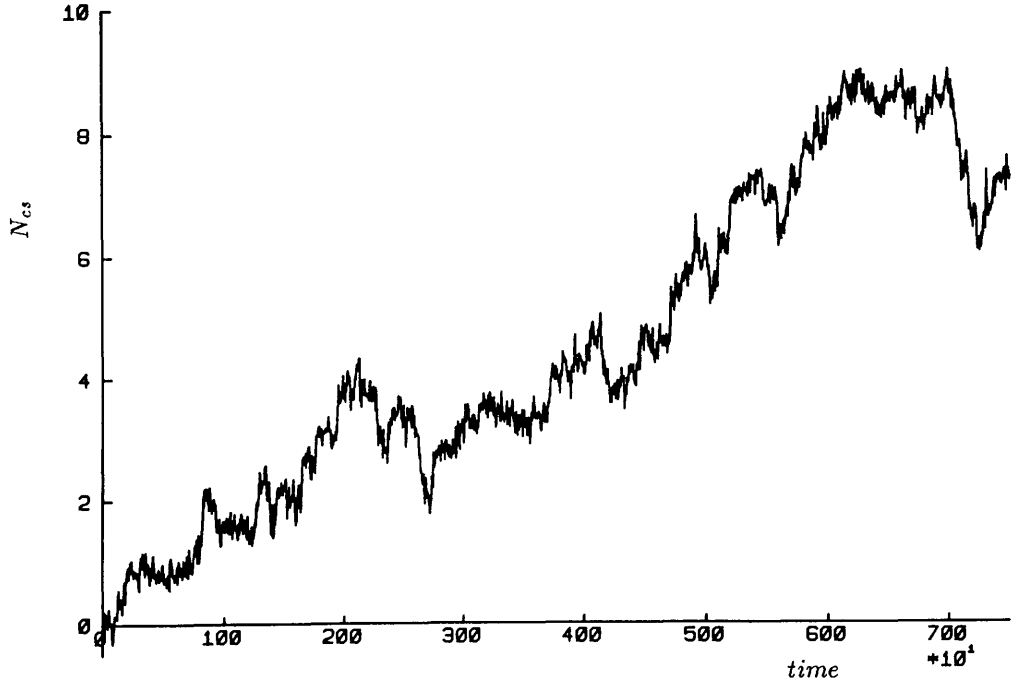

Figure 6.9

1^{st} order time evolution of N_{cs} for $\beta_G = 9.0$, $\beta_H = 0.34$ and $\beta_R = 0.0016$. The lattice size is 12^3 and $\Delta t = 0.05$.

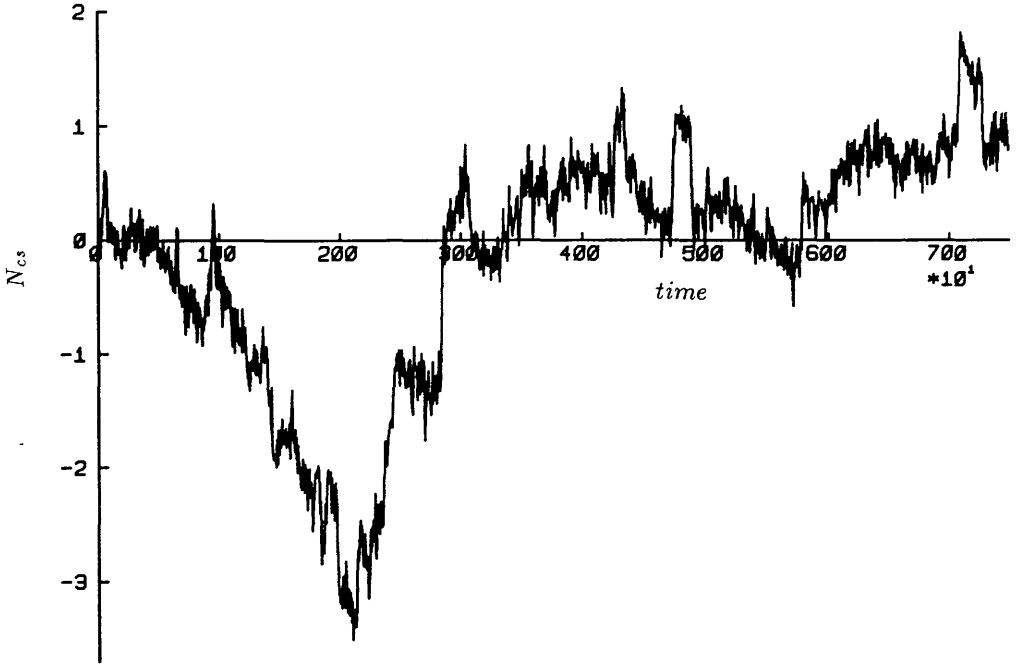

Figure 6.10

1^{st} order time evolution of N_{cs} for $\beta_G = 10.0$, $\beta_H = 0.34$ and $\beta_R = 0.0014$. The lattice size is 12^3 and $\Delta t = 0.05$.

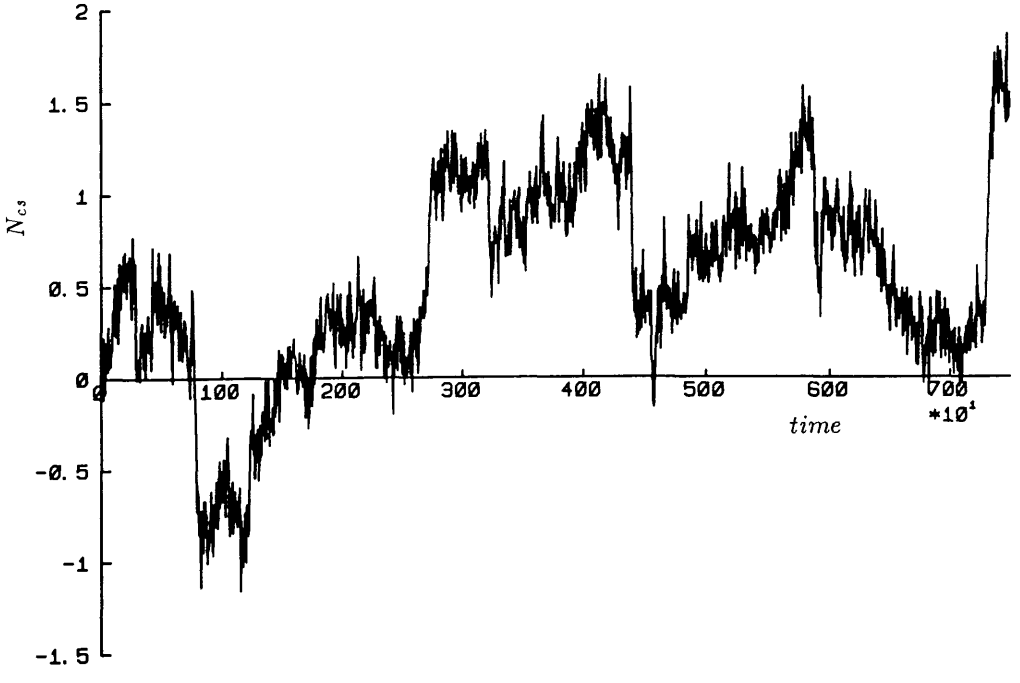

Figure 6.11

1^{st} order time evolution of N_{cs} for $\beta_G = 10.0$, $\beta_H = 0.34$ and $\beta_R = 0.0014$. The lattice size is 12^3 and $\Delta t = 0.05$.

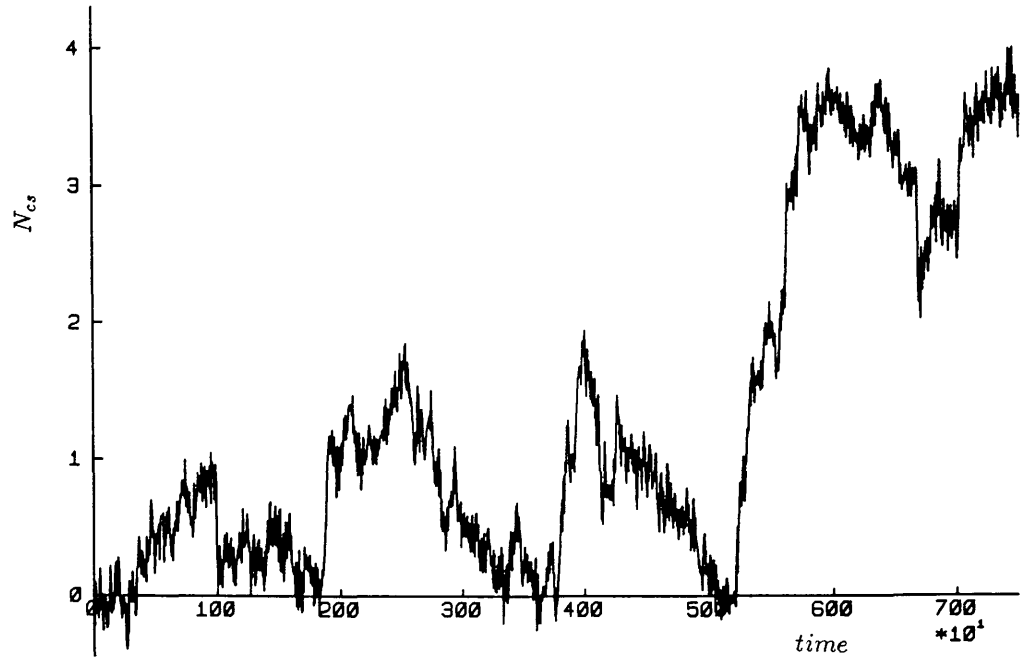

Figure 6.12

1^{st} order time evolution of N_{cs} for $\beta_G = 10.0$, $\beta_H = 0.34$ and $\beta_R = 0.0014$. The lattice size is 12^3 and $\Delta t = 0.05$.

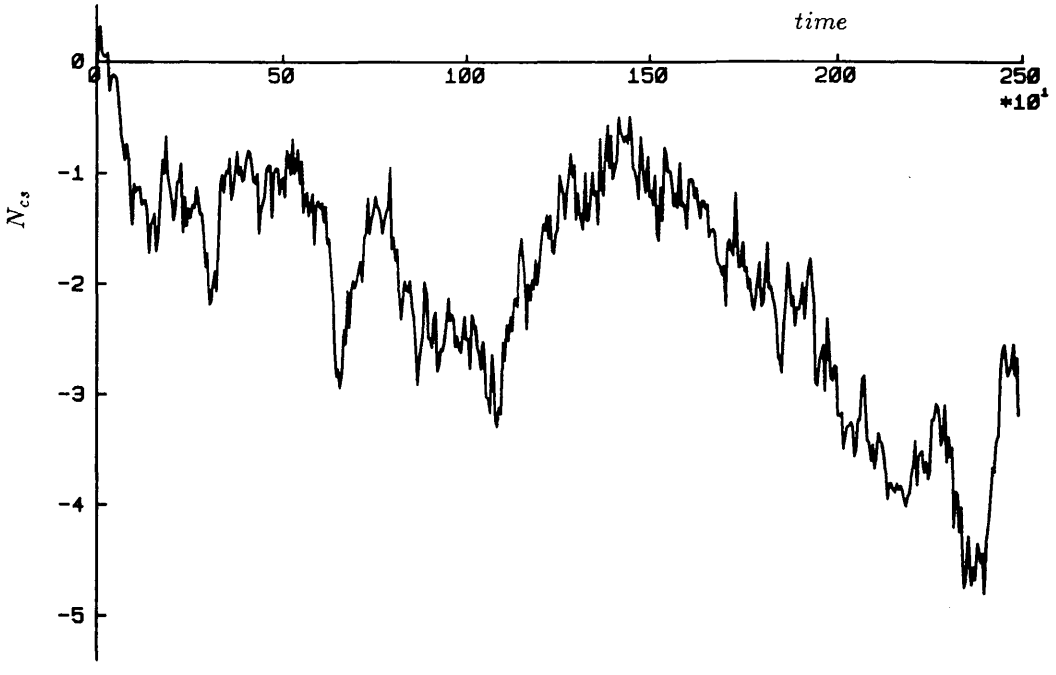

Figure 6.13

1^{st} order time evolution of N_{cs} for $\beta_G = 10.0$, $\beta_H = 0.34$ and $\beta_R = 0.0014$. The lattice size is 16^3 and $\Delta t = 0.05$.

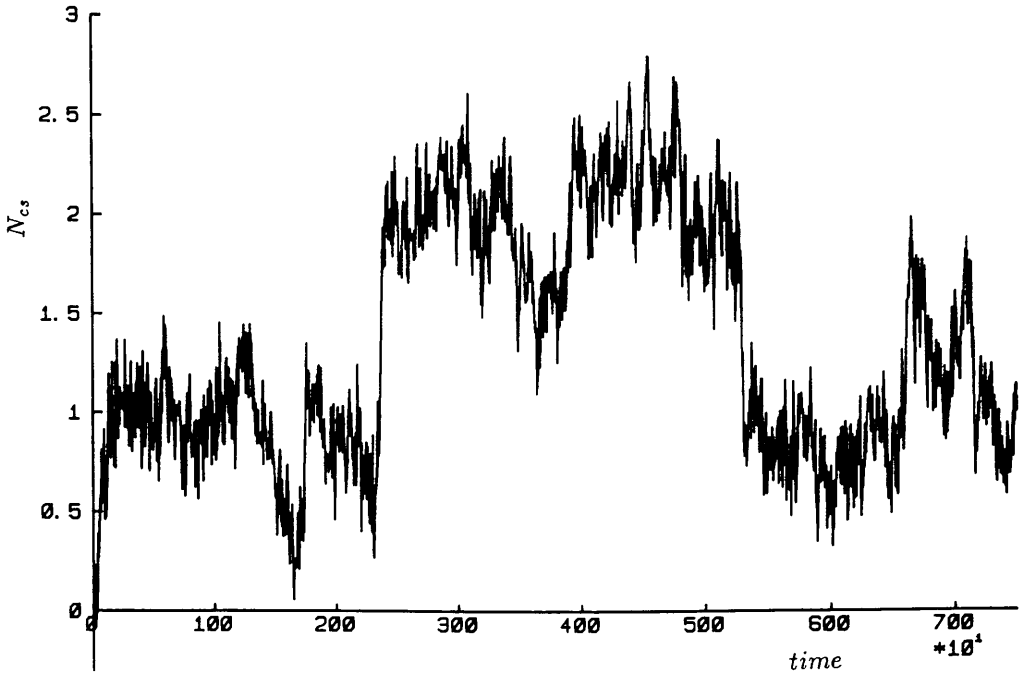

Figure 6.14

1^{st} order time evolution of N_{cs} for $\beta_G = 12.0$, $\beta_H = 0.34$ and $\beta_R = 0.0014$. The lattice size is 16^3 and $\triangle t = 0.05$.

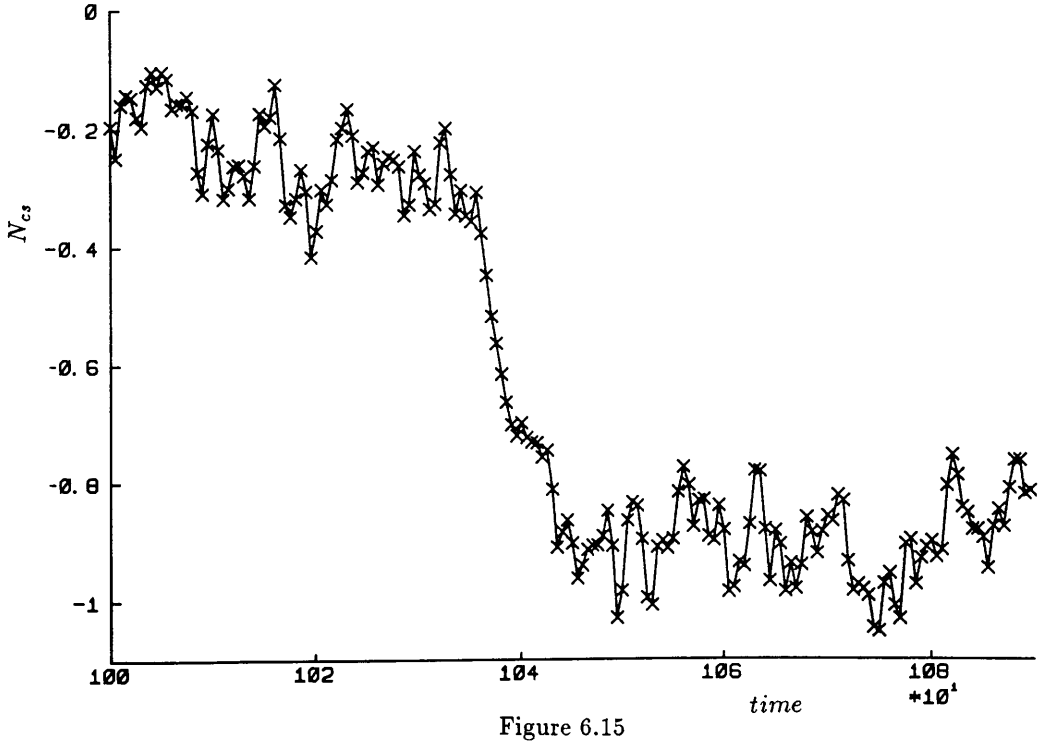

Figure 6.15

Close-up of figure 6.2 showing an apparant sphaleron transition. $\beta_G = 8.0$, $\beta_H = 0.34$, $\beta_R = 0.00181$ and the lattice size is 8^3.

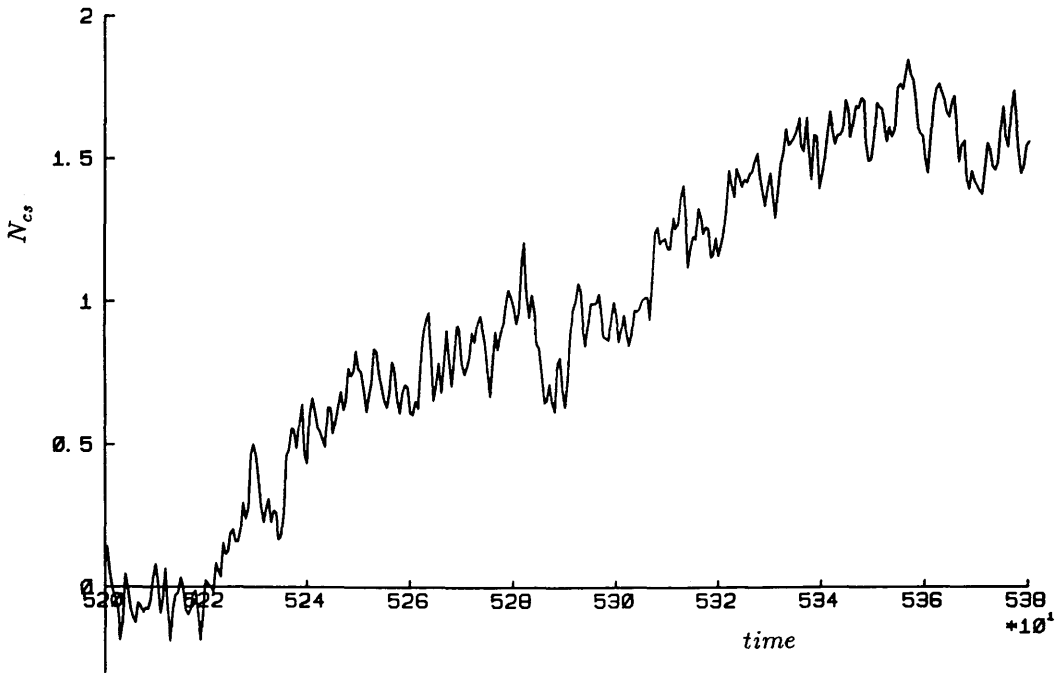

Figure 6.16

Close-up of figure 6.12 showing an apparant sphaleron transition. $\beta_G = 10.0$, $\beta_H = 0.34$, $\beta_R = 0.0014$ and the lattice size is 12^3.

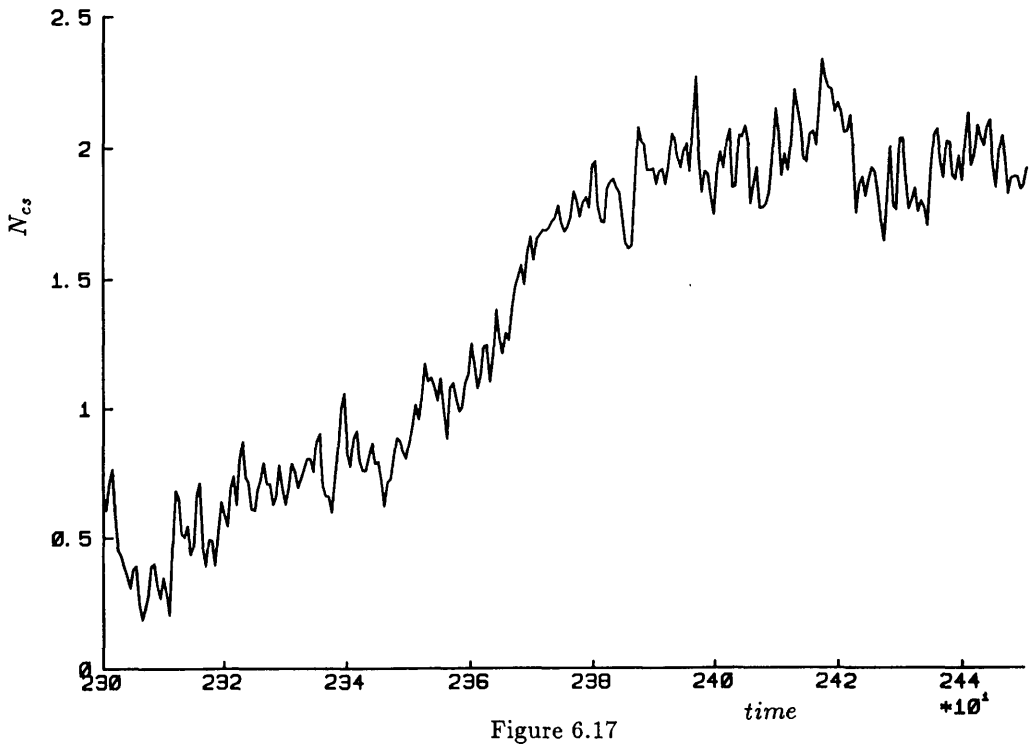

Figure 6.17

Close-up of figure 6.14 showing an apparant sphaleron transition. $\beta_G = 12.0$, $\beta_H = 0.34$, $\beta_R = 0.0014$ and the lattice size is 16^3.

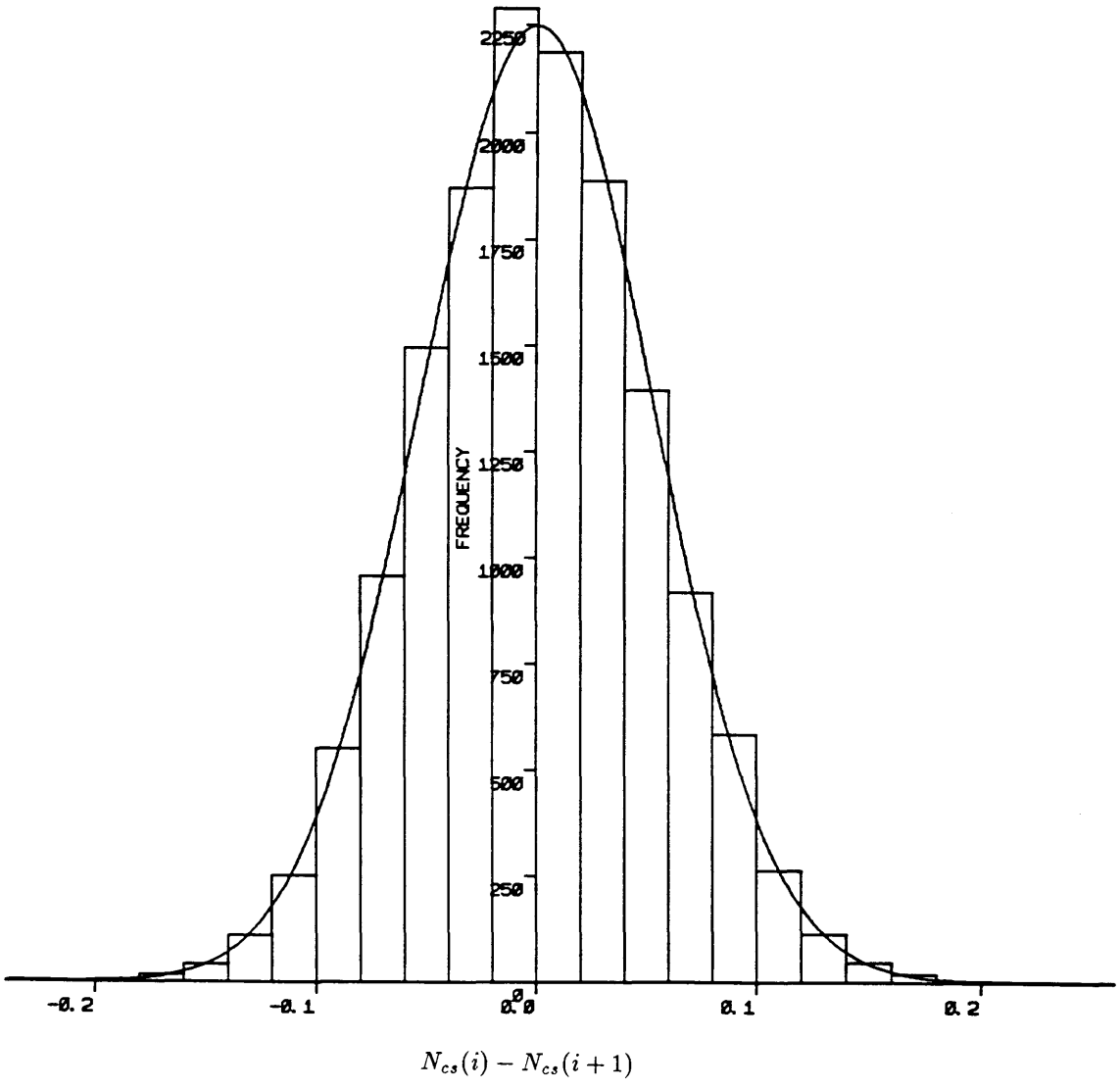

Figure 6.18

A typical histogram of $N_{cs}(i) - N_{cs}(i+1)$ with a gaussian distribution which has the same mean and standard deviation superimposed (solid line). Consecutive measurements of N_{cs} have been made every 0.5 units of lattice time, so that there are 15000 measurements contributing to the histogram.

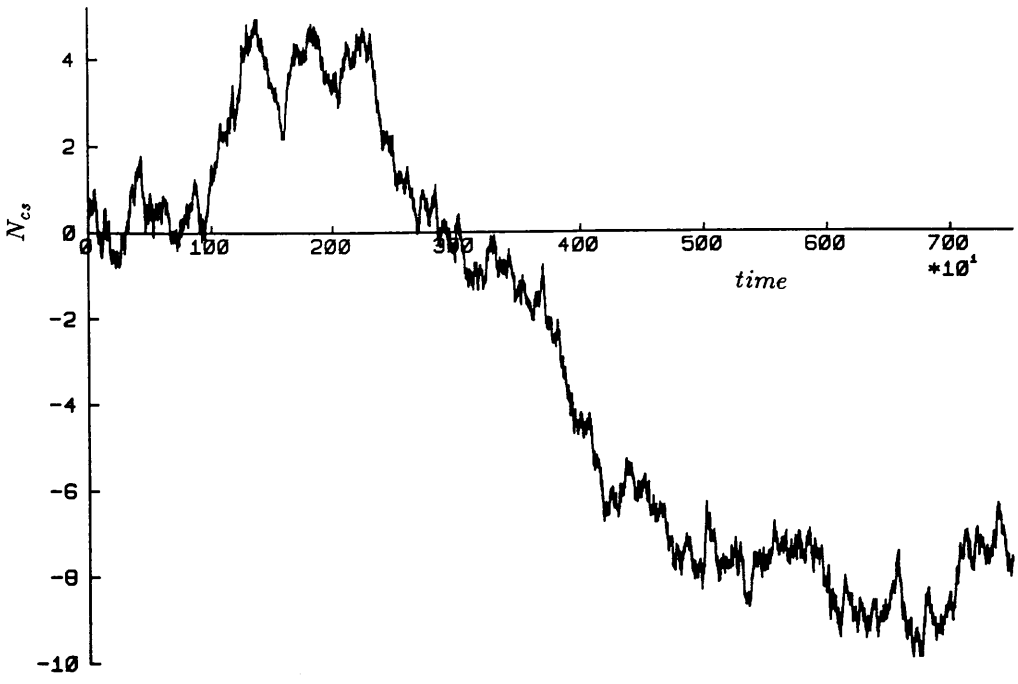

Figure 6.19

A random walk in N_{cs} generated from a gaussian probability function with a mean and standard deviation corresponding to the lattice data set plotted out in figure 6.2.

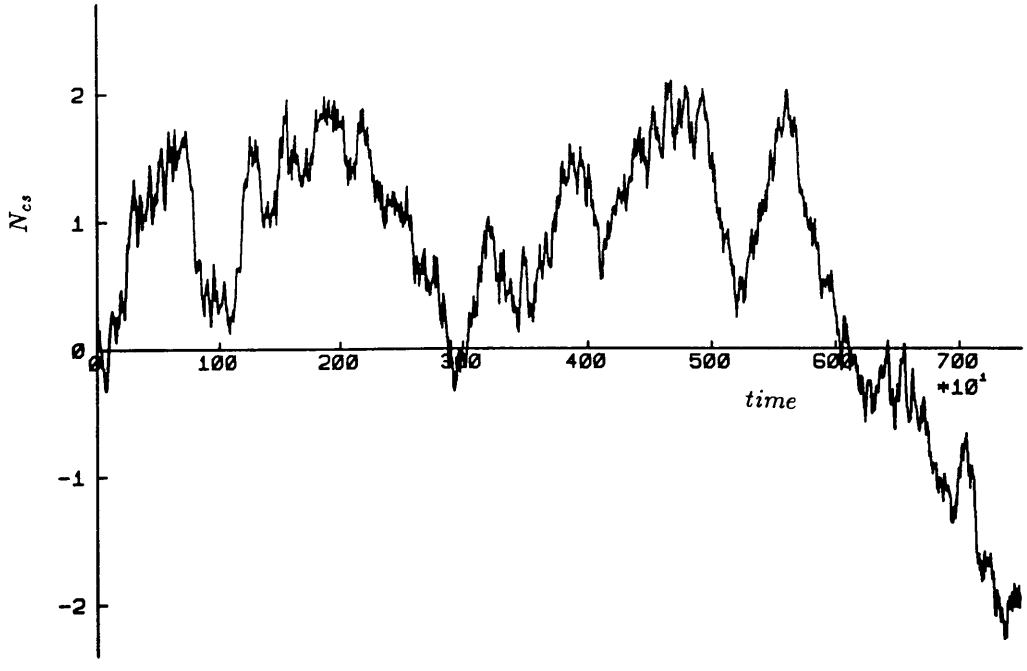

Figure 6.20

A random walk in N_{cs} generated from a gaussian probability function with a mean and standard deviation corresponding to the lattice data set plotted out in figure 6.4.

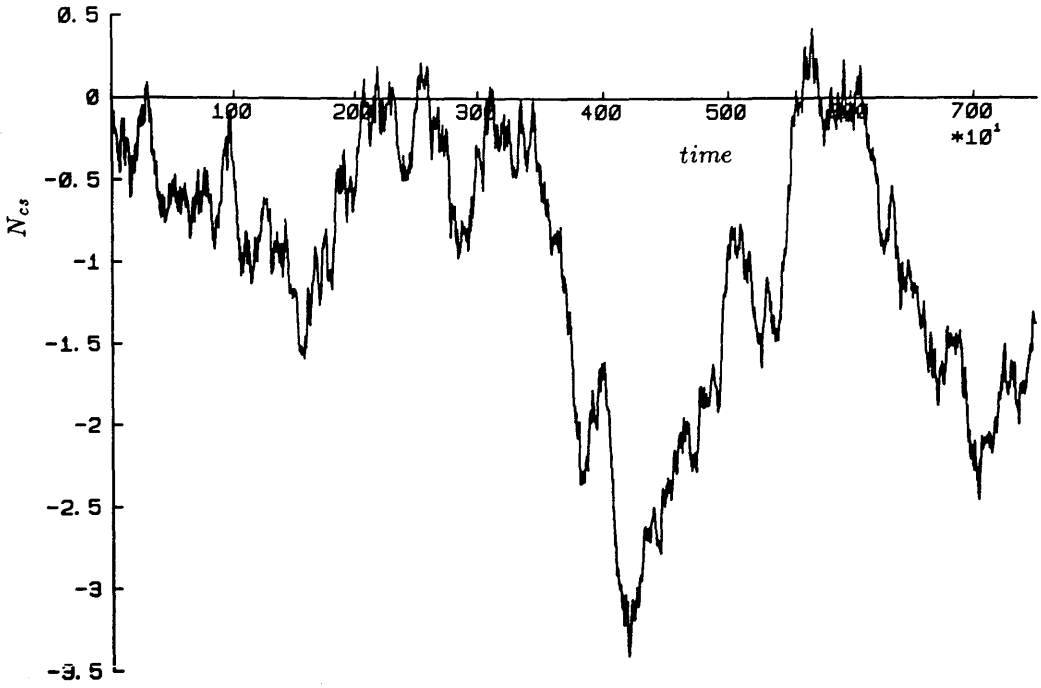

Figure 6.21

A random walk in N_{cs} generated from a gaussian probability function with a mean and standard deviation corresponding to the lattice data set plotted out in figure 6.5.

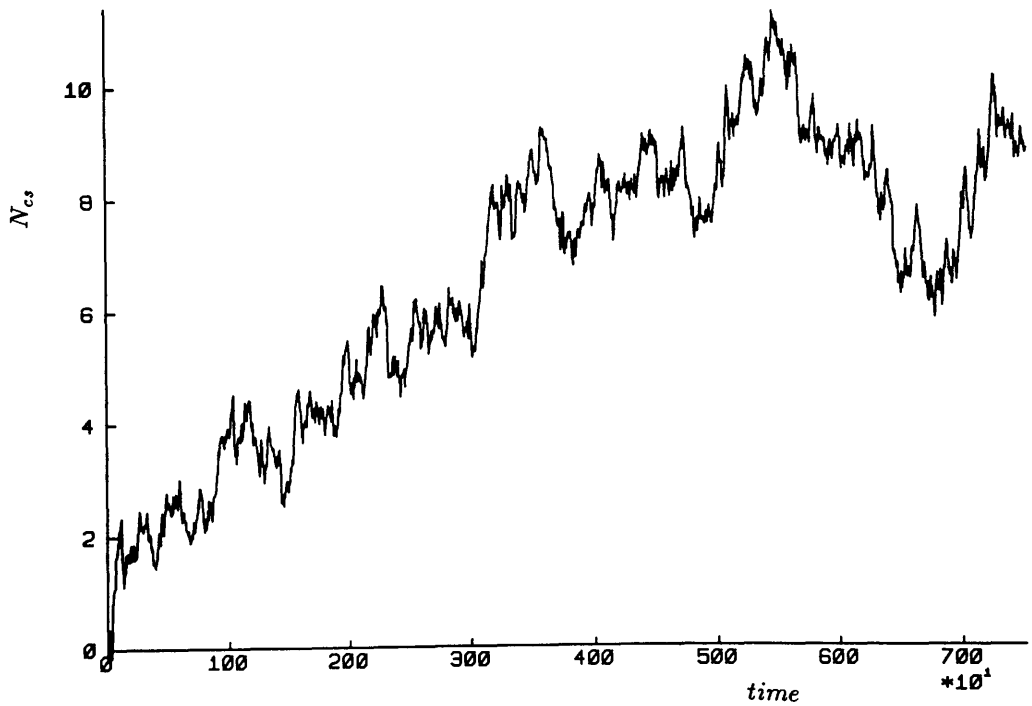

Figure 6.22

A random walk in N_{cs} generated from a gaussian probability function with a mean and standard deviation corresponding to the lattice data set plotted out in figure 6.8.

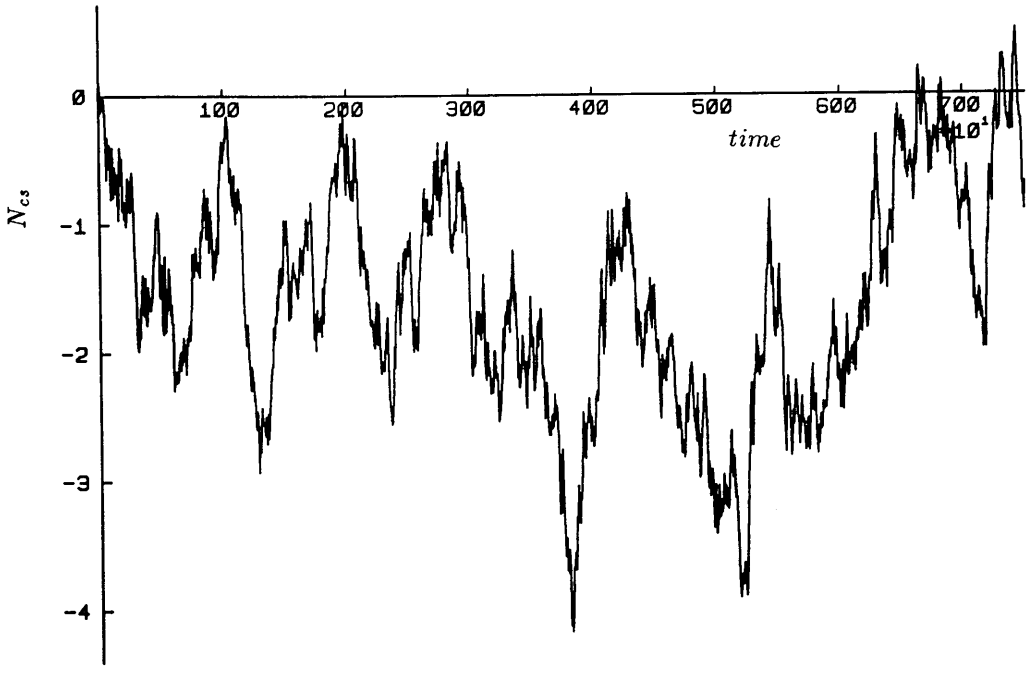

Figure 6.23

A random walk in N_{cs} generated from a gaussian probability function with a mean and standard deviation corresponding to the lattice data set plotted out in figure 6.11.

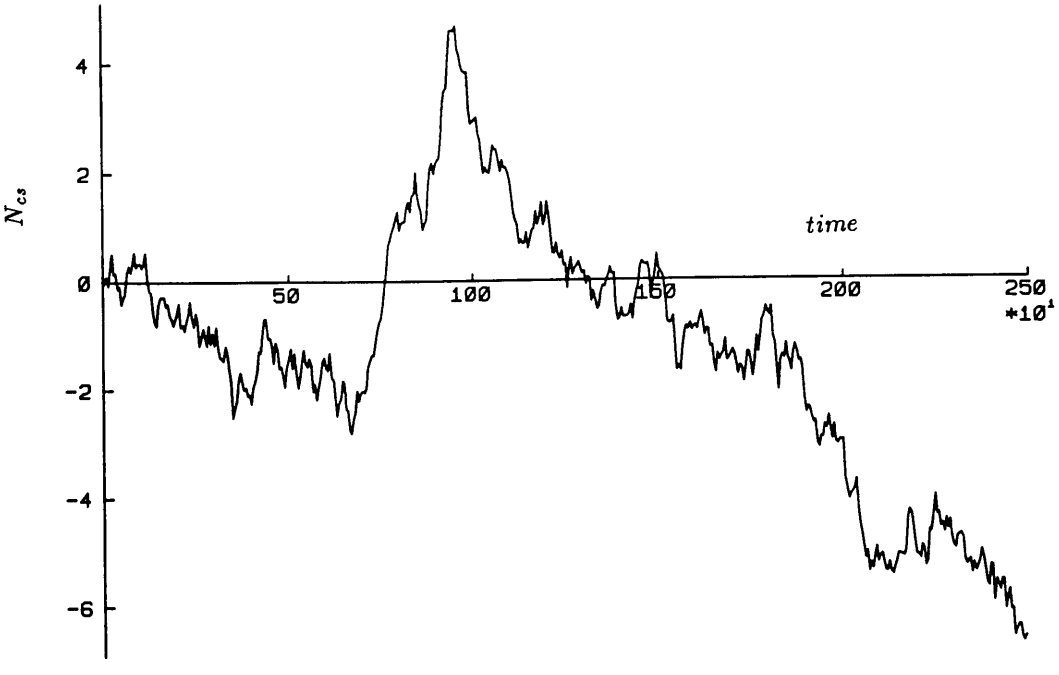

Figure 6.24

A random walk in N_{cs} generated from a gaussian probability function with a mean and standard deviation corresponding to the lattice data set plotted out in figure 6.13.

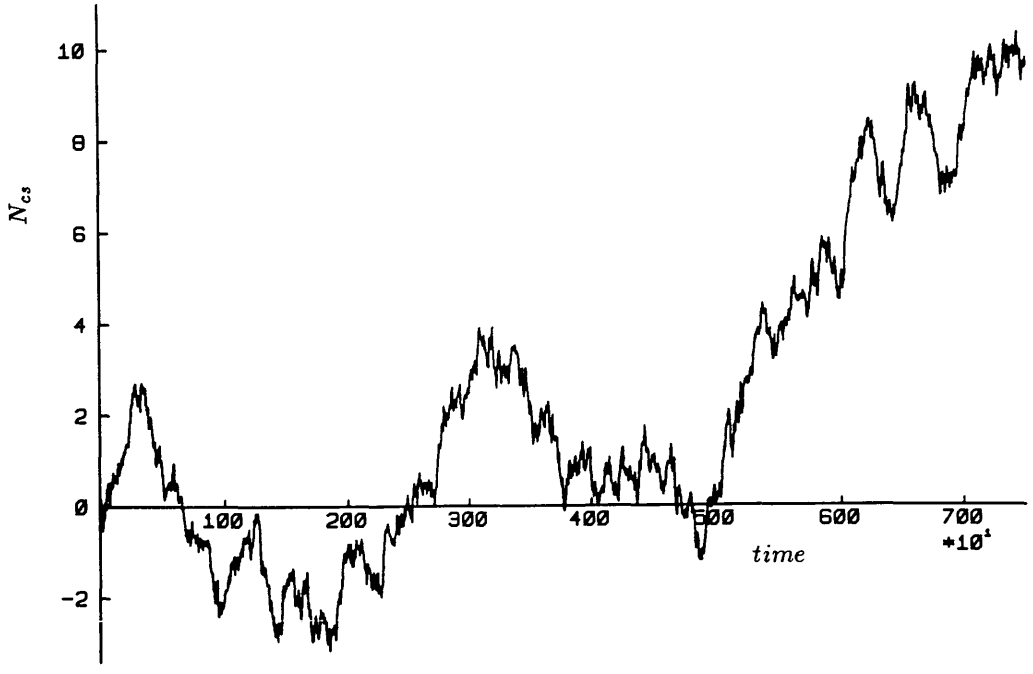

Figure 6.25

A random walk in N_{cs} generated from a gaussian probability function with a mean and standard deviation corresponding to the lattice data set plotted out in figure 6.14.

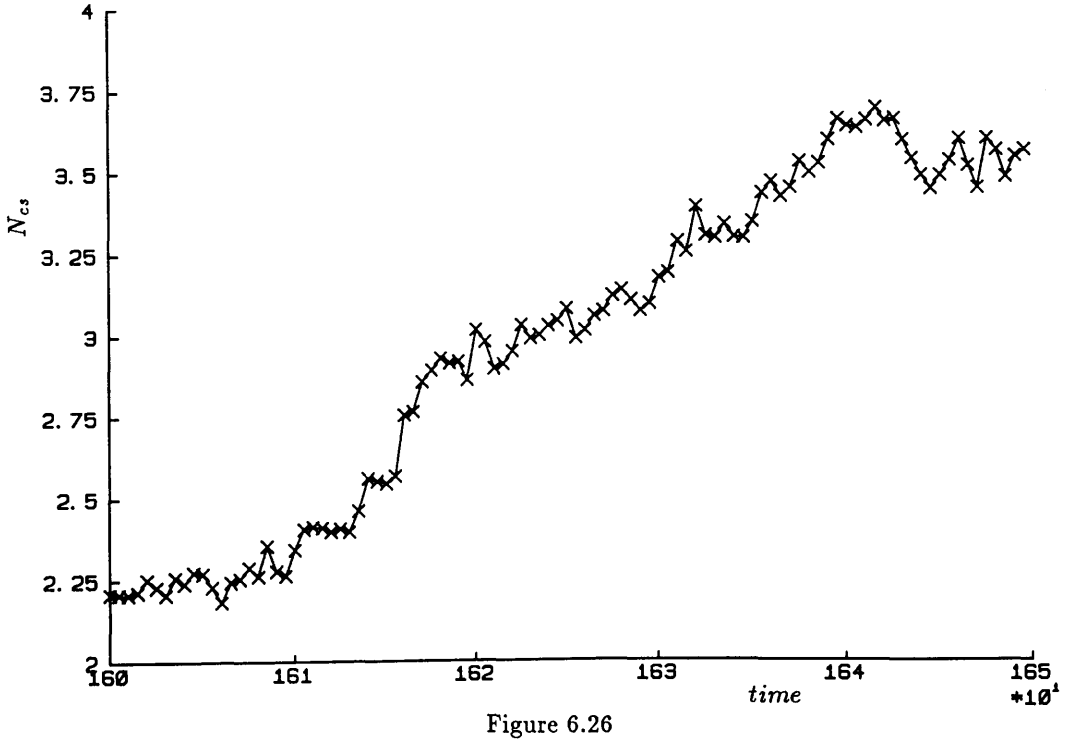

Figure 6.26

Close-up of the random walk of figure 6.19.

Figure 6.27

Close-up of the random walk of figure 6.20.

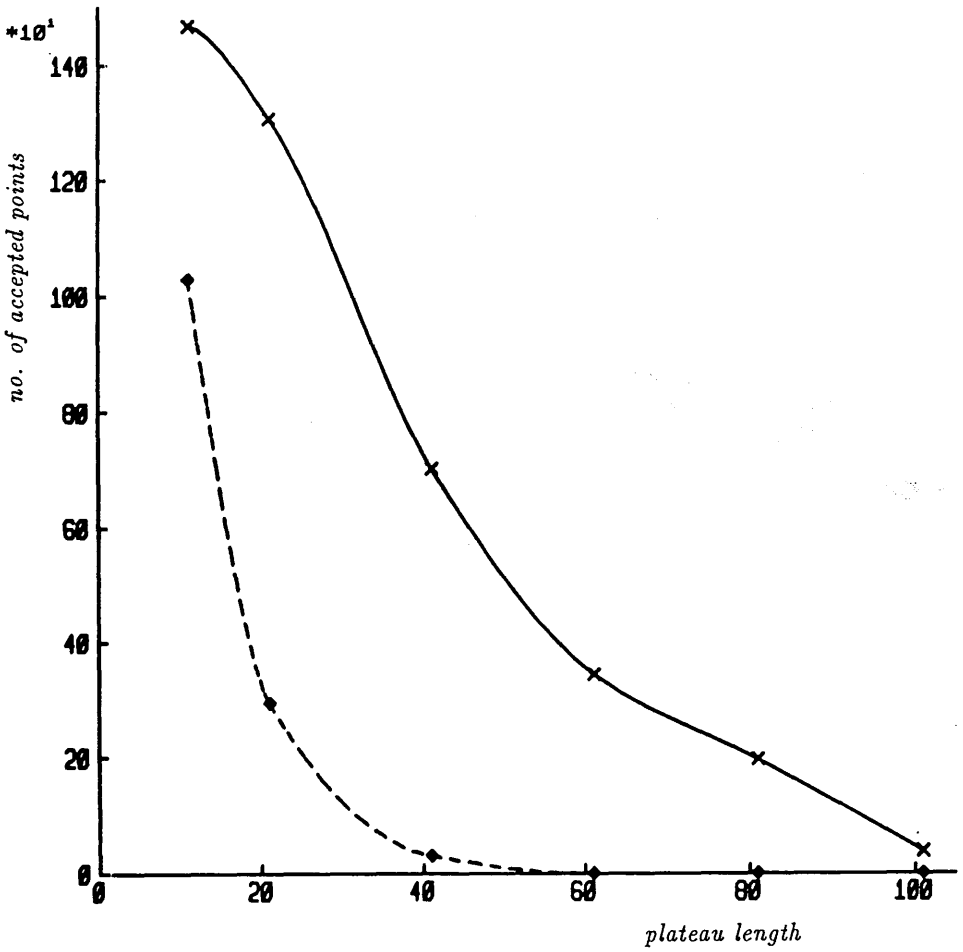

Figure 6.28

The variation of the number of accepted points with the plateau length being imposed. The lattice data (solid line) has many more points associated with plateaus than its corresponding random walk (broken line). The full lattice data set of 1500 measurements of N_{cs} is shown in figure 6.4. The plateau length is expressed as the number of consecutive measurements of N_{cs} being used.

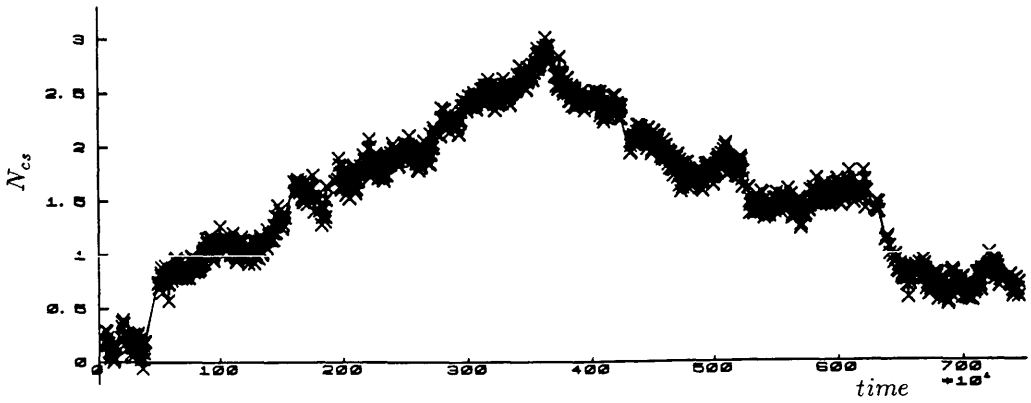

6.29a

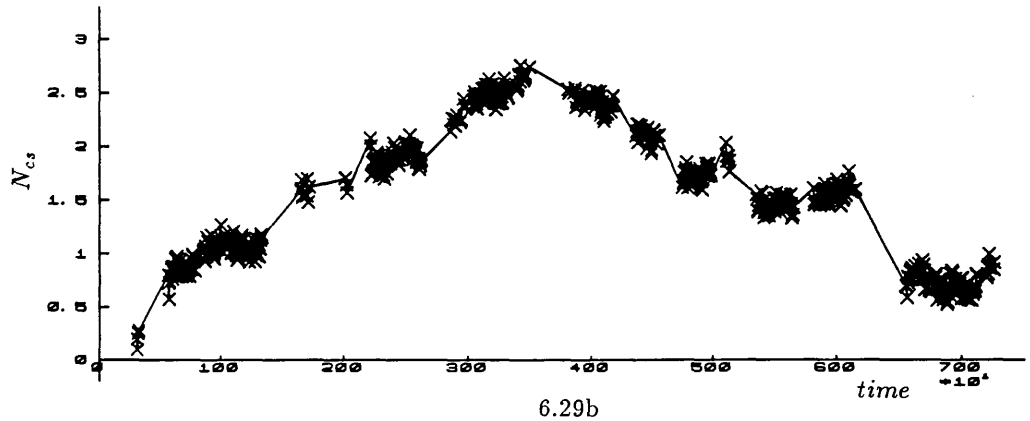

6.29b

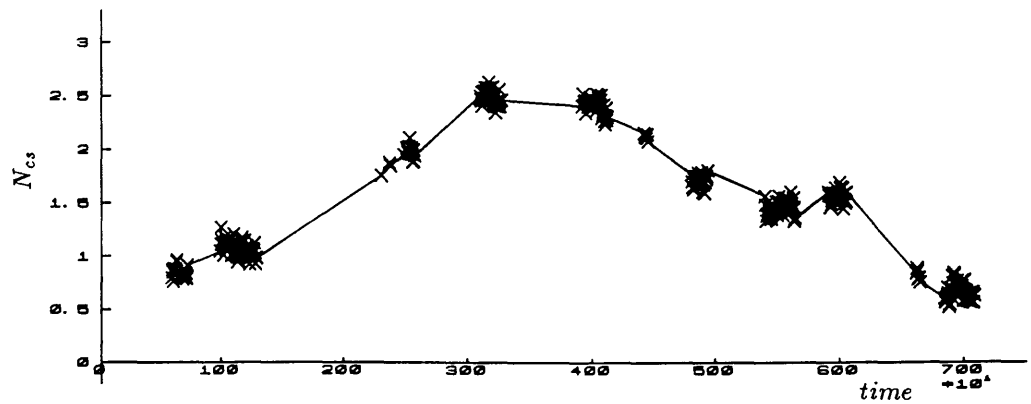

6.29c

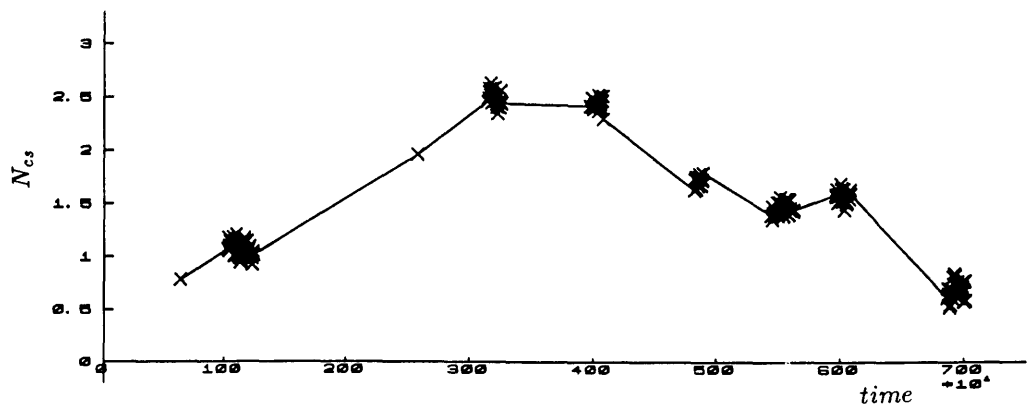

6.29d

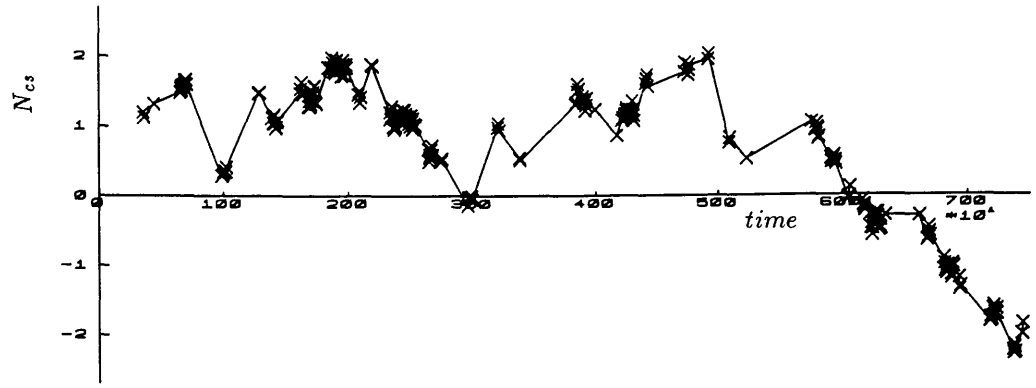

6.29e

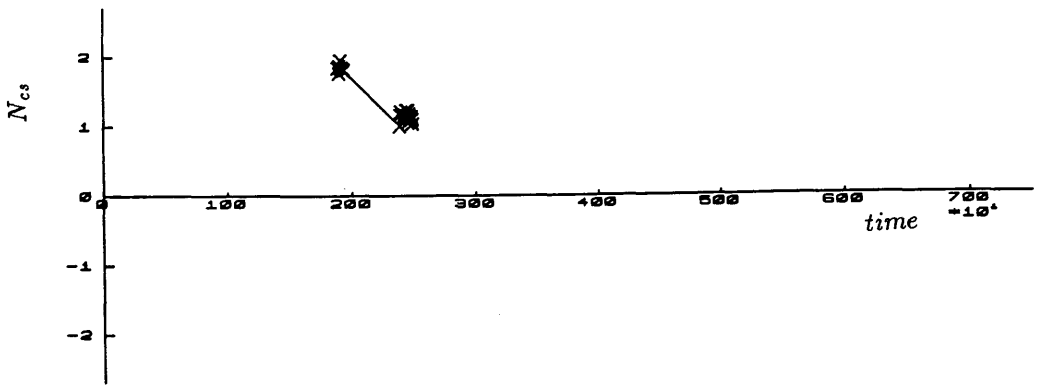

6.29f

Figure 6.29

The evolution of N_{cs} in time showing only those points which are accepted by the plateau selection technique. Graphs a to d show the results of this treatment on a lattice data set using plateau lengths 21, 41, 61 and 81 respectively; again the plateau length is expressed as the number of consecutive measurements of N_{cs}. Graphs e and f show the results for the corresponding random walk using plateau lengths 21 and 41. The full lattice data set is shown in figure 6.4 and the corresponding random walk is shown in figure 6.20.

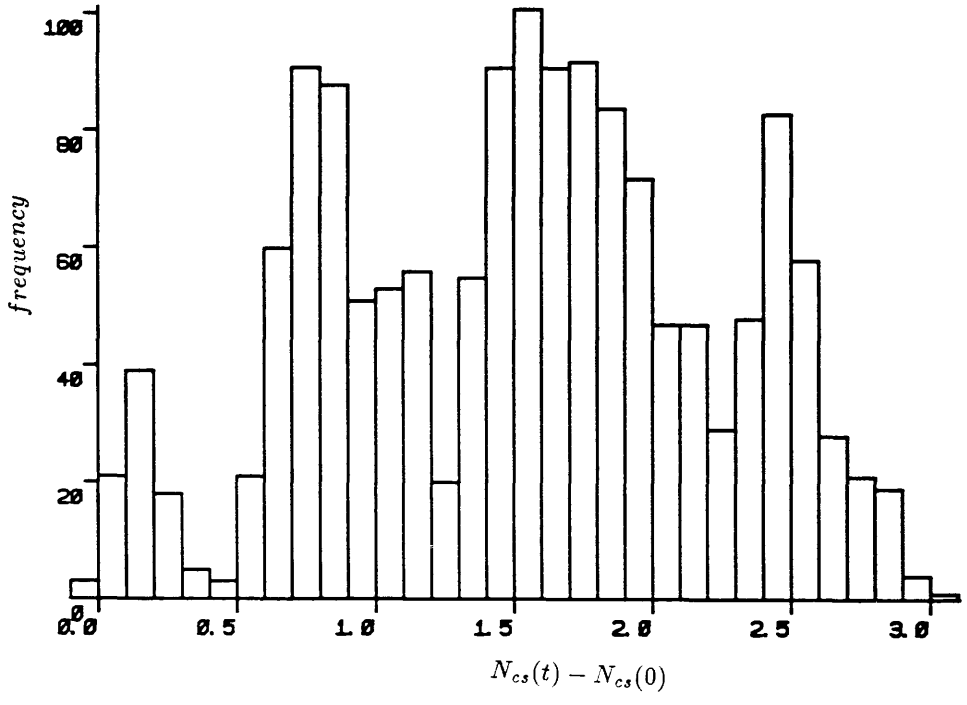

Figure 6.30

Histogram of N_{cs} for $\beta_G = 9.0$, $\beta_H = 0.34$ and $\beta_R = 0.0016$. The lattice size is 8^3. The corresponding plot of N_{cs} versus time is shown in figure 6.4. This histogram seems to highlight a preference for the system to stick around integer values of N_{cs}.

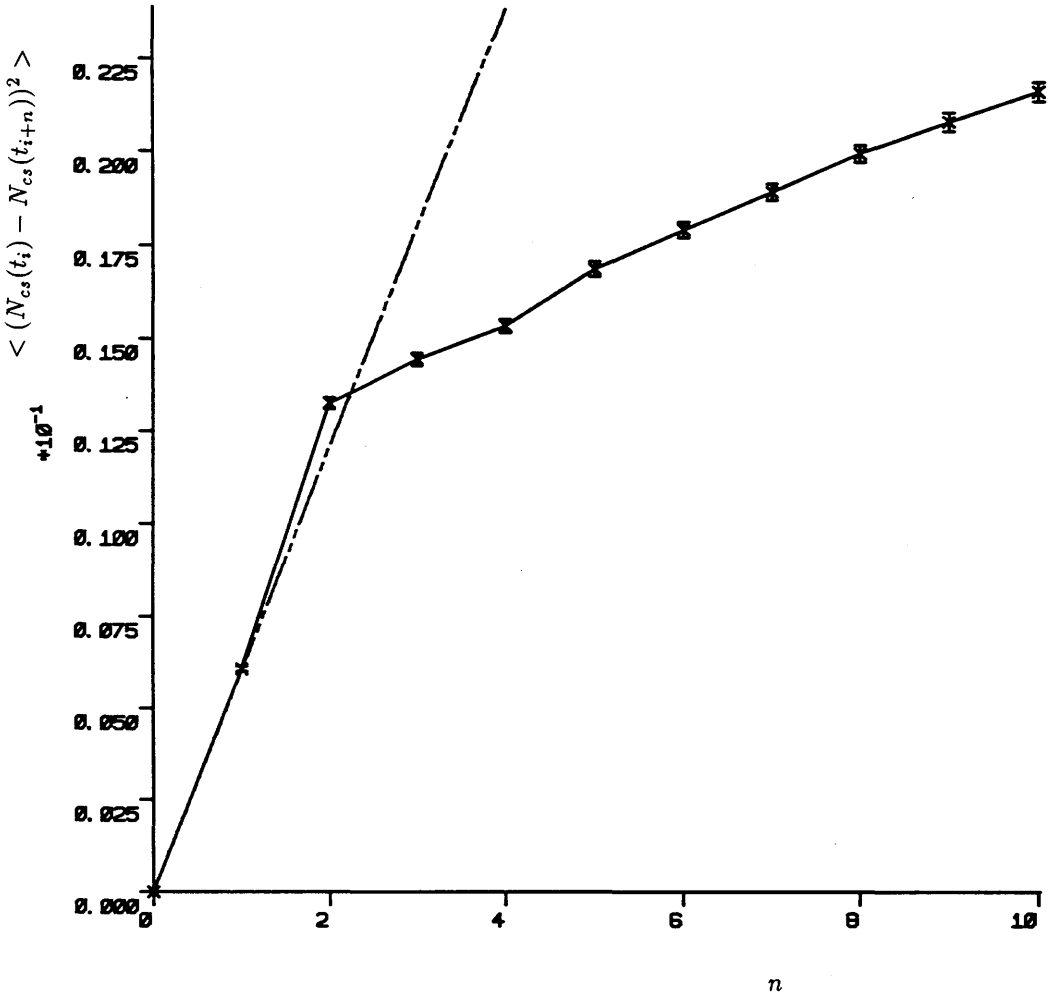

Figure 6.31

$< (N_{cs}(t_i) - N_{cs}(t_{i+n}))^2 >$ as a function of the separation of measurements, n. The solid line shows the case of the lattice data for which $\beta_G = 10.0$, $\beta_H = 0.34$ and $\beta_R = 0.0014$ on a 12^3 lattice. The error bars are a measure of the statistical error only; it seems clear that there is a much larger systematic error present. The broken line indicates the behaviour of random walk data.

Chapter 7

Simulations With a Non-Zero Chern-Simons Density

7.1 Introduction

We want to study the effect of having the additional term $\mu_B N_{cs}$ in the effective action. As outlined in Chapter 3, this term arises from a non-zero fermionic density at high temperature. Shaposhnikov has suggested that such a term could be responsible for B.A.U., provided that the Chern-Simons potential is flat bottomed. The inclusion of $\mu_B N_{cs}$ allows us to explore the shape of this potential. The original aim was to make a large number of independent simulations of a gauge-Higgs system in the hot phase, with a sufficiently long time evolution for the additional term to influence the dynamics. In the early Universe the timescale over which the extra term had effect would be of the order of the age of the Universe at the time of the electroweak phase transition, $t \sim 10^{-11}$secs. After completion of the time development the system would be taken through a first order phase transition and the topological charge, Q, measured. On the lattice this first order phase transition is modelled by an abrupt increase in the gauge Higgs coupling, β_H, to one well inside the broken symmetry regime. The resultant Q distribution would be expected to reflect the asymmetry of the modified Chern-Simons potential. This is in some ways similar to the original work of Ambjørn, Laursen and Shaposhnikov; but they had neither real time development nor the $\mu_B N_{cs}$ term. The motivation now is that it is much easier to detect an asymmetry in a distribution than a difference in terms of flat-

tening from a Gaussian shaped distribution. The original results of Ambjørn et al. were ambiguous because of finite size lattice effects which may distort the distribution of Q anyway. Shaposhnikov and Grigoriev have studied the effect of such a finite chemical potential on a $1+1$ Abelian Higgs model [52]. Although they found no convincing evidence for a degenerate Chern-Simons effective potential, $U(n_{cs})$, this may not rule it out in the full theory. The difference between a $1+1$ Abelian-Higgs model and a $3+1$ non-Abelian Higgs model is non-trivial. For example, as we shall see, the chemical potential is multiplied by a magnetic field in 3 spatial dimensions, but in only one spatial dimension the magnetic field simply does not enter the equations. In practise, rather than perform many different simulations from distinct starting configurations, each yielding a single measurement of Q, we used a few longer runs and measured Q at intervals. If the system is truly ergodic then; provided that the time intervals between measurements is sufficiently long; the consecutive values of Q should be independent and we may build up a distribution using considerably less computer time.

In section 7.2 we describe how the driving term $\mu_B N_{cs}$, is incorporated into the system by the introduction of the magnetic field, B, onto the lattice. The following section describes some preliminary results. Section 7.4 considers how the magnetic field allows a possible alternative approach for the measurements of topological charge. We conclude with a discussion of the problems which seem to be associated with the introduction of the magnetic field, and comment about directions of future work.

7.2 Implementation of the Driving Term, $\mu_B N_{cs}$ on the Lattice

There is no convenient lattice version of N_{cs}. However, if we use the Hamiltonian formalism we find that we have no need for N_{cs} explicitly; the extra term affects

the dynamics only through the E field equations of motion. We have

$$\partial_0 \pi = -\frac{\delta H}{\delta \phi} \tag{7.1}$$

where ϕ is some field and π its conjugate momentum. Putting in the $\mu_B N_{cs}$ term gives

$$H_{eff} = H_0 + \mu_B N_{cs} \tag{7.2}$$

where H_0 is the original Hamiltonian. If we consider the field A_i^a then

$$\partial_0 \pi_i^a = -\frac{\delta H_0}{\delta A_i^a} - \mu_B \frac{\delta N_{cs}}{\delta A_i^a} \tag{7.3}$$

In the continuum

$$\begin{aligned} \frac{\delta N_{cs}}{\delta A_i^a} =& \frac{g^2}{16\pi^2} \epsilon_{ijk} F_{jk}^a \\ =& \frac{g^2}{8\pi^2} B_i^a \end{aligned} \tag{7.4}$$

where B_i^a is the "magnetic" field associated with F_{ij}^a.

$$B_i^a = \frac{1}{2} \epsilon_{ijk} F_{jk}^a \tag{7.5}$$

The problem has become one of putting the magnetic field onto the lattice. To do this we consider

$$Tr(\tau^c U_\Box(x; \hat{j}, \hat{k})) \tag{7.6}$$

where $Tr(\tau^c U_\Box(x; \hat{j}, \hat{k}))$ is a plaquette originating at site x and the j, k^{th} directions. Taking $a \to 0$ we see

$$\begin{aligned} Tr(\tau^c U_\Box(x; \hat{j}, \hat{k})) =& Tr(\tau^c \exp(-ia^2 g F_{jk}^b \frac{\tau^b}{2})) \\ \simeq& -ia^2 g F_{jk}^c \end{aligned} \tag{7.7}$$

We have some approach to discretizing the B field. Next we consider π_i^a, the momentum conjugate to A_i^a. Since

$$\pi_i = \frac{\partial \mathcal{L}}{\partial \dot{\phi}_i} \tag{7.8}$$

We obtain

$$\pi_i^a = -\mathcal{E}_i^a \tag{7.9}$$

where $\mathcal{E}_i^a \equiv F_{0i}^a$; or in the $A_0 = 0$ gauge we have $\mathcal{E}_i^a = \partial_0 A_i^a$. The continuum electric field is closely related to the lattice variable E. To see this we start from eq(4.31) and expand in terms of a.

$$\begin{aligned} E(x,\hat{i})_t =& \frac{1}{\triangle t} U^\dagger_{x,\hat{i}} U_{x+\hat{0},\hat{i}} \\ =& \frac{1}{\triangle t} \exp(iagA_i^a(x)_t) \exp(-iagA_i(x)_{t+\triangle t}) \\ =& \frac{1}{\triangle t}(I + iag(A_i(x)_t - A_i(x)_{t+\triangle t})) \end{aligned} \tag{7.10}$$

But $\triangle t E(x,\hat{i})_t$ is an $SU(2)$ matrix, and in the limit $\triangle t \to 0$, $\triangle t E^4(x,\hat{i})_t$ is very close to 1. So

$$i\tau^a E^a(x,\hat{i})_t = -\frac{iag}{2}\tau^a \frac{\partial A_i^a}{\partial t}(x)_t \tag{7.11}$$

Thus from the definition of $\mathcal{E}_i^a$

$$E^a(x,\hat{i}) = -\frac{ag}{2}\mathcal{E}_i^a \tag{7.12}$$

Using eq.(7.3) we find that the E field equations are modified

$$\frac{dE_i^a}{dt} = -i\frac{\mu_B}{8\pi^2\beta_G}\epsilon_{ijk} Tr(\tau^a U_\Box(x;\hat{j},\hat{k})) + ... \tag{7.13}$$

so we add on a term

$$-i\frac{\mu_B}{8\pi^2\beta_G}\triangle t \epsilon_{ijk} Tr(\tau^a U_\Box(x;\hat{j},\hat{k})) \tag{7.14}$$

to the right hand side of eq.(4.38).

It is trivial to see that $\delta N_{cs}/\delta A_0 = 0$, so that in the the continuum the additional term is perfectly compatible with the Gauss constraint. Unfortunately it is impossible to impose the Bianchi identity exactly on the lattice for a non-Abelian gauge theory. The Bianchi identity takes the form

$$D_\mu F_{\nu\rho} + D_\nu F_{\rho\mu} + D_\rho F_{\mu\nu} = 0 \tag{7.15}$$

The violation on the lattice is well known and can be seen by simply studying the flux out of a cube on the lattice.

To understand what is happening we consider a simple Abelian system for which eq.(7.3) becomes

$$\frac{dE_i^a}{dt} = -\mu B_i^a \tag{7.16}$$

Thus

$$\frac{d}{dt}(\partial_i E_i^a) = -\mu(\partial_i B_i^a) \tag{7.17}$$

so if the Bianchi identity $\partial_i B_i^a$ is non-zero then the time independence of the value of the Gauss constraint disappears.

The problem of the violation of this constraint is clearly worrying, and it remains an important consideration in all lattice simulations which use the approach outlined above.

In adding the extra term $\mu_B B$ to the lattice it was found to be best to average over the four plaquettes which originate at site x and are associated with the plane orthogonal to $E(x,\hat{i})$; averaging reduced the growth of the size of the Gauss constraint compared with picking only one of the plaquettes. The reason that we may only consider plaquettes *originating* from site x, is that then the E field and the plaquette transform in the same way under a gauge transformation $V(x)$.

$$\begin{aligned} E(x,\hat{i}) &\rightarrow V(x)E(x,\hat{i})V^\dagger(x) \\ U_\Box(x;\hat{i},\hat{j}) &\rightarrow V(x)U_\Box(x;\hat{i},\hat{j})V^\dagger(x) \end{aligned} \tag{7.18}$$

The next section discusses the behaviour of the lattice system with the $\mu_B N_{cs}$ term added to the E field equations of motion.

7.3 Preliminary Results

Measurements of N_{cs} against time for a range of μ_B were obtained exactly as for $\mu_B = 0$, except that Gauss cooling was used during the real time evolution to control the constraint. An approximate guide to appropriate values of μ_B to use on the lattice is provided be eq.(7.13). Since $E^a \sim \triangle t$, the additional term in the E field equations must be small compared to $\triangle t$ if it is be considered as

a perturbation on the system.

$$-i\frac{\mu_B}{8\pi^2\beta_G}\epsilon_{ijk}Tr(\tau^a U_\Box(x;\hat{j},\hat{k})) \ll 1 \tag{7.19}$$

or defining

$$\mu_L = -\frac{\mu_B}{8\pi^2\beta_G} \tag{7.20}$$

then

$$\mu_L \ll \frac{1}{4} \tag{7.21}$$

Figure 7.1 shows time evolution pictures for a very large positive and negative value of μ_L; the drift in N_{cs} is an obvious effect and its sign is determined by that of μ_L. In figure 7.2 a much smaller value of μ_L has been used and the systematic drift in N_{cs} is much less pronounced. Problems with energy conservation and lack of computer time have prevented a more thorough study of non-zero μ_B. Despite similar problems with energy conservation our collaborators in Denmark have studied the distribution of Q between the unbroken and broken symmetry phases, but have seen no evidence of an asymmetry which would signal non-trivial degeneracy of $U(n_{cs})$ [51]. It should be clear that the large N_{cs} values obtained by using relatively large values of μ_L have nothing to do with the production of the baryon asymmetry. The corresponding physical picture is illustrated schematically by figure 3.3.

7.4 The Magnetic Field and Topology

Here we discuss a suggestion made by Ambjørn that the possibility of using the alternative expression for Q based on expressing $F\tilde{F}$ in terms of the product of the electric and magnetic fields, $\mathcal{E}.B$, may be fruitful in both the time development of the hot phase and in the cooling procedures.

Q may be expressed in terms of the electric and magnetic fields:

$$Q = \frac{g^2}{8\pi^2}\int \mathcal{E}_i^a B_i^a d^4x \tag{7.22}$$

where $\mathcal{E}_i^a \equiv F_{0i}^a$ and $B_i^a \equiv 1/2\epsilon_{ijk}F_{jk}^a$. The most immediate advantage of such an approach is that there is no longer any need to embed the 3-dimensional

lattice in a 4-dimensional one. In addition where $\mu_B \neq 0$ we should already have an expression for the magnetic field B_i^a; and so the algorithm to calculate the change in the Chern-Simons number within the hot phase, during the time evolution, would become relatively simple and thus computationally efficient. Even measuring Q, the change in topological charge from cooling the system from the hot phase into the cold broken symmetry phase, might become faster, again because although formalism for the magnetic field would be required, the need to embed the system would vanish.

Lack of computer resources has prevented a proper study of this possibility, we were only able to try measuring N_{cs} in addition to the original method for a few of the runs at $\mu_B = 0$. The results were very disappointing, and did not seem to bear any resemblence to the measurement of N_{cs} used elsewhere. For this reason these results were not discussed in Chapter 6. One reason for mistrusting this method of measuring N_{cs} is that the implementation of the magnetic field may not be reliable, we have seen in the previous section how the addition of the $\mu_B B$ term to the electric field equations of motion seems to be causing problems, and it may well be that the rather naïve approach to discretizing the magnetic field is responsible for the problems here. Clearly further investigation is needed to address these problems.

7.5 Conclusions

Both Section 7.3 and 7.4 have uncovered difficulties with our approach to the lattice. A possible explanation for the problems at $\mu_B \neq 0$ could be that the magnitude of $D_i B_i$ is large. Great effort has been made to ensure that $D_i E_i$, the Gauss constraint, is as small as possible and yet if the Bianchi identities are to be at least approximately satisfied on the lattice then $D_i B_i$ should be small too. It is tempting to suggest that all the problems are due entirely to our lattice prescription for the B field. If we are averaging over four plaquettes to get the B field along some link then the four individual contributions should be reasonably close in magnitude. In fact, it appears that the four plaquettes

are not at all equal, preliminary investigations show that they vary in sign and quite widely in magnitude. The most obvious way forward would be to find some more satisfactory approach to discretizing the magnetic field and seeing if this improves energy conservation at $\mu_B \neq 0$ or measurement of Q through the approach outlined in Section 7.4. Further, a measurement of $D_i B_i$ on the lattice would be extremely useful.

Although it is disappointing not to have more positive results, the work here has indicated areas of difficulty that are important considerations for lattice simulations which aim to test Baryon number production at the electroweak phase transition.

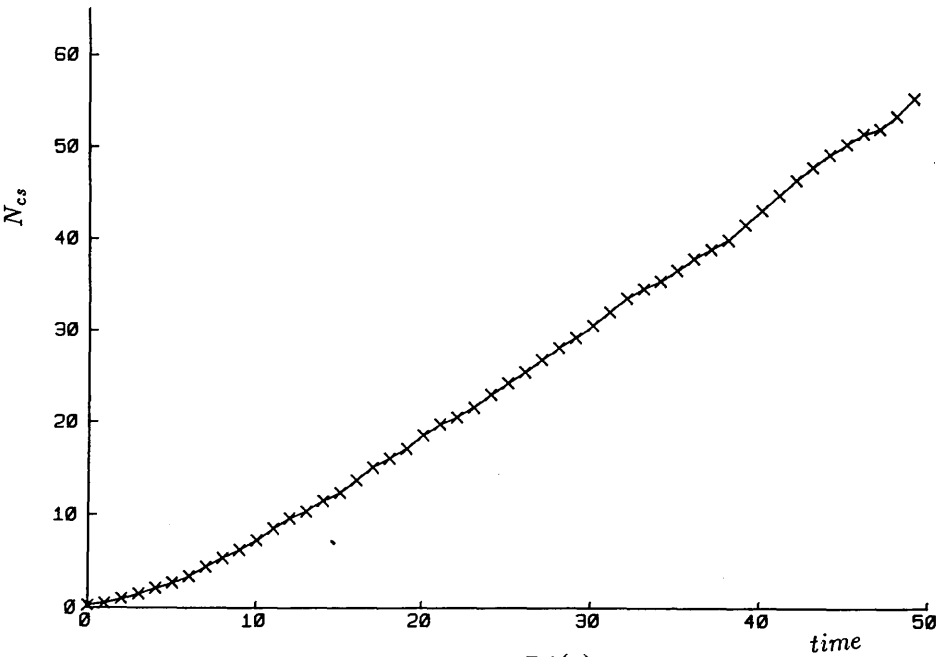

7.1(a)

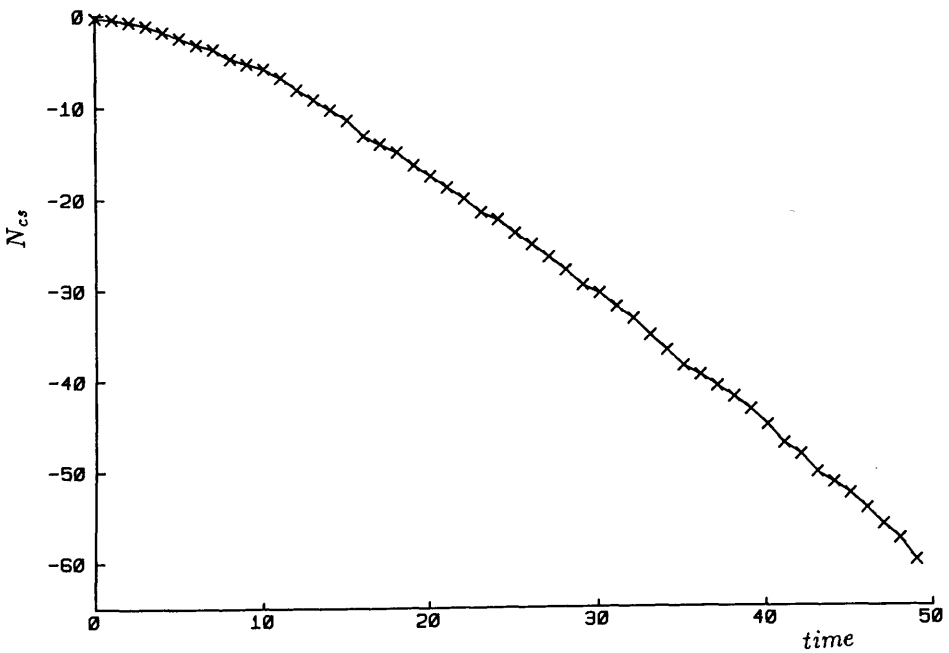

7.1(b)

Figure 7.1

N_{cs} as a function of time for (a) $\mu_L = 0.2$ and (b) $\mu_L = -0.2$. $\beta_G = 8.0$, $\beta_H = 0.32$ and $\beta_R = 0.0016$. $\triangle t = 0.01$ and the lattice size is 8^3.

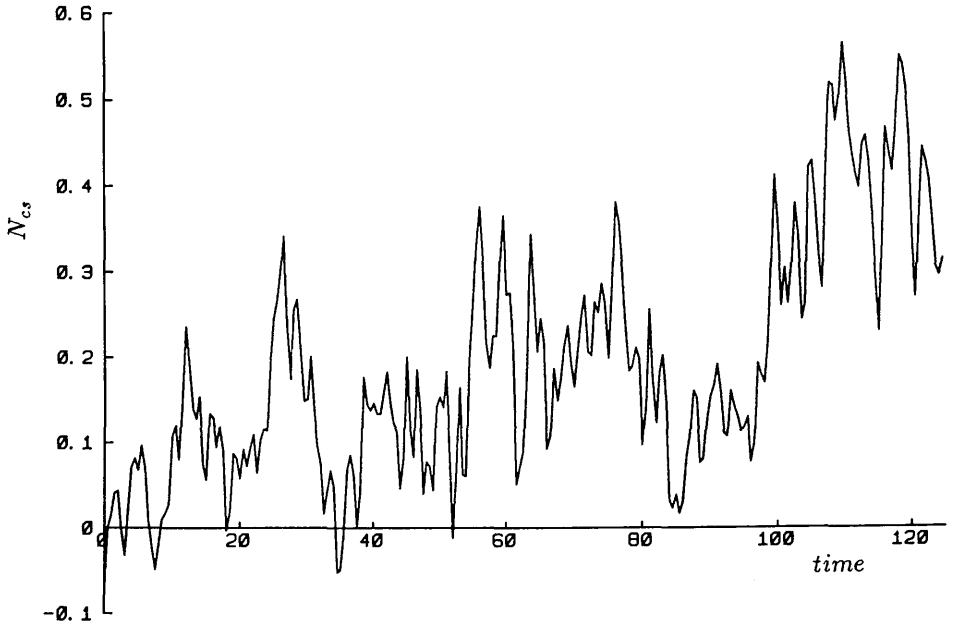

Figure 7.2

N_{cs} as a function of time for $\mu_L = 0.01$ and $\Delta t = 0.05$. $\beta_G = 8.0$, $\beta_H = 0.32$ and $\beta_R = 0.0016$. The lattice size is 8^3.

Conclusions

Our conclusions regarding Chapters 1 and 2 are reasonably straightforward. Ma's claim that his new model could quite easily give a large $\Delta I = 1/2$ amplitude for $K \to 2\pi$ has been shown to be incorrect. The existence of an algebraic error in his calculation has been highlighted. Additionally, the neglect of pseudoscalar terms in the interaction Lagrangian ensures that the matrix element for $K \to 2\pi$, mediated solely by the new particles, is zero. However, even with the pseudoscalar interactions restored, the new model seems unable to provide a mechanism that is sufficient to explain the $\Delta I = 1/2$ selection rule without resorting to non-perturbative coupling strengths and new particle masses at the TeV. scale. Of course, we have little guarantee that our approach to the calculation of the model's contribution is accurate, we have discussed the uncertainties that surround the evaluation of the hadronic matrix elements, and further the difficulties of including the contribution of soft gluon propagators if we use a perturbative approach. The same problems plague the Standard Model calculation. Even if it could be shown that the calculational techniques that we have used give an underestimate of the new model's contribution then it is likely that the same applies to the Standard Model calculation. Thus we are left with the choice that either some as yet unknown mechanism is responsible for the $\Delta I = 1/2$ rule, or that the Standard Model may itself be sufficient.

The remaining work of the thesis is more complicated when considering its implications. The formalism of our approach has been used successfully in $1+1$ dimensions previously, and we have good reason to believe that it is equally valid in $3+1$ dimensions. We are close to having agreement with the equipartition of energy theorem, we have good energy conservation during the time evolution and further, the Gauss constraint remains almost constant for $\mu_B = 0$. Despite the problems associated with the measurement of topological quantities on a lattice, the investigations to determine the sphaleron transition rate by measuring the change in the Chern-Simons number, N_{cs}, at $\mu_B = 0$ in the hot

phase were encouraging. Not only was a rate measured, but it lent weight to the claim that the transitions are unsuppressed in the hot phase, promoting the more general suggestion that the electroweak theory has a major role to play in baryogenesis. In addition, the thermal average $< N_{cs}^2 >$ measured on the lattice was in surprisingly good agreement with the first order perturbative estimate. As always in lattice gauge theory we claim that larger lattices would give improved results, but in the broken symmetry phase it seems to be impossible to measure the sphaleron transition rate given the limits on available lattice sizes. The determination of such a rate would also be very significant, although there seems to be less disagreement about the theoretical estimates of this rate in the literature. Lack of computing time prevented an examination of the distribution of the time intervals between successive sphaleron jumps.

The situation at $\mu_B \neq 0$ clearly requires considerable future effort, our naïve approach of adding a magnetic field B onto the equations of motion to simulate the $\mu_B N_{cs}$ term is not working. It may be that a more satisfactory approach to putting B onto the lattice can be found, or else a fresh approach to the problem uncovered. Topological measurements are more of a problem here, the distribution of the difference in N_{cs} between the hot and cold phases is needed because it is an asymmetry in this distribution that would signal non-trivial degeneracy of the Chern-Simons potential above the phase transition. The dependence of the value of Q on the choice of cooling equations has been discussed, but hopefully an asymmetric signal would be fairly robust to the choice of such equations.

This thesis has studied two diverse facets of the electroweak theory. There are naturally other areas of interest relating to this theory, but the the one feature that combines the two chosen topics has been the incontravertable experimental evidence that remains unsatisfactorily explained despite many years of effort.

Appendix A

Correction to Ma's Model

The error in equation (17) of the paper by Ma is pointed out and corrected here.

Choosing $m_1 = M$ and defining $x = m_2/M$ and substituting into the given expression for the Kaon mass difference leads to

$$\Delta m_K \propto \frac{g_1^2 g_2^2 \sin^2\theta \cos^2\theta}{16\pi^2 M^2} h(x) \tag{A.1}$$

where

$$h(x) \equiv \left(\frac{(1 - 4x - 6x^2 - 4x^3 + x^4)}{4(1-x^2)^2} - \frac{x^2(1 + x^2 + 4x)}{(1-x^2)^3} \ln x \right) \tag{A.2}$$

rather than

$$\Delta m_K \propto \frac{g_1^2 g_2^2 \sin^2\theta \cos^2\theta}{16\pi^2 M^2} h'(x) \tag{A.3}$$

and

$$h'(x) \equiv \left(\frac{(1 - 4x - 6x^2 - 4x^3 + x^4)}{4(1-x^2)^2} - \frac{x^2(1 + x)^2)}{(1-x^2)^3} \ln x \right) \tag{A.4}$$

as quoted by Ma.

The difference between $h(x)$ and $h'(x)$is shown in the graph below; $h(x)$ has only one root at $x = 1$; so Δm_K is small only when m_1 and m_2 are close. However $h'(x)$ has two roots, away from $x = 1$, incorrectly suggesting that it is possible to obtain a small $K_L - K_S$ mass difference other than at $m_1 = m_2$. This is significant because it can be shown that a large penguin amplitude is only obtained away from $m_1 = m_2$; at $m_1 = m_2$ the penguin amplitude is zero.

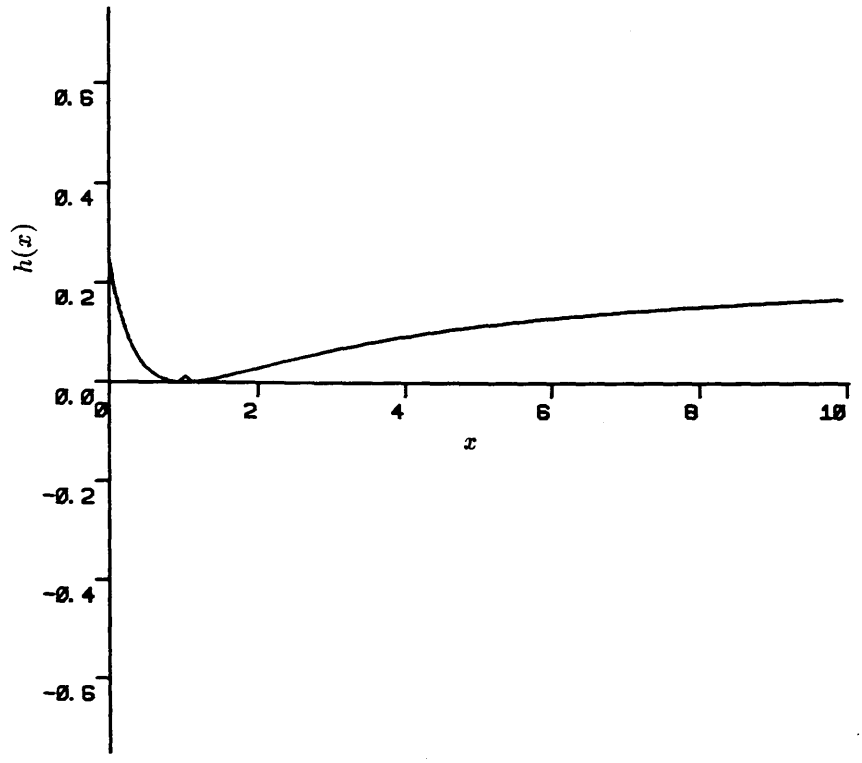

Figure A.1

The function $h(x)$.

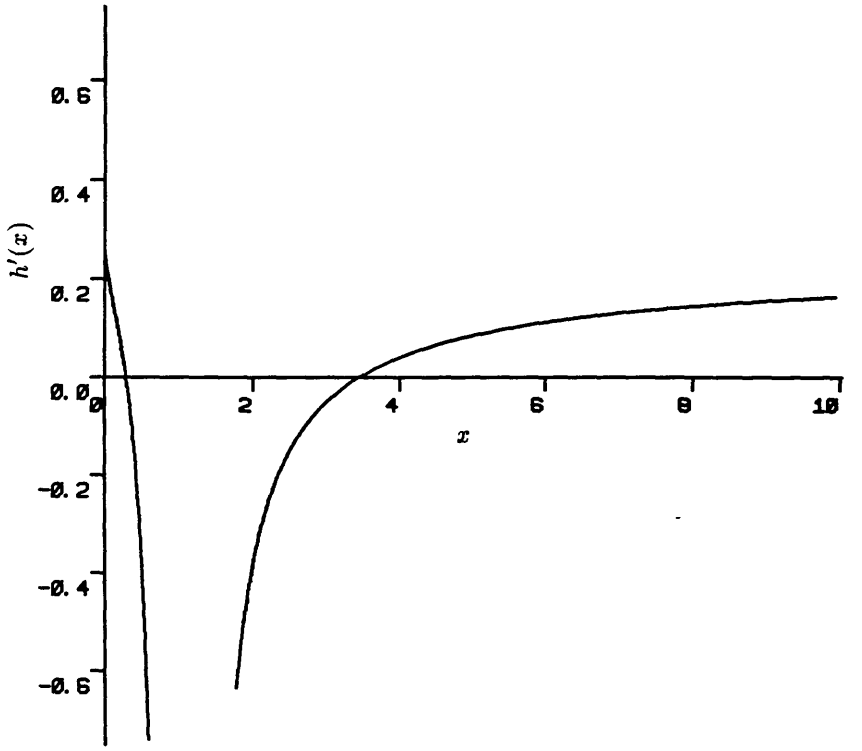

Figure A.2

The function $h'(x)$.

Appendix B

Notation and Feynman Rules

B.1 Mixing Angles

$$\begin{pmatrix} h_1 \\ h_2 \end{pmatrix} = \begin{pmatrix} \cos\theta & \sin\theta \\ -\sin\theta & \cos\theta \end{pmatrix} \begin{pmatrix} H_1 \\ H_2 \end{pmatrix} \tag{B.1}$$

$$\begin{pmatrix} \phi_1 \\ \phi_2 \end{pmatrix} = \begin{pmatrix} \cos\alpha & \sin\alpha \\ -\sin\alpha & \cos\alpha \end{pmatrix} \begin{pmatrix} \Phi_1 \\ \Phi_2 \end{pmatrix} \tag{B.2}$$

B.2 Feynman Rules for the Lagrangian eq(2.2)

Vertex Factors

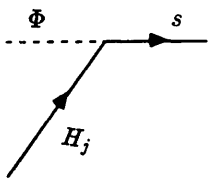

$$i\frac{g_B}{2}(-1)^j(\sin\theta)^{2-j}(\cos\theta)^{j-1}\cos\alpha(1-\gamma_5) \tag{B.3}$$

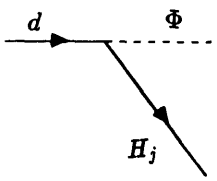

$$-i\frac{g_C}{2}(\sin\theta)^{j-1}(\cos\theta)^{2-j}\sin\alpha(1-\gamma_5) \tag{B.4}$$

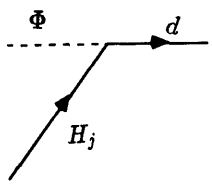

$$-i\frac{g_C}{2}(\sin\theta)^{j-1}(\cos\theta)^{2-j}\sin\alpha(1+\gamma_5) \tag{B.5}$$

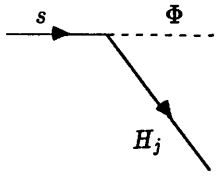

$$i\frac{g_B}{2}(-1)^j(\sin\theta)^{2-j}(\cos\theta)^{j-1}\cos\alpha(1+\gamma_5) \qquad \text{(B.6)}$$

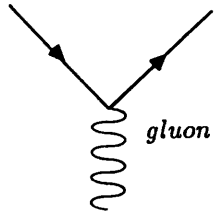

$$ig_S\gamma^\mu\frac{\lambda^\alpha}{2} \qquad \text{(B.7)}$$

Propagators

$$\frac{i}{(k^2-M^2+i\epsilon)} \qquad \text{(B.8)}$$

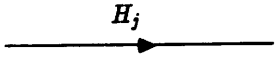

$$\frac{i}{(\not{k}-m_j+i\epsilon)} \qquad \text{(B.9)}$$

Appendix C

Derivation of the Lattice Equations

Suppose we have an element of a Lie algebra, U, then

$$U = e^{i\theta^a T^a} \tag{C.1}$$

where the T^a are the generators of the group.

$$[T^a, T^b] = if^{abc}T^c \tag{C.2}$$

and

$$TrT^aT^b = \frac{1}{2}\delta^{ab} \tag{C.3}$$

so for $SU(2)$, $T^a = \tau^a/2$ with τ^a the Pauli matrices. We consider a function f:

$$\begin{aligned} f(Ue^{i\epsilon^a T^a}) \simeq & f(U(1 + i\epsilon^a T^a)) \\ \simeq & f(U) + i\epsilon^a (UT^a)_{ij} \frac{\partial}{\partial U_{ij}} f(U) \end{aligned} \tag{C.4}$$

Thus

$$f(Ue^{i\epsilon^a T^a}) \simeq f(U) + i\epsilon^a \nabla^a f \tag{C.5}$$

$$\nabla^a f = (UT^a)_{ij} \frac{\partial}{\partial U_{ij}} f(U) \tag{C.6}$$

This is the right Lie derivative, the left derivative is of course equally valid and is just a consequence of multiplying U to the left rather than on the right.

C.1 E Field Equations of Motion

These are obtained by variation with respect to $U_{x,\hat{k}}$. We may gauge fix $U_{x,\hat{0}} = 1$ since these links do not affect the derivation.

The relevant part of the Minkowski action is given by

$$\begin{aligned} S = &- \frac{\beta_G}{2\triangle t^2} \sum_x \sum_i Tr(U_{x,\hat{i}} U^\dagger_{x+\hat{0},\hat{i}}) + \frac{\beta_G}{4} \sum_x \sum_{j\neq i} \sum_j Tr(U_{x,\hat{i}} U_{x+\hat{i},\hat{j}} U^\dagger_{x+\hat{j},\hat{i}} U^\dagger_{x,\hat{j}}) \\ &+ \frac{\beta_H}{2} \sum_x \sum_i (\Phi^\dagger_x U_{x,\hat{i}} \Phi_{x+\hat{i}} + \Phi^\dagger_{x+\hat{i}} U^\dagger_{x,\hat{i}} \Phi_x) + ... \end{aligned} \tag{C.7}$$

For convenience we use the left handed Lie derivative.

$$\nabla^a S = (T^a U_{x,\hat{k}})_{rs} \frac{\partial S}{(\partial U_{x,\hat{k}})_{rs}} \tag{C.8}$$

Then

$$\begin{aligned} \nabla^a S = &- \frac{\beta_G}{2\triangle t^2} Tr(T^a U_{x,\hat{k}} U^\dagger_{x+\hat{0},\hat{k}} - U_{x-\hat{0},\hat{k}} U^\dagger_{x,\hat{k}} T^a) \\ &+ \frac{\beta_G}{4} Tr \{ \sum_{j\neq k} (T^a U_{x,\hat{k}} U_{x+\hat{k},\hat{j}} U^\dagger_{x+\hat{j},\hat{k}} U^\dagger_{x,\hat{j}}) + \sum_{i\neq k} (U_{x-\hat{i},\hat{i}} T^a U_{x,\hat{k}} U^\dagger_{x-\hat{i}+\hat{k},\hat{i}} U^\dagger_{x-\hat{i},\hat{k}}) \\ &\quad - \sum_{j\neq k} (U_{x-\hat{j},\hat{k}} U_{x-\hat{j}+\hat{k},\hat{j}} U^\dagger_{x,\hat{k}} T^a U^\dagger_{x-\hat{j},\hat{j}}) - \sum_{j\neq k} (U_{x,\hat{i}} U_{x+\hat{i},\hat{k}} U^\dagger_{x+\hat{k},\hat{i}} U^\dagger_{x,\hat{k}} T^a) \Big\} \\ &+ \frac{\beta_H}{2} (\Phi^\dagger_x T^a U_{x,\hat{k}} \Phi_{x+\hat{k}} - \Phi^\dagger_{x+\hat{k}} U^\dagger_{x,\hat{k}} T^a \Phi_x) \end{aligned} \tag{C.9}$$

but

$$U_{x+\hat{0},\hat{k}} = \triangle t E(x,\hat{k}) U_{x,\hat{k}} \tag{C.10}$$

It follows that

$$\begin{aligned} \nabla^a S = &- \frac{\beta_G}{2\triangle t} Tr(T^a E^\dagger(x,\hat{k}) - E^\dagger(x-\hat{0},\hat{k}) T^a) \\ &+ \frac{\beta_G}{2} \sum_{i\neq k} Tr(T^a U_{x,\hat{k}} U_{x+\hat{k},\hat{i}} U^\dagger_{x+\hat{i},\hat{k}} U^\dagger_{x,\hat{i}} + T^a U_{x,\hat{k}} U_{x-\hat{i}+\hat{k},\hat{i}} U^\dagger_{x-\hat{i},\hat{k}} U^\dagger_{x-\hat{i},\hat{i}}) \\ &+ i\beta_H Im(\Phi^\dagger_x T^a U_{x,\hat{k}} \Phi_{x+\hat{k}}) \end{aligned} \tag{C.11}$$

Then since $\triangle t E(x,\hat{k})$ is an $SU(2)$ matrix we finally find that setting $\nabla^a S = 0$

gives:

$$E^a(x,\hat{k}) = E^a(x-\hat{0},\hat{k}) - \triangle t \sum_{i\neq k}(U_{x,\hat{k}}U_{x+\hat{k},\hat{i}}U^\dagger_{x+\hat{i},\hat{k}}U^\dagger_{x,\hat{i}} + U_{x,\hat{k}}U^\dagger_{x-\hat{i}+\hat{k},\hat{i}}U^\dagger_{x-\hat{i},\hat{k}}U_{x-\hat{i},\hat{i}})^a$$
$$- 2\frac{\beta_H}{\beta_G}\triangle t Im(\Phi^\dagger_x T^a U_{x,\hat{k}}\Phi_{x+\hat{k}}) \tag{C.12}$$

C.2 P Field Equations of Motion

These are obtained from $\partial S/\partial\phi_j(x)$. The relevant part of the Minkowski action is then:

$$S = \frac{\beta_H}{2}\sum_x\left\{\frac{1}{\triangle t^2}(2\Phi^\dagger_x\Phi_x - \Phi^\dagger_x\Phi_{x+\hat{0}} - \Phi^\dagger_{x+\hat{0}}\Phi_x)\right.$$
$$\left. - (6\Phi^\dagger_x\Phi_x - 2Re\sum_i(\Phi^\dagger_x U_{x,\hat{i}}\Phi_{x+\hat{i}}))\right\} \tag{C.13}$$
$$- \beta_R\sum_x(\Phi^\dagger_x\Phi_x - v^2)^2 + ...$$

Thus

$$\frac{\partial S}{\partial\phi_j} = \beta_H\left\{\frac{1}{\triangle t^2}(2\phi_j(x) - \phi_j(x+\hat{0}) - \phi_j(x-\hat{0})) - 6\phi_j(x)\right.$$
$$\left. + \sum_i(U_{x,\hat{i}}\Phi_{x+\hat{i}})_j + \sum_i(U^\dagger_{x-\hat{i},\hat{i}}\Phi_{x-\hat{i}})_j\right\} - 4\beta_R\phi_j(x)(\Phi^2_x - v^2)^2 \tag{C.14}$$

Setting $\partial S/\partial\phi$ to zero yields:

$$0 = -\frac{\beta_H}{\triangle t}(p_j(x) - p_j(x-\hat{0})) - 6\beta_H\phi_j(x) - 4\beta_R\phi_j(x)(\Phi^2 - v^2)$$
$$+ \beta_H\sum_i(U_{x,\hat{i}}\Phi_{x+\hat{i}} + U^\dagger_{x-\hat{i},\hat{i}}\Phi_{x-\hat{i}})_j \tag{C.15}$$

$$P_x = P_{x-\hat{0}} + \triangle t\left\{\sum_i(U_{x,\hat{i}}\Phi_{x+\hat{i}} + U^\dagger_{x-\hat{i},\hat{i}}\Phi_{x-\hat{i}}) - \left(6 + 4\frac{\beta_R}{\beta_H}(\Phi^2_x - v^2)\right)\Phi_x\right\} \tag{C.16}$$

the P field equations of motion.

C.3 Derivation of the Gauss Constraint

We need to calculate

$$\nabla^a S = (U_{x,\hat{0}} T^a)_{rs} \frac{\partial S}{(\partial U_{x,\hat{0}})_{rs}} \tag{C.17}$$

So the relevant part of the action is

$$\begin{aligned} S = &- \frac{\beta_G}{2\triangle t^2} \sum_x \sum_i Tr(U_{x,\hat{0}} U_{x+\hat{0},\hat{i}} U^\dagger_{x+\hat{i},\hat{0}} U^\dagger_{x,\hat{i}}) \\ &- \frac{\beta_H}{2\triangle t^2} \sum_x (\Phi^\dagger_x U_{x,\hat{0}} \Phi_{x+\hat{0}} + \Phi^\dagger_{x+\hat{0}} U^\dagger_{x,\hat{0}} \Phi_x) + ... \end{aligned} \tag{C.18}$$

Then after some algebra

$$\begin{aligned} \nabla^a S = &- \frac{\beta_G}{2\triangle t^2} \sum_i Tr(U_{x,\hat{0}} T^a U_{x+\hat{0},\hat{i}} U^\dagger_{x+\hat{i},\hat{0}} U^\dagger_{x,\hat{i}} - U_{x-\hat{i},\hat{0}} U_{x-\hat{i}+\hat{0},\hat{i}} T^a U^\dagger_{x,\hat{0}} U^\dagger_{x-\hat{i},\hat{i}}) \\ &- \frac{\beta_H}{2\triangle t^2} (\Phi^\dagger_x U_{x,\hat{0}} T^a \Phi_{x+\hat{0}} - \Phi^\dagger_{x+\hat{0}} T^a U^\dagger_{x,\hat{0}} \Phi_x) \end{aligned} \tag{C.19}$$

Having differentiated we may now fix the gauge, $U_{x,\hat{0}} = 1$. Further,

$$U_{x+\hat{0},\hat{i}} U^\dagger_{x,\hat{i}} = \triangle t E(x,\hat{i}) \tag{C.20}$$

and

$$U^\dagger_{x-\hat{i},\hat{i}} U_{x-\hat{i}+\hat{0},\hat{i}} = \triangle t U^\dagger_{x-\hat{i},\hat{i}} E(x-\hat{i},\hat{i}) U_{x-\hat{i},\hat{i}} \tag{C.21}$$

We also replace $\Phi_{x+\hat{0}}$ by $\Phi_x + \triangle t P_x$ and using $Im(\Phi_x \tau^a \Phi_x) = 0$ we find:

$$\nabla^a S = -i \frac{\beta_G}{2\triangle t} \sum_i (E(x,\hat{i}) - U^\dagger_{x-\hat{i},\hat{i}} E(x-\hat{i},\hat{i}) U_{x-\hat{i},\hat{i}})^a - i \frac{\beta_H}{2\triangle t} Im(\Phi^\dagger_x \tau^a P_x) \tag{C.22}$$

Using

$$E^a = -(E^\dagger)^a \tag{C.23}$$

and

$$(U^\dagger E U)^a = -(U^\dagger E^\dagger U)^a \tag{C.24}$$

We finally arrive at the form of the Gauss constraint given in Chapter 4.

$$G_x \equiv \frac{-i}{\triangle t} \left\{ \frac{\beta_G}{2} \sum_i (U^\dagger_{x-\hat{i},\hat{i}} E^\dagger(x-\hat{i},\hat{i}) U_{x-\hat{i},\hat{i}} - E^\dagger(x,\hat{i}))^a + \frac{\beta_H}{2} Im(\Phi^\dagger_x \tau^a P_x) \right\} = 0 \tag{C.25}$$

Appendix D

The Leapfrog Scheme

Suppose we have a variable h which is a function of time. Then a first order scheme would approximate

$$h(t + \Delta t) = h(t) + \dot{h}(t)\Delta t + \mathcal{O}(\Delta t^2) \tag{D.1}$$

The leapfrog method is a second order scheme using

$$h(t + \frac{\Delta t}{2}) = h(t - \frac{\Delta t}{2}) + \dot{h}(t)\Delta t + \mathcal{O}(\Delta t^3) \tag{D.2}$$

Effectively, the integral $\int_{t_1}^{t_2} dt\, \dot{h}(t)$ is evaluated at the midpoint of the two limits t_1 and t_2, rather than simply at t_1 as in the first order scheme. Thus we have a method of obtaining second order accuracy in t without having to calculate $\ddot{h}(t)$. The main difficulty of this method is that the boundary conditions give $h(t_0)$ but we need $h(t_0 + \Delta t/2)$ as well. In fact the overall accuracy of the method depends quite critically on the accuracy of $h(t_0 + \Delta t/2)$, so $h(t_0 + \Delta t/2)$ must be carefully evaluated by some other method. We used the first order approach but with a smaller timestep to maintain accuracy.

In terms of the specific fields used in the work of this thesis the leapfrog

equations become

$$\begin{aligned}
U(t+\Delta t) &= \Delta t E(t+\frac{\Delta t}{2})U(t) \\
\Phi(t+\Delta t) &= \Phi(t) + \Delta t P(t+\frac{\Delta t}{2}) \\
E(t+\Delta t) &= E(t) + \Delta t f(\Phi(t+\frac{\Delta t}{2}), U(t+\frac{\Delta t}{2})) \\
P(t+\Delta t) &= P(t) + \Delta t g(\Phi(t+\frac{\Delta t}{2}), U(t+\frac{\Delta t}{2}))
\end{aligned} \tag{D.3}$$

f and g are the functions multiplying Δt in equations (4.38) and (4.39).

We begin by evaluating $U(t+\Delta t/2)$ and $\Phi(t+\Delta t/2)$ using the first order scheme with a reduced timestep. The next stage is the evaluation of $E(t+\Delta t)$ and $P(t+\Delta t)$. The following step is then the evaluation of $U(t+3\Delta t/2)$ and $\Phi(t+3\Delta t/2)$. The last two stages are repeated for as long as necessary.

Appendix E

Calculation of $< N_{cs}^2 >$

Here we derive the perturbative estimate of $< N_{cs}^2 >$ which is quoted in Section 6.2. The calculation follows an approach used by Linde [53], and is a first order classical approximation in which all terms of order g^3 or higher are completely neglected. Thus we have

$$< N_{cs}^2 >= 4\left(\frac{g^2}{32\pi^2}\right)^2 \int\int d^3x d^3y \epsilon^{ijk}\epsilon^{lmn} < (\partial_i A_j^a A_k^a)(x).(\partial_l A_m^b A_n^b)(y) > \tag{E.1}$$

Using the finite temperature average of the gauge fields

$$< A_i^a(x) A_j^b(y) >= \frac{1}{V}\int \frac{d^3\underline{k}}{(2\pi)^3 2k^0} 2\delta^{ab}\delta_{ij} n_B(k) e^{-ik(x-y)} \tag{E.2}$$

where $n_B(k)$ is the Bose distribution function, we have two contributions to $< N_{cs}^2 >$. The first by considering:

$$< \partial_i A_j^a(x).A_n^b(y) >< A_k^a(x).\partial_l A_m^b(y) > \tag{E.3}$$

and the second from

$$< \partial_i A_j^a(x).\partial_l A_m^b(y) >< A_k^a(x).A_n^b(y) > \tag{E.4}$$

We will consider the contribution of eq.(E.3).

$$
\begin{aligned}
< N_{cs}^2 > = & 4\frac{1}{V^2}\left(\frac{g^2}{32\pi^2}\right)^2 \int\int d^3x d^3y \epsilon^{ijk}\epsilon^{lmn} \\
& \times \int \frac{d^3\underline{k}}{(2\pi)^3 k^0} \delta^{ab}\delta_{jn} n_B(k)(-ik_i) e^{-ik(x-y)} \\
& \times \int \frac{d^3\underline{q}}{(2\pi)^3 q^0} \delta^{ab}\delta_{km} n_B(q)(-iq_i) e^{-iq(x-y)}
\end{aligned}
\tag{E.5}
$$

The integration over x is done first:

$$
\int d^3x e^{ix(q-k)} = V e^{ix^0(q^0-k^0)}(2\pi)^3\delta^3(\underline{q}-\underline{k}) \tag{E.6}
$$

Then the integral over $\underline{q}$ is straightforward and we obtain:

$$
\begin{aligned}
< N_{cs}^2 > = & 4V\left(\frac{g^2}{32\pi^2}\right)^2 \epsilon^{ijk}\epsilon^{lkj}\delta^{ab}\delta^{ab} \\
& \times \frac{1}{(2\pi)^3}\int \frac{d^3\underline{k}}{(k^0)^2}\frac{1}{(e^{|k|/T}-1)^2}(-k_i k_l)
\end{aligned}
\tag{E.7}
$$

where we have also performed the integral over y.

Then since

$$
\delta^{ab}\delta^{ab} = 3 \tag{E.8}
$$

and

$$
\epsilon^{ijk}\epsilon^{ljk}k_i k_l = 2|k|^2 \tag{E.9}
$$

it follows that

$$
\begin{aligned}
< N_{cs}^2 > = & \frac{4V}{8\pi^3}3\left(\frac{g^2}{32\pi^2}\right)^2 \int d^3\underline{k}\frac{2}{(e^{|k|/T}-1)^2} \\
= & \frac{48V}{2\pi^2}\left(\frac{g^2}{32\pi^2}\right)^2 T^3(\zeta(2)-\zeta(3))
\end{aligned}
\tag{E.10}
$$

where ζ is Riemann's zeta function. The second contribution from eq.(E.4) gives an identical result, so that the complete estimate is given by:

$$
< N_{cs}^2 > = \frac{48VT^3}{\pi^2}\left(\frac{g^2}{32\pi^2}\right)^2 (\zeta(2)-\zeta(3)) \tag{E.11}
$$

Bibliography

[1] T.P.Cheng and L.F.Li "Gauge theory of elementary particle physics" (Oxford University Press, 1984)

[2] H-Y. Cheng, Int. J. Mod. Phys. A4 (1989) 495

[3] Particle Data Group, Phys. Lett. 204B (1988) 1

[4] M.Shifman, A.Vainshtein and V.Zakharov, Nucl. Phys. B120 (1977) 316; JETP Lett. 22 (1975) 55

[5] M.Shifman, A.Vainshtein and V.Zakharov, Sov. Phys. JETP 45 (1977) 670

[6] E.Papantonopoulos, N.Tracas and G.Zoupanos, Phys. Lett. 188B (1987) 493

[7] E.Ma, Phys. Rev. Lett. 57 (1986) 287

[8] J.Hewett and T.Rizzo, Phys. Rep. 183 (1989) 193

[9] C.Froggatt and H.Porter, Glasgow University Preprint GUPTA/89/5-1

[10] S.Choudhury and G.Joshi, Phys. Rev. Lett. 57 (1986) 2870

[11] N.G.Deshpande, Phys. Rev. D23 (1981) 2654

[12] J.Donoghue and B.Holstein, Phys. Rev. D32 (1985) 1152

[13] E.Kolb and M.Turner, Ann. Rev. Nucl. Part. Sci. 33 (1983) 645

[14] A.Sakharov, Sov. Phys. JETP Lett. 5 (1967) 24

[15] T.Eguchi, P.Gilkey and A.Hansen, Phys. Rep. 66 (1980) 213

[16] S.Coleman "Aspects of Symmetry"(Cambridge University Press, 1985)

[17] R.Jackiw "Current Algebra and Anomalies" (World Scientific, 1985) edited by S.Treiman, R.Jackiw, B.Zumino and E.Witten

[18] S.Adler, Phys. Rev. 177 (1969) 2426; J.Bell and R.Jackiw, Nuovo Cimento 60 (1969) 47; W.Bardeen, Phys. Rev. 184 (1969) 1848

[19] G.'t Hooft, Phys. Rev. Lett. 37 (1986) 8

[20] V.Kuzmin, V.Rubakov and M.Shaposhnikov, Phys. Lett. 155B (1985) 36

[21] R.Dashen, B.Hasslacher and A. Neveu, Phys. Rev. D10 (1974) 4138

[22] F.Klinkhamer and N.Manton, Phys. Rev. D30 (1984) 2212

[23] P.Arnold and L.McLerran, Phys. Rev. D36 (1987) 581; Phys. Rev. D37 (1988) 1020

[24] S.Khlebnikov and M.Shaposhnikov, Nucl. Phys. B308 (1988) 885

[25] J.Cornwall, Phys. Rev. D40 (1989) 4130

[26] M.Shaposhnikov, Nucl. Phys. B287 (1987) 757

[27] M.Shaposhnikov, Nucl. Phys. B299 (1988) 797; Proc. XXIV Int. Conf. High Energy Physics edited by R.Kotthaus and J.Kühn (Springer-Verlag, Berlin, 1989)

[28] A.Redlich and L.Wijewardhana, Phys. Rev. Lett. 54 (1985) 970; A.Niemi and G.Semenoff, Phys. Rev. Lett. 54 (1985) 2166; K.Tsokos, Phys. Lett. 157B (1985) 413

[29] M.Shaposhnikov, talk at the annual informal particle theory meeting at RAL, 18-20 Dec 1989.

[30] A.Bocharev, S.Khlebnikov and M.Shaposhnikov, Nucl. Phys. B329 (1990) 493

[31] A.Bocharev and M.Shaposhnikov, Mod. Phys. Lett. A2 (1987) 417

[32] A.Linde, Phys. Lett. 92B (1980) 119

[33] ALEPH collaboration, Phys. Lett. 246B (1990) 306

[34] CDF collaboration, Phys. Rev. Lett. 64 (1990) 142

[35] A.Bocharev, S.Kuzmin and M.Shaposhnikov, Niels Bohr Institute Preprint NBI-HE-90-08 (1990)

[36] N.Turok and J.Zadrozny, Princeton preprint PUPT-90-1183

[37] E.Witten, Nucl. Phys. B177 (1981) 477; A.Guth and E.Weinberg, Phys. Rev. Lett. 45 (1980) 1131

[38] D.Gross, R.Pisarski and L.Yaffe, Rev. Mod. Phys. 53 (1981) 43

[39] M.Creutz, "Quarks, Gluons and Lattices" (Cambridge University Press, 1983)

[40] J.Ambjørn, M.Laursen and M.Shaposhnikov, Phys. Lett. 197B (1987) 49; Nucl. Phys. B316 (1989) 483

[41] K.Wilson, Phys. Rev. D10 (1974) 2445

[42] K.Bowler and C.Rebbi, contribution to "Statistical and Particle Physics", edited by K.Bowler and A.McKane (SUSSP Publications 1983)

[43] D.Grigoriev and V.Rubakov, Nucl. Phys. B299 (1988) 67

[44] D.Grigoriev, V.Rubakov and M.Shaposhnikov, Phys. Lett. 216B (1989) 172; Nucl. Phys. B326 (1989) 737

[45] A.Bocharev and M.Shaposhnikov, Mod. Phys. Lett. A2 (1987) 991

[46] J.Jersak, Preprint, DESY 89-115, HLRZ 89-45 (1989)

[47] J.Kogut and L.Susskind, Phys. Rev. D11 (1975) 395

[48] A.D.Kennedy, Fermilab Preprint FERMILAB CONF-89/237-T, SCRI Preprint FSU-SCRI-89-147

[49] P.Di Vecchia, K.Fabricus, G.C.Rossi and G.Veneziano, Nucl. Phys. B192 (1981) 392

[50] J.Ambjørn, T.Askgaard, H.Porter and M.Shaposhnikov, Phys. Lett. 244B (1990) 479

[51] J.Ambjørn, T.Askgaard, H.Porter and M.Shaposhnikov, Preprint, NBI-HE-90-48 (1990)

[52] D.Grigoriev and M.Shaposhnikov, Preprint, NBI-HE-90-05 (1990)

[53] A.Linde, "Inflation and Quantum Cosmology", Newton Centenary Volume (Cambridge University Press)